A study of regional and global myocardial morphology and function in various substrates of cardiac remodelling

Čikeš, Maja

UNIVERSITY OF ZAGREB
SCHOOL OF MEDICINE

Maja Čikeš

A Study of Regional and Global Myocardial Morphology and Function in Various Substrates of Cardiac Remodelling

PhD THESIS

Zagreb, 2009.

The scientific work on which this Thesis is based has been conducted at the Department of Cardiovascular Diseases, University Hospital Centre Zagreb, University of Zagreb School of Medicine and University of Zagreb, Faculty of Engineering and Computing as well as at St. George's Hospital, St George's University, London, United Kingdom and University Hospital Würzburg, Würzburg, Germany.

This work was financed by the Ministry of Science, Education and Sport of the Republic of Croatia (Project Nr. 108-1081875-1991), the National Foundation for Science, Higher Education and Technological Development of the Republic of Croatia (Brain gain - Senior Programme, Project "An integrated, model based, approach for the quantification of cardiac function based on cardiac imaging") and the L'Oreal-UNESCO Scholarship for Women in Science.

Thesis mentors: Professor Bart Bijnens, PhD
ICREA Research Professor
Department of Information & Communication Technologies
Universitat Pompeu Fabra
Barcelona, Spain

Professor Jadranka Šeparović Hanževački, MD, PhD
Department of Cardiovascular Diseases
University of Zagreb School of Medicine

I owe my deepest gratitude to Professor Bart Bijnens for his endless research enthusiasm and great patience. Looking at echoes through Bart's prism has shown me an intriguing view at the heart, inspiring to question the facts rather then to always accept them as they are. Although I was often not allowed to take shortcuts, I thank him for his immaculate guidance through this thesis, giving me the opportunity to enrich my knowledge along the way.

I would like to thank Professor Jadranka Šeparović Hanževački for being my mentor from my student's days and for her enthusiasm for haemodynamics.

I am also grateful to Professor Davor Miličić for his great support as well as providing a progressive clinical and academic environment. The confidence he had in me was indebting to pursue these projects; his continuous drive and motivating energy was essential to finalise the thesis in due time.

I have to particularly thank Professor George Sutherland for his enormous experience and eagerness in teaching echocardiography as well as giving invaluable clinical advice in our research projects. The time I have spent in his echolab was most important for my training in echocardiography and cardiology.

This thesis is based on true team work: I thank Professor Sven Lončarić and engineer Hrvoje Kalinić (University of Zagreb Faculty of Engineering and Computing) as well as dozent Frank Weidemann (University Hospital Würzburg) for their time, effort and fruitful discussions. I also thank my colleagues from the Department of Cardiovascular Diseases (particularly the members of the Echolab), Department of Cardiac Surgery and the Division of Endocrinology for being part of our multidisciplinary, multicentre environment.

Last but not least, I thank my parents for their unconditional support and, in this case, particularly my father for "infecting" me with his love for cardiology.

Contents

List of Abbreviations

α – gal A	α - galactosidase A
AA	secondary amyloidosis
AL	primary amyloidosis
AS	aortic stenosis
ASE	American Society of Echocardiography
asymm	asymmetry index
A-V	atrio-ventricular
AV	aortic valve
AVA	aortic valve area
AVC	aortic valve closure
AVO	aortic valve opening
AVR	aortic valve replacement
BMI	body mass index
BP	blood pressure
CABG	coronary artery bypass grafting
CARE-HF	Cardiac Resynchronization in Heart Failure
CMR	cardiac magnetic resonance imaging
CMR LE	late enhancement by cardiac magnetic resonance imaging
CO	cardiac output
CRT	cardiac resynchronization therapy
CT	computed tomography
CW	continuous wave Doppler
DBP	diastolic blood pressure
DM	diabetes mellitus
DMI	Doppler Myocardial Imaging
dP/dt	change of pressure over time
DSE	dobutamine stress echocardiography
DSE_{neg}	patients without resting wall motion abnormalities or signs of inducible ischaemia on DSE
DSE_{pos}	patients with resting wall motion abnormalities or a positive DSE
E	early mitral flow velocities
E’	early basal myocardial velocities
ECG	electrocardiogram
EDWT	end-diastolic wall thickness
EF	ejection fraction
ESWT	end-systolic wall thickness
ET	ejection time
ET_{mod}	ejection time derived by mathematical modelling
ET_{man}	ejection time by manual analysis of the Doppler signal
ET/R-R	relative ejection time
FPR	false positive rate
GH	growth hormone
$GRAD_{neg}$	patients without an inducible intracavitary gradient by dobutamine stress echocardiography
$GRAD_{pos}$	patients with an inducible intracavitary gradient by dobutamine stress echocardiography
HCM	hypertrophic cardiomyopathy
HR	heart rate
HTN	hypertension
IGF-I	insulin-like growth factor-I

IVCT	isovolumic contraction time
IVD	interventricular delay
IVRT	isovolumic relaxation time
IVS	interventricular septum
IVSd	interventricular septum thickness at end-diastole
LA	left atrium
LV	left ventricle
LVEDV	left ventricular volume at end-diastole
LVESV	left ventricular volume at end-systole
LVETI	left ventricular ejection time index
LVH	left ventricular hypertrophy
LVIDd	left ventricular internal diastolic dimension at end-diastole
LVIDs	left ventricular internal diastolic dimension at end-systole
LVM AS	left ventricular mass, American Society of Echocardiography Formula
LVMI	left ventricular mass index
LVOT	left ventricular outflow tract
LVPWd	left ventricular posterior wall thickness at end-diastole
MI	myocardial infarction
MR dP/dt	change of pressure over time derived from the mitral regurgitation jet
MVO	mitral valve opening
no	number
ns	not significant
NYHA	New York Heart Association Classification
P	area
Pa	Pascal
PAP	pulmonary artery systolic pressure
PCI	percutaneous coronary intervention
PG	pressure gradient
POST	postoperative
PRE	preoperative
PSS	post-systolic strain
pts	patients
R – R	R – R interval
ROC	receiver operating characteristic
RWT	regional wall thickness
S	end-systolic strain
SBP	systolic blood pressure
SD	standard deviation
SR	peak systolic strain-rate
SV	stroke volume
TEE	transesophageal echocardiography
T_rise	rise time
T_fall	fall time
T_{mod}	time from onset of aortic flow to peak aortic flow derived by mathematical modelling
T_{man}	time from onset of aortic flow to peak aortic flow by manual analysis of the Doppler signal
T_{mod}/ET_{mod}	ratio of time to peak and ejection time flow by analysis of the modelled signal
TPR	true positive rate
Vmax	maximal velocity
VTI	velocity time integral

Chapter 1

General Introduction

1.1. Cardiac Function

For the management of a broad range of heart diseases, a quantitative, reproducible approach for the assessment of *cardiac (dys-) function* is of great importance. However, cardiac (dys-) function is a very general and non-specific entity that is defined depending on the context. This makes it difficult to unambiguously define, and thus quantify, (dys-) function in a clinical context. Intrinsic cardiac function implies the assessment of true contractility of the myocardium. Using non-invasive approaches, this is currently not measurable and in clinical practice surrogates for true cardiac contractility are assessed and reported as reflecting *cardiac function*.

Figure 1.1 gives an overview of an integrated view on 'cardiac function'. First of all, two different levels are distinguished: *intrinsic myocyte function* (often referred to as *contractility*) and *ventricular pump function*. At both levels, function consists of two components, namely force development (resulting in the generation of sufficient pressure to open the cardiac valves) and deformation (resulting in volume ejection). Additionally, ventricular function can be interpreted either from a global perspective as overall pump performance, or from a regional perspective where the contributions of individual wall segments are taken into account. The interactions between the components force development and deformation is determined by the boundary conditions in which the heart functions. These include: a) wall properties such as tissue composition/elasticity, fibre structure and global geometry, which determine the local segment interactions and the resulting wall stress; b) interaction between the heart and peripheral circulation, mostly described as (pressure & volume) loading conditions.

In summary, cardiac function can qualitatively be defined as the ability of the myocardium to work (pump) and keep on working sufficiently in order to maintain an adequate stroke volume (as demanded by the peripheral organs) by developing force to generate pressure and by deforming to displace volume.

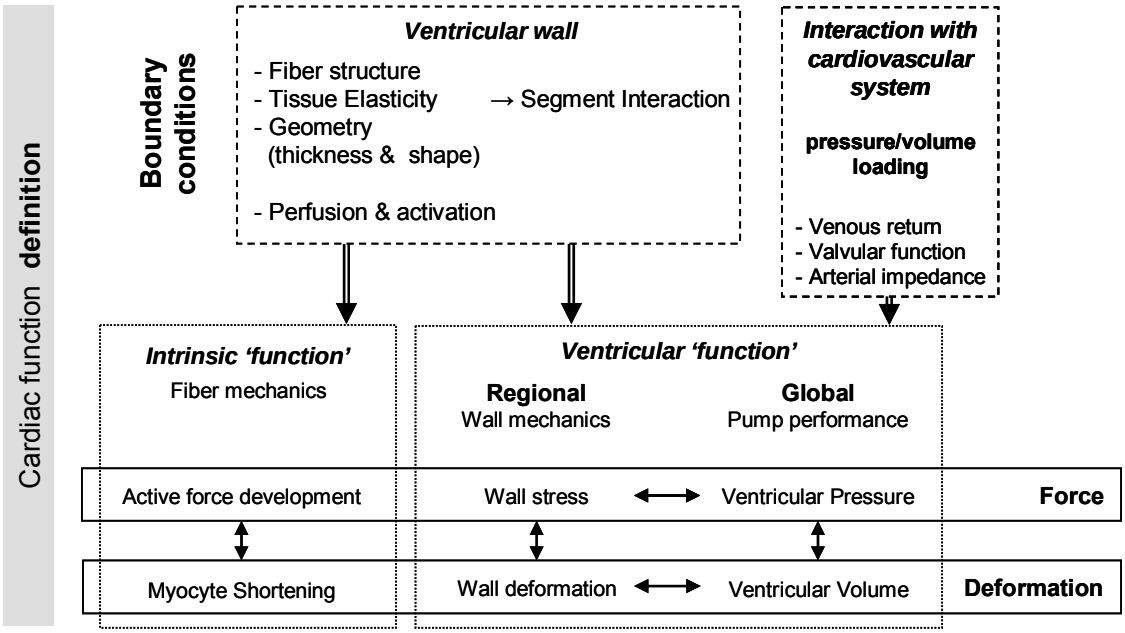

Figure 1.1: An integrated view on cardiac function.

1.2. Cardiac Remodelling

Ventricular remodelling is an adaptive mechanism used by the ventricle to cope with a problem, either within the myocardium itself or the environment it has to work in, intended to generate sufficient cardiac output to fulfil the needs of the body (figure 1.2). However, since this is an abnormal situation with inherent disadvantages, on the long term it will lead to irreversible damage to the myocardium which can evolve into ventricular dysfunction and heart failure.

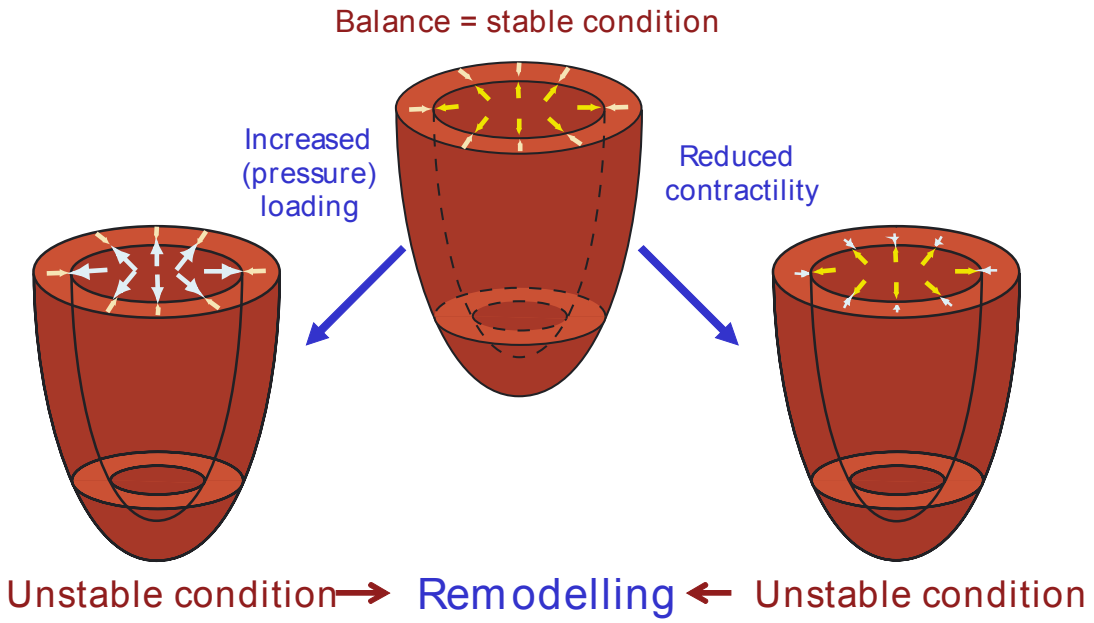

Figure 1.2: Balance of cardiac contractility and loading.

Several cardiac conditions are associated with progressive remodelling of the ventricle. Examples of this are pressure or volume overload due to valvular stenosis or regurgitation, ischaemic remodelling in coronary artery disease, pressure remodelling in severe hypertension, electrical remodelling in certain conduction abnormalities (e.g. LBBB), genetic abnormalities resulting in progressive development of local hypertrophy and fibrosis etc.

Most non-ischemic remodelling, like left ventricular hypertrophy (LVH), has classically been considered as a substrate affecting the ventricle *globally*. However, it has been shown that e.g. arterial hypertension results in localised LVH due to regional differences in wall stress, suggesting that *regional* phenomena might play a more important role than previously assumed. This implies that enhanced understanding of LV remodelling might still lead to optimized clinical treatment of these patients.

For the clinical evaluation of patients with signs of ventricular remodelling, a good method for the evaluation and follow up of the evolution of intrinsic ventricular function is required. This is however hampered by two factors: both the abnormal loading and the altered geometry associated with several of these heart diseases importantly affect the current methods used to evaluate cardiac function. To study cardiac function in the context of ventricular remodelling, techniques which are as load-independent as possible are required since pressure or volume loading will mostly be abnormal. In clinical routine, indirect measurements of contractility and volume ejection are being used, mainly based on non-invasive imaging techniques (echocardiography, cardiac magnetic resonance imaging (CMR) or computed tomography (CT)).

1.3. Aims and Outline of the Thesis

The main aim of this thesis was to study cardiac function in different types of myocardial remodelling. We sought to follow these objectives:

- To describe the impact of *Velocity and deformation imaging* on the assessment of myocardial dysfunction. Chapter 2 addresses the assessment of cardiac function, myocardial motion and deformation as well as clinical applications of Velocity and deformation imaging.

- To propose a novel method for Doppler signal analysis. Chapter 3 describes the method underlying the (semi)automatic analysis of continuous wave (CW) Doppler aortic outflow traces and its segmentation, providing a theoretical basis for the following clinical applications of this approach.

- To define parameters useful in the detection of myocardial (dys-)function in groups of patients with *ischaemic remodelling* and *remodelling in valvular heart disease* (aortic stenosis). In Chapters 4 and 5 the previously described dedicated signal modelling algorithm is applied on the LV outflow traces in these patient groups, providing specific parameters of myocardial (dys-)function based on the aortic outflow profile traces (instantaneous peak velocities).

- To assess the influence of *electrical remodelling* in patients with left bundle branch block on myocardial dysfunction as well as to study acute *reverse remodelling* in these patients immediately after cardiac resynchronization therapy. In Chapter 6, the mechanical consequence of the underlying electrical abnormality and its acute reversal are studied.

- To examine a group of patients with early acromegalic cardiomyopathy in which hypertrophy occurs without significant changes in wall stress. In Chapter 7, *hypertrophy and hypercontractility* in early stage acromegalic cardiomyopathy resulting in increased cardiac output and inducing additional signs of vascular remodelling are discussed.

- To describe different entities leading to hypertrophic remodelling and define the differences in regional deformation based on the various underlying substrates. Chapter 8 addresses the changing role of echocardiography in the diagnosis of the *hypertrophically remodelled myocardium*.

1.4. Hypothesis

The application of different modalities of echocardiographic imaging in various substrates of ventricular remodelling enhances the understanding of the underlying pathophysiological mechanisms and its relation to global and/or regional functional impairment, thus aiding clinical decision making in such patients.

Chapter 2

Velocity and Deformation Imaging for the Assessment of Myocardial Dysfunction*

2.1. Introduction

Recent developments in echocardiographic imaging technology and processing enabled the quantification of myocardial motion and deformation in a clinical setting. Echocardiographic strain (-rate) imaging (either based on Doppler Myocardial Imaging (DMI) [1] or speckle tracking [2]) provides a relatively easy way to study myocardial deformation.

It has been shown, both in the early animal lab work based on microcrystal measurements, and more recently using the non-invasive image based methodologies, that analyzing myocardial velocities and deformation, especially when combined with the response to a dobutamine challenge, enables the assessment of myocardial dysfunction in a wide range of cardiovascular pathologies (amongst which: coronary artery disease and stress echo [3-6]; valvular diseases [7,8]; hypertension [9, 10]; hypertrophic cardiomyopathy [11]; cardiac resynchronization therapy [12]; amyloidosis [13]; heart transplantation [14]; genetic cardiomyopathies [15, 16]). One of the major strengths of quantitative deformation analysis is the discrimination of different ischemic substrates, ranging from acute ischemia, over stunning to chronic ischemia with sub-endocardial fibrosis [17].

For a proper interpretation of velocity and deformation data in a clinical setting, it is required to understand cardiac function/mechanics in normality and pathologies, combined with knowledge on how intrinsic cardiac function influences motion and deformation.

2.2. Assessing Cardiac Function

For the management of a broad range of heart diseases, a quantitative, reproducible approach for the assessment of *cardiac (dys-) function* is of great importance. However, *cardiac (dys-) function* is a very general and non-specific entity that is defined depending on the context. This makes it difficult to unambiguously define, and thus quantify, (dys-) *function* in a clinical context. Intrinsic cardiac function implies the assessment of true contractility of the myocardium. Using non-invasive approaches, this is currently not measurable and in

* With permission from: Bijnens BH, Cikes M, Claus P, Sutherland GR. Velocity and deformation imaging for the assessment of myocardial dysfunction. Eur J Echocardiogr. 2009;10(2):216-26.

clinical practice surrogates for true cardiac contractility are assessed and reported as reflecting *cardiac function*.

Figure 2.1 illustrates how the heart (simplified to the LV) manages to fulfil its task: *maintaining a constant and adequate blood (volume) flow*. The contractile elements of the myocardium can develop a contractile force and can shorten. These contractile elements are imbedded, with a very specific distribution, in the LV with a certain overall geometry (shape, thickness) and with specific elastic properties. By the initial force development of the contractile elements, the ventricle can increase its internal pressure up to the point that this is high enough to open the aortic valve. From that moment on, the shortening of the contractile elements will decrease the cavity size so that its internal blood content is ejected.

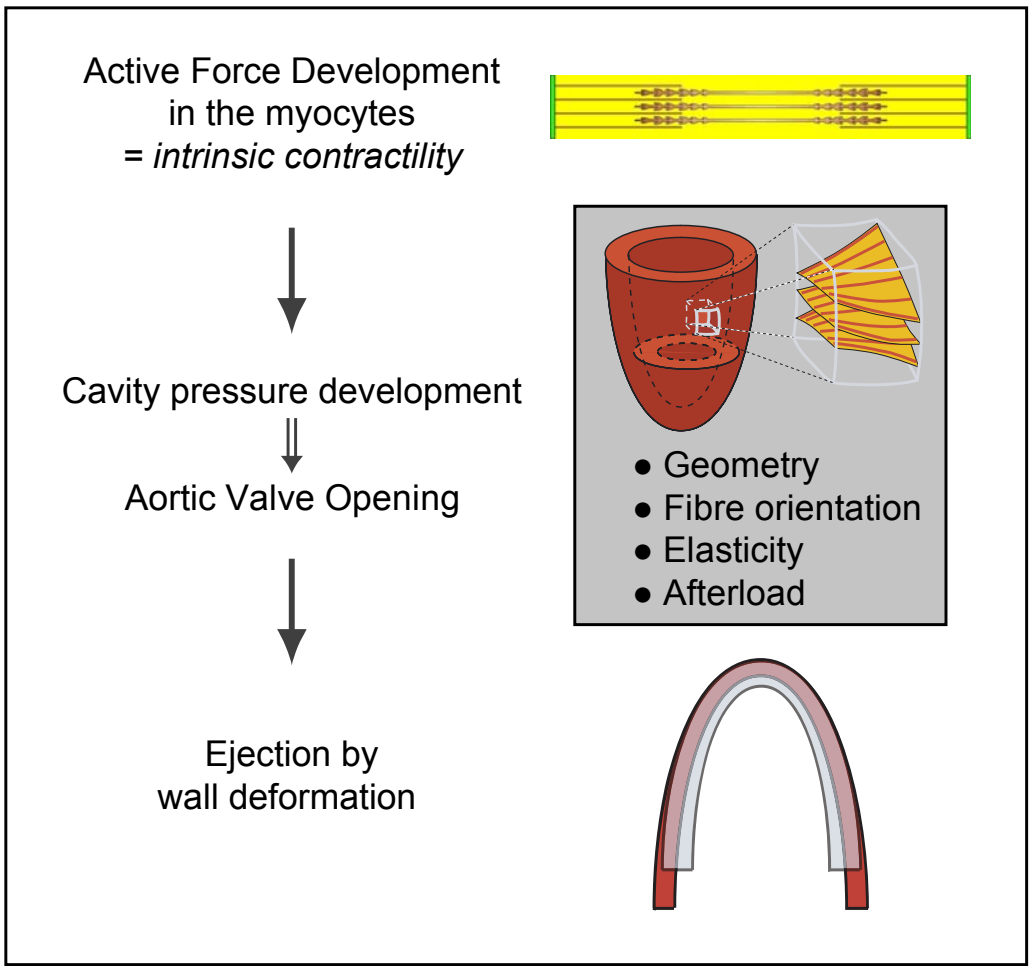

Figure 2.1: The functioning of the heart.

From Figure 2.1, it is clear that in order to understand the functioning of the heart, all aspects, involved in both the development of the internal pressure and the ejection of the blood by the reduction (deformation) of the cavity volume, have to be taken into account. Just

measuring e.g. the EF, leaves out all information on pressure, tissue properties and the transformation from shortening of the individual contractile elements into the global deformation of the LV.

Thus, to fully describe *cardiac function*, two aspects and their interaction should be distinguished: *force development* (contractility of the myocytes, resulting in the generation of sufficient pressure to open the cardiac valves) and *deformation* (shortening of the myocytes, resulting in the actual volume ejection). Additionally, ventricular function can be interpreted either from a global perspective as overall pump performance, or from a regional perspective where the contributions of individual wall segments are taken into account. The interactions between the components *force development* and *deformation* are determined by the boundary conditions in which the heart functions.

These include:

- *Wall properties* such as tissue composition and elasticity, fiber structure and global geometry, which determine the local segment interactions and the resulting wall stress
- *Interaction between the heart and peripheral circulation, mostly described as (pressure and volume) loading conditions.*

The interpretation of cardiac function data by examining either wall mechanics (regional deformation-stress analysis) or pump performance (pressure-volume analysis) requires an integration of their measurement in the global picture of the working of the heart (Figure 1).

In clinical practice, this integration is usually performed in the mind of the investigator and only indirect measurements of force development and volume ejection are used to study *cardiac function*. These are mainly based on non-invasive imaging techniques (echocardiography, CMR or CT). Usually, patients are followed clinically using echocardiography. Two-dimensional and Doppler echocardiography allow both the direct anatomical evaluation of the myocardium and the evaluation of haemodynamics. Cardiac geometry and the degree of myocardial hypertrophy can be determined by measuring ventricular size, wall thickness and myocardial mass index [18].

For the evaluation of (systolic) cardiac function, the intrinsic properties of the fibres and myocytes are the most important, since these determine whether the myocardium is affected by the chronic condition and their properties reflect when irreversible damage is induced. However, current evaluation is based on global indices such as ejection fraction and fractional shortening. These volume based parameters have important limitations in reflecting contractility in the context of abnormal loading conditions because:

- The assessment of intrinsic function based on volume parameters, like fractional shortening and ejection fraction, depends on geometric assumptions. It is not well understood how these are influenced by wall thickness or ventricular shape. Often

'supra-normal' values of EF are measured in hypertrophied or volume overloaded ventricles. It is unclear whether these really reflect actual changes in contractility [7].

- All volume based indices are load-dependent. During disease progression, changes in loading or geometry will affect functional evaluation. For the serial assessment of myocardial contractility in such patients, an integrated approach, which takes into consideration geometry and loading, is required.
- Conventional parameters only assess global function. In most conditions, which show alterations in myocardial contractility, the assessment of regional ventricular function is important. Additionally, several of the methods for global assessment concentrate only on radial function, ignoring longitudinal function, which in most cardiac pathology is altered before changes occur in radial indices [19]. Increased radial function often acts as a compensation for the reduction in global longitudinal function.
- Global measurements do not take into account segment interactions that e.g. only result in local wall deformation which does not contribute to pressure build up or a reduction in global ventricular volume [20].

To overcome some of these concerns, new echocardiographic methods have been proposed to assess regional ventricular function based on myocardial motion and deformation. One of these, which has proven to be both important for understanding cardiac physiology and of clinical value is Tissue Doppler imaging, which allows the quantification of myocardial velocities [1]. Post processing techniques, based on acquired velocity data, allow the calculation of regional myocardial deformation (strain rate or rate of deformation and strain or amount of deformation) while post processing of grayscale images (using speckle tracking or registration techniques) can provide information on displacement and deformation. In a lot of cardiac pathologies, the reduction in myocardial deformation correlates well with the severity of the disease [21, 22]. However, it is yet unclear whether this is entirely due to a decrease in function or rather related to changes in cardiac geometry and loading.

2.3. Myocardial Motion and Deformation

Using either Doppler Myocardial Imaging (also referred to as Tissue Doppler Imaging or Myocardial Velocity Imaging) or grayscale speckle tracking, motion of myocardial segments can be recorded and quantified.

Figure 2.2A shows the motion components that can be assessed based on echocardiographic imaging. From an apical view, the longitudinal motion (the base of the LV moving towards the (normally) fixed apex) can be assessed while from using a parasternal (short or long-axis) view, the inward radial motion can be measured.

Either by calculating the spatial gradients of the obtained myocardial velocities [1] or by using a grayscale imaging approach (speckle tracking) [23], local myocardial deformation can be quantified. In reality, the deformation of a myocardial segment during the cardiac cycle is very complex [24] (Fig 2.2B) and contains both *normal* deformation (longitudinal shortening/lengthening, radial thickening/thinning and circumferential shortening/lengthening) and *shear* (base-apex twisting, epi-endo circumferential shear and epi-endo longitudinal shear) [1, 25, 26].

Figure 2.2C shows a typical longitudinal velocity and displacement (the temporal integral of the velocity) from a normal individual (using high frame-rate DMI). Figure 2.2D represents the corresponding deformation (strain) and speed of deformation (strain-rate). Note that there is a clear gradient from base to apex in both velocity and displacement, which corresponds to the stationarity of the apex within the thorax while the base moves towards it. In contrast, deformation is more or less homogenous throughout the (normal) myocardial wall. These patterns will be altered in cardiac pathologies (see further). Using Doppler based approaches, mainly longitudinal and radial motion/deformation is studied, since it is difficult to align the circumferential motion with the ultrasound beam, as is required with this technique. With speckle tracking, longitudinal and circumferential motion/deformation is most commonly analyzed, since the intrinsic spatial resolution of the images is limited, making it difficult to track the tissue within the (thin) wall. Moreover, the lateral resolution of ultrasound images is intrinsically less than in the axial direction, making it more difficult to assess radial deformation from an apical view [27, 28]. Additionally, speckle tracking allows the assessment of cardiac rotation and torsion (if measured at different levels) [29]. When using either of the approaches, it is important to note the inherent differences in the results. DMI works at higher temporal resolution (>150 Hz), making that it is more suited to assess that fast events, as are observed in velocities and strain-rates (especially in the iso-volumic periods), while for the quantification of displacements and strain, the inherent lower frame-rate used for speckle tracking (<90Hz) would be sufficient. Speckle tracking has shown to be more reproducible and requires less user expertise, but inherently uses more spatial and temporal averaging of the obtained profiles, resulting in significantly lower values when compared to DMI and a decreased ability in detecting smaller abnormal regions [27, 28, 30, 31].

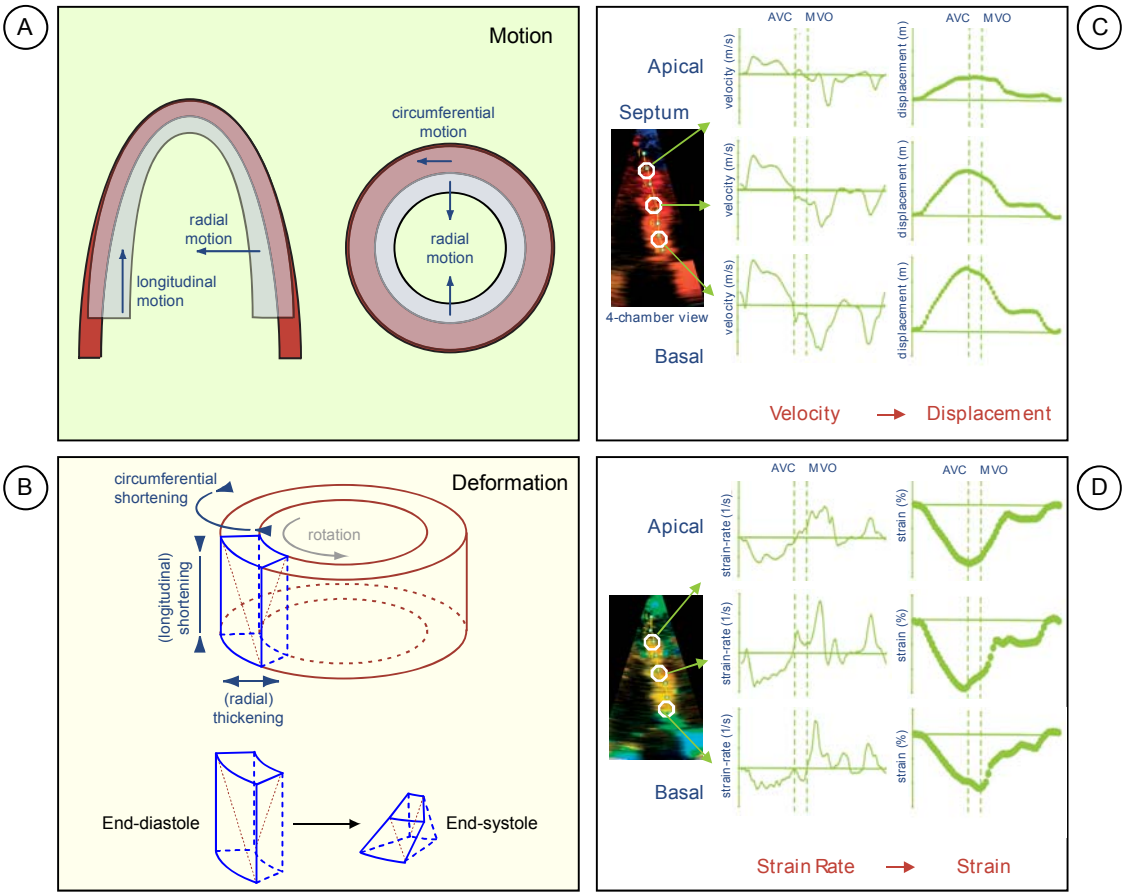

Figure 2.2: Myocardial motion and deformation consists of 3 major components: longitudinal, radial and circumferential (A, B). The total deformation, from end-diastole to end-systole, of a myocardial segment is very complex and includes shortening, thickening and shearing (B). Typical profiles for the velocity, displacement (C) and strain-rate, strain (D) traces during one cardiac cycle in normal myocardium.

2.4. The Relation between Myocardial Function (Contractility) and Regional Deformation

When using myocardial motion or deformation to assess (dys-) function, it is important to understand the relation between intrinsic function (contractility) and the resulting motion/deformation.

In general, the relation between the forces acting up on an object and the resulting deformation of that object is described by *Hooke's law*. This law states that forces (mostly expressed as *stress* and with units *pascal* (*Pa)*) and deformation (mostly Lagrangian (relative) deformation and expressed as a *percentage*) are linked by the elasticity (with units *Pa*) of the object. The more elastic an object, the more it will be deformed by a certain force.

This relation (which is also time-variant), when applied to myocardium, is illustrated in Figure 2.3.

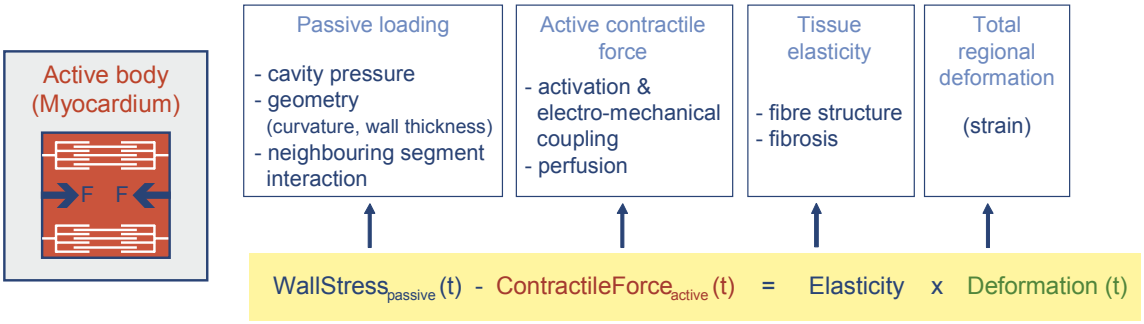

Figure 2.3: The relationship between local forces and deformation.

In a myocardial segment, both the force developed *by* the segment, as well as all forces developed *on* the segment have to be taken into account. Obviously, the *internal* contractile force (the intrinsic *contractility* of the myocardium, a force trying to shorten the myocytes, thus resulting in negative deformation) is the most important. However, it has to be kept in mind that any piece of myocardium is always imbedded in a ventricle, resulting in *external* forces acting up on it (and mostly working in the opposite direction of the contractile force). These forces are described as the *loading* of the tissue and consist of the local wall stress, caused by the intra-cavity pressure (whose influence is related to local geometry of the ventricle), and the interaction with neighboring, contracting, segments (each contracting neighboring segment will *pull* the segment under investigation).

As for any object, the relation between all acting forces and the resultant deformation is ruled by the regional elasticity, which, for myocardium, translates in the fiber/matrix structure and the presence or absence of fibrosis and depositions. Also, it must be kept in mind that elasticity is not a constant, since, due to the matrix structure of the tissue, the more myocardium is stretched, the more difficult it becomes to stretch it even further.

In summary, the main factors influencing regional myocardial deformation are (Figure 2.4):

- *Intrinsic contractility* i.e. the contractile force developed by the myocardium (influenced by tissue perfusion and electrical activation and being developed in the early part of the ejection phase, peaking around one third of it) [32].
- *Cavity pressure* (often referred to as afterload and influenced by preload), whose influence is related to the local ventricular geometry [33].
- *Segment interaction* (the influence of the contracting neighbouring segment) [20].
- *Tissue elasticity* (which is dependent on the local histology (fibrosis) and on the amount that the myocardium is already stretched) [34].

Thus, these influencing factors consist of one active force (contractility), two passive forces (pressure and segment interaction) and the tissue properties. This is graphically presented in Figure 2.4, which shows a schematic short-axis cross section of the left ventricle.

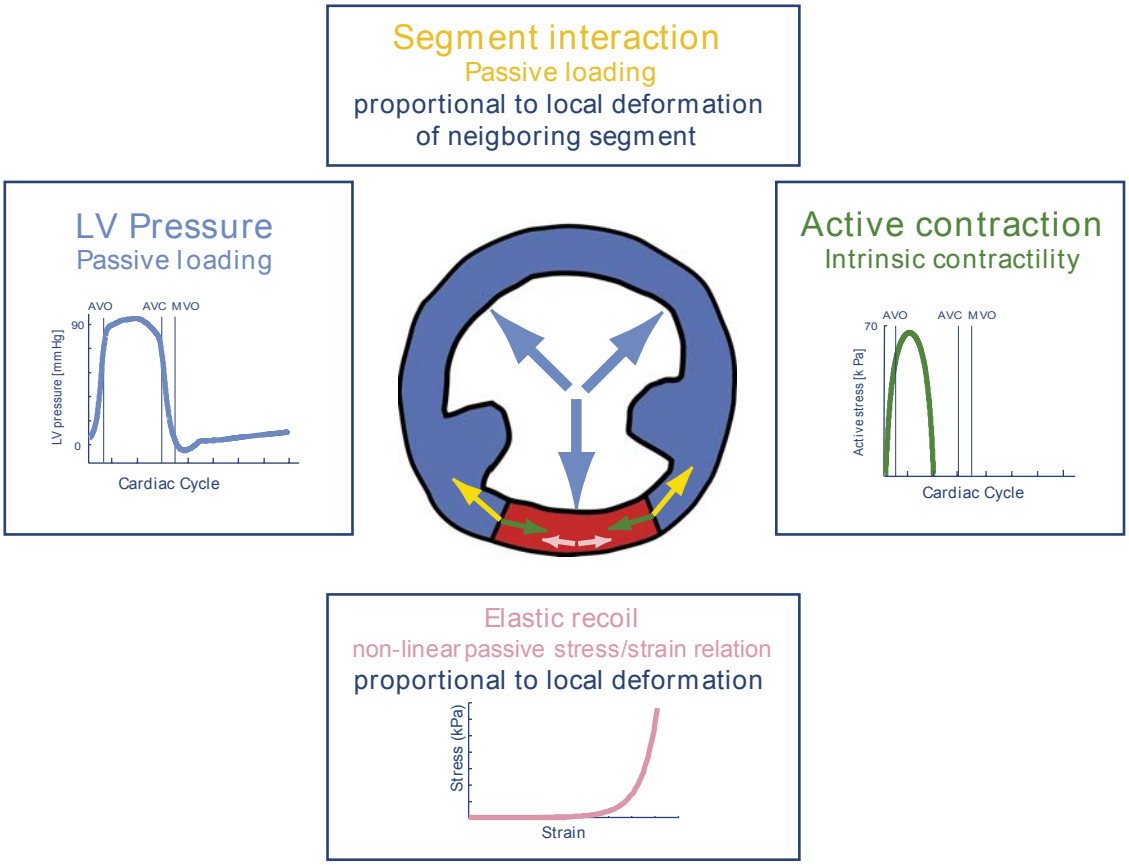

Figure 2.4: The local forces acting upon a myocardial segment.

2.5. Clinical Application

2.5.1. Coronary Artery Disease

Coronary artery disease and the underlying ischemic substrates have been studied extensively using velocities and deformation (both based on invasive ultrasound crystal measurement and non-invasive imaging (echocardiography and magnetic resonance imaging)) [21, 35-37]. It was shown that myocardial motion and deformation react very predictably on changes in regional perfusion of the presence of infarction [17].

In summary, regional velocities as well as peak systolic strain-rate and end-systolic strain reduce linearly with a reduction in regional perfusion or the presence of sub-endocardial fibrosis. Simultaneously, post-systolic motion/deformation is developing. When challenged with dobutamine, acutely ischemic tissue will show even less deformation, while post-systolic deformation is increased, whereas normal tissue shows increased deformation (continuously increasing strain-rate and increasing strain as long as filling is not reduced by increased heart-rate). In contrast, partial thickness chronic infarction will show a very moderate deformation increase (depending on the transmurality) when stimulated with dobutamine. Interestingly, while stunned myocardium shows decreased deformation at rest, associated with post-systolic deformation, when stimulated with dobutamine, systolic deformation almost restores to normal and post-systolic deformation almost completely disappears [17]. This behavior of stunned myocardium can be attributed to myofibrillar oedema, increasing the spacing within the contractile elements of the myocardium and thus reducing the effective force it can develop [38].

Additionally, it was shown that full pressure reperfusion of an acute infarct influences deformation. If reperfusion is within a short period of time after the onset of symptoms, the myocardial deformation will normalize quickly (potentially after some period of stunning). However, when reperfusion is within a time-span of about 1.5 to 6 hours, interstitial myocardial oedema will develop, resulting in a sudden increase in end-diastolic wall thickness of the infarcted segment at the moment of reperfusion. This is associated with the total absence of regional deformation [39, 40]. With reperfusion later than about 6 hours after onset of symptoms, the myocardial wall has thinned and does not deform and reperfusion does not alter this significantly.

Thus, deformation analysis at baseline and its response to a dobutamine challenge enables to uniquely distinguish the different ischemic substrates (Figure 2.5).

This makes the combination of the measurement of baseline deformation (in a lesser extent: motion), combined with the response to a dobutamine stress echo, a potent clinical tool for the assessment of the ischemic substrate in a clinical patient.

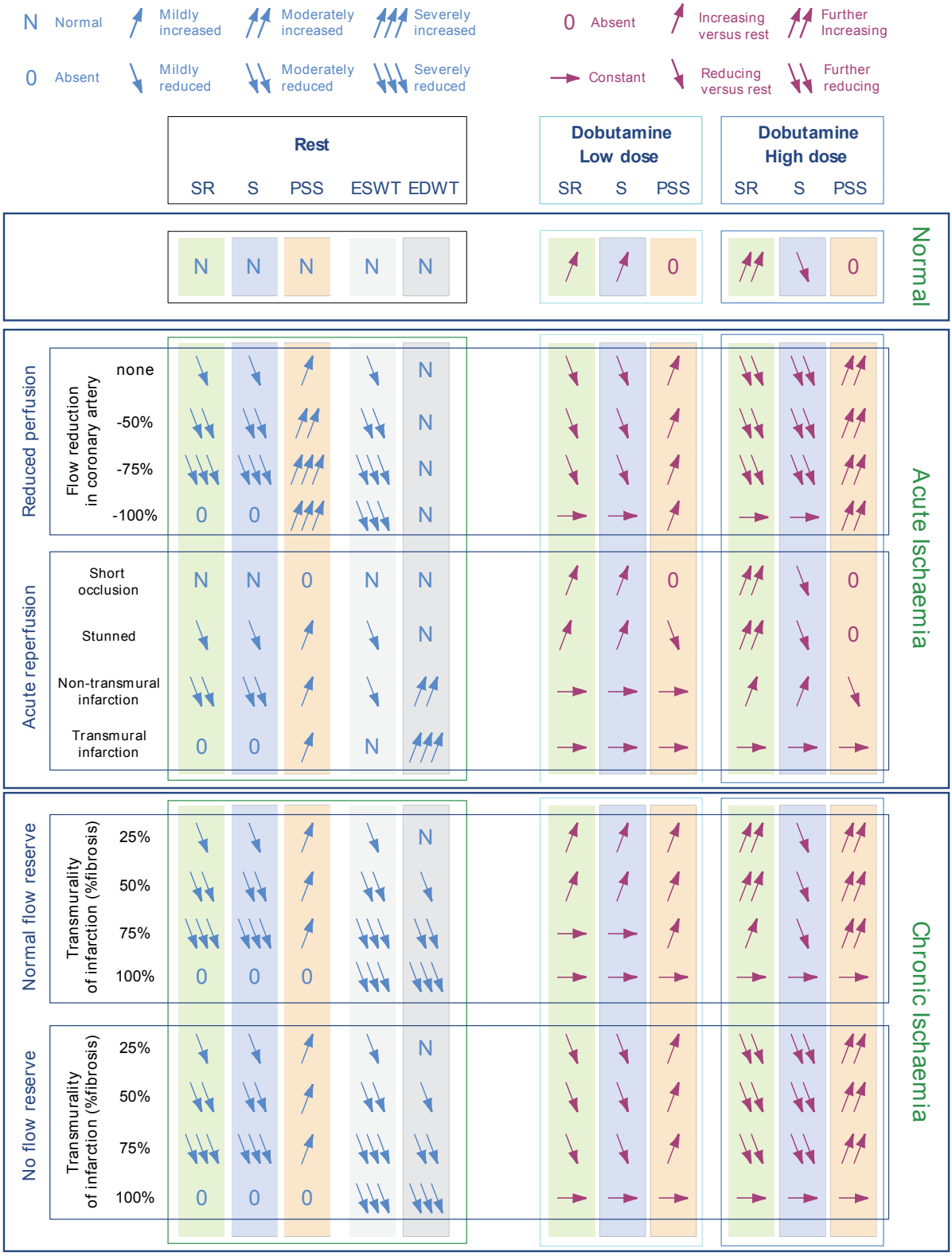

Figure 2.5: An overview of the regional deformation and wall thickness of the different ischaemic substrates at rest and how they respond to dobutamine. From [1], with permission.

2.5.2. Volume Overload

As discussed above, deformation is also related to ventricular geometry. Dilatation is an adaptive mechanism used by the ventricle to cope with the problem of generating sufficient cardiac output to fulfil the needs of the body. There is a clear relationship between ventricular size and the generated stroke volume for a certain available contractile force. An enlarged ventricle can more easily generate a larger stroke volume than a smaller one. This can be easily understood since in a spherical or ellipsoid object, the volume of the outermost part is always larger than the volume of the innermost part, which means that similar deformation (determined by the contractile force) can generate a larger stroke volume in a dilated heart. Similarly, the same amount of stroke volume can be generated with less contractility in a dilated heart. Thus, as the ventricle dilates, with a preservation of stroke volume, regional deformation reduces without any change in contractility. However, when stroke volume increases (as in valve regurgitation), myocardial deformation can increase. In these cases, only when contractility additionally reduces, there is a marked decrease in deformation [7]. Normalising deformation with ventricular volume might be a useful approach to isolate the effect of geometry and changing contractility in volume overloaded ventricle [7].

2.5.3. Pressure Overload

Several cardiac conditions are associated with progressive remodelling of the ventricle. Examples of this include pressure or volume overload due to valvular stenosis or regurgitation, coronary artery disease with associated decreased contractility and fibrosis leading to ventricular dilatation, genetic abnormalities resulting in hypertrophy and progressive development of local fibrosis, severe hypertension, conduction abnormalities, etc.

Remodelling is in the first instance a response to a problem with either the muscle itself or the environment in which it has to work and is an attempt to keep on fulfilling the heart's task - circulating the blood. However, since this is an abnormal situation with inherent mechanical disadvantages, in the long term, this will lead to irreversible damage to the muscle which evolves into ventricular dysfunction and heart failure. The early detection and follow-up of changes in cardiac function and myocardial properties is thus of major importance.

Myocardial velocities and deformation have proven useful in several conditions with altered myocardial properties or geometry.

With pressure overload pathology, the basal septal segment is the first to show changes (figure 6). Both a decrease in strain (-rate) and the development of post-systolic motion/deformation is observed, as well as the development of localized hypertrophy [9]. With increasing overload the whole ventricle becomes hypertrophic and deforms less. The

development of regional fibrosis further diminishes deformation. Thus, basal septal deformation is the most sensitive to changes in pressure overload pathology.

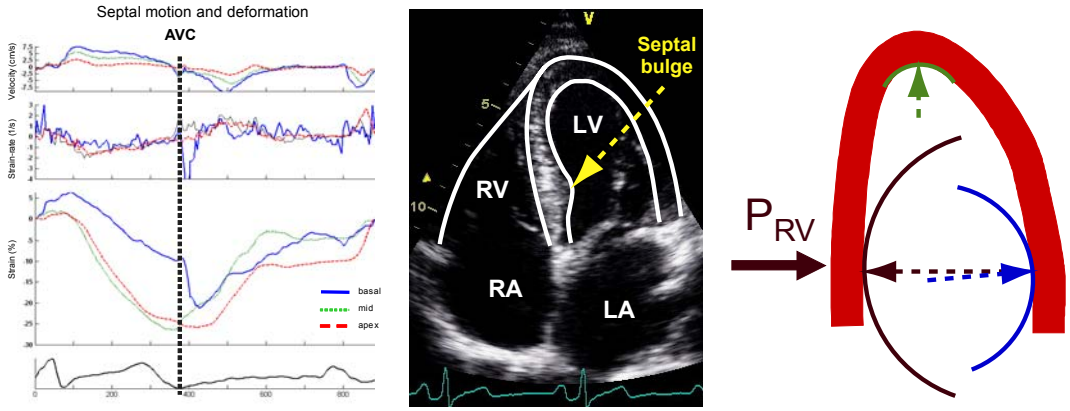

Figure 2.6: Hypertension results in ventricular remodelling, with the initial development of basal septal hypertrophy (septal bulge) due to increased wall stress associated with the bigger local radius of curvature. This is associated with reduced systolic deformation and the development of post-systolic deformation.

2.5.4. Genetic Cardiomyopathies

Hypertrophic cardiomyopathy is associated with the presence of regional abnormalities in myocardial fibre arrangement, resulting in local dysfunctional myocardium. Using regional deformation analysis, these areas of histological abnormalities can be easily localized since they do not show any systolic deformation, while the rest of the (hypertrophic) segments still deform (although mostly much reduced compared to normal).

In genetic diseases such as Friedreich's Ataxia, Fabry Disease or Duchenne Cardiomyopathy, regional deformation is first changing in the infero-lateral segment. As fibrosis develops first in this area, local strain-rates reduce and post-systolic deformation becomes apparent. This knowledge can be used to assess the efficacy of novel (very expensive) medical therapies [15].

2.5.5. Left Bundle Branch Block and Cardiac Resynchronization Therapy

The availability of cardiac resynchronization therapy (CRT) has drastically changed the management of heart failure patients with dilated cardiomyopathies and left bundle branch block. In these patients, it is assumed that the abnormal conduction leads to a late activation of the lateral wall, resulting in an important reduction in cardiac function. Although about 70% of these patients clearly benefit from biventricular pacing, there is still a lot of debate about the best method to assess those patients that will most benefit from the treatment [41, 42].

The current approach to select potential responders is to get a more direct evaluation of late contractility by (echocardiographically) searching for the presence of mechanical dyssynchrony and trying to identify a severely delayed wall with potentially recruitable function, rather than looking only for ECG manifestations of ventricular conduction delay which poorly correlate with the actual ventricular mechanical events. Many methods have been proposed to quantify dyssynchrony. These can be classified as evaluating either the Inter-ventricular delay (assessing the time difference between right and left ventricular contraction) or the Intra-ventricular delay (looking at timing of the motion/deformation of opposite ventricular walls).

To assess intra-ventricular delays, both M-mode (measuring the time difference between maximal septal and posterior excursion) and velocity/deformation based methods have been proposed.

Velocity and deformation based methods mostly assess the time differences between maximal values from different myocardial segments. However, most methods are based on longitudinal motion. Patients eligible for CRT mostly have dilated ventricles with complex motion (including *rocking*) and low velocities. Especially the additional presence of infarcted areas makes the interpretation of the (longitudinal) velocity traces very challenging. Because local myocardial motion reflects both contractile function and the influence of other myocardial segments (tethering), using local velocities to extract information on timing of contraction is almost impossible. Especially in dilated hearts, with poor LV function, local motion can be importantly influenced, even by right ventricular motion [43]. This makes that most imaging parameters have proven to be not ideal to assess potential response to CRT [44].

A more appropriate approach to assess these patients is searching for the underlying pathophysiological aethiology of their heart failure [1]. Besides problems with diastolic filling resulting from inappropriate atrio-ventricular delays, in a subgroup of patients there are typical and specific signs of LBBB and associated changes in cardiac mechanics.

'True' mechanical dyssynchrony originates from a delayed electrical activation of one of the myocardial walls. In a normal left ventricle, all segments are activated almost simultaneously and are thus deforming (longitudinal shortening and radial thickening) at the same time (Figure 2.7A). While the septum starts contracting, it contributes to pressure build up and ejection, but at the same time, it also pulls the lateral wall towards it. Similarly, the lateral wall will contribute to the pressure build up and ejection and will pull the septum towards it with an equal strength. The result is that both the septal and lateral annuli are dragged towards the apex, which remains stationary.

However, if there is a significant delay in the activation (and thus onset of contraction) of the lateral wall, the interaction between the walls changes significantly. When the septum is

activated, there is a period where it is actively developing a contractile force and shortening while the contralateral wall is not. This means that it exerts a pulling effect on the latent opposite wall which is not counterbalanced by contraction of the latter. Because it now contracts against a reduced load, it will move/shorten faster than it would in a normal ventricle (Figure 2.7B). Additionally, this will result in an early stretching of the, still relaxed, lateral wall. As soon as the lateral wall is electrically activated, it starts to contract and thus will start in its turn to influence the septum. The pulling force from the (later activated) contracting lateral wall will stretch the septum.

This sequence of motion and deformation in septal and lateral wall can be easily appreciated from the regional motion and deformation traces. Figure 2.7C shows the (radial) velocities of the septal and infero-lateral wall of a normal individual and a patient with LBBB. While normally, the septal and infero-lateral wall show similar, but mirrored velocity (both moving inward, thus with opposite directions with regard to the transducer), in LBBB the septum shows a very large inward velocity as soon as it is activated, almost immediately followed by a fast outward motion when the infero-lateral wall is starting to contract. This can also be appreciated from slowed-down grayscale images, where the septum rapidly moves in and outward, resulting in a 'septal flash' motion. This 'septal flash' is not only fast septal motion, but is a result of fast septal deformation (Fig 2.7D, E, F) where there is rapid thickening of the septum (while the lateral wall is stretched) followed by thinning when the lateral wall contracts and thickens.

The combination of the unloaded contraction of the septum stretching the lateral wall followed by the late lateral wall contraction stretching the septum will result in very inefficient global contraction, in which a lot of energy and force is wasted in deforming opposing myocardium without contributing to ejection. This will ultimately lead to symptomatic heart failure. Correcting the difference in local activation and deformation using CRT will result in a marked improvement in cardiac function and reverse geometrical remodelling in patients showing these specific mechanical signs of LBBB.

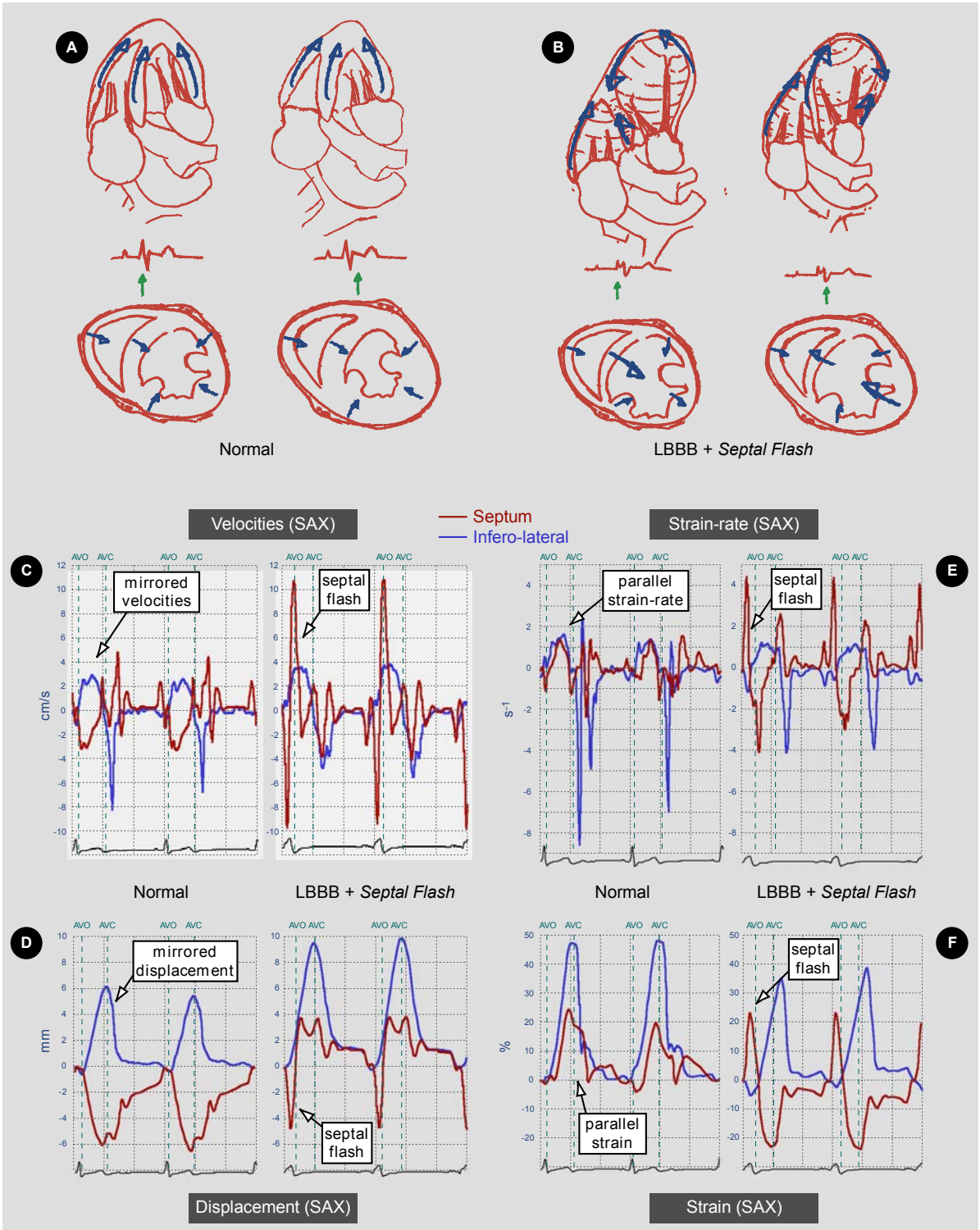

Figure 2.7: Myocardial velocities and deformation in patients with LBBB, compared to normal individuals.

2.5.6. Diastolic Function

Myocardial velocities have been suggested to be useful to assess diastolic function. Especially the ratio of early mitral flow velocities (E) and early basal myocardial velocities (E') was shown to correlate with relaxation abnormalities [45] and filling pressures [46].

However, in order to understand its use and recognize the pitfalls of this approach, it is important to keep in mind what these velocities represent. When assessing diastolic function, one wants to get an idea on how much (volume) filling is happening in the early relaxation phase (related to ventricular compliance and intrinsic myocyte relaxation) and at which pressures (elevated end-diastolic and atrial pressure) this is taking place. When quantifying mitral blood flow velocities, one assesses the pressure gradient, between the atrium and the ventricle, driving the flow (figure 2.8, left). This means that a high E can reflect as well (normal) low LV pressure with normal LA pressure, as well as elevated LA pressures (pseudo-normalization). When measuring basal myocardial velocities or ring motion, one assesses the dynamics of the basal LV displacement, which can be seen as a surrogate of global LV volume change (global LV deformation) (figure 2.8, right). Thus, E' provides information on how much volume is entering the LV in the early filling period. This makes that the ratio E/E' provides information on how much volume enters the ventricle for a given LA-LV pressure gradient. This means that in all situations where E' does not properly reflect global LV volume changes (large infarctions, LV dilatation, LBBB, primary mitral regurgitation, hypertrophy, etc.), the ratio E/E' is not reflecting diastolic function and should be used with caution [47, 48].

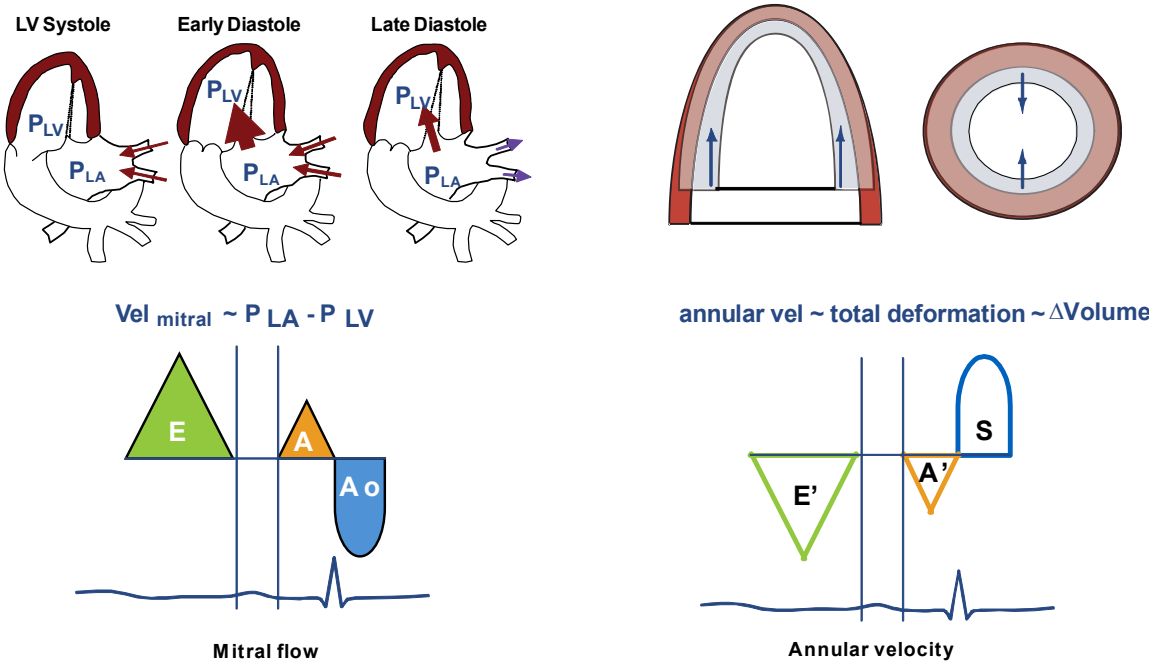

Figure 2.8: Myocardial velocities and deformation in patients with LBBB, compared to normal individuals.

2.6. Conclusion

Regional myocardial velocities and deformation prove to be a powerful tool to understand and quantify myocardial (dys-) function. Several cardiac conditions are associated with very specific changes in motion and deformation, which can be quantified using echocardiographic techniques. Analyzing myocardial deformation has provided important insights in cardiac mechanics and in the understanding of changes induced by a range of cardiac pathologies. Although none of the current techniques for ultrasound deformation assessment is perfect (DMI-strain has a steep learning curve and is very sensitive to the acquisition while speckle tracking strain works with low temporal resolution and important spatial and temporal smoothing), they still provide insight for the assessment of cardiac function in individual patients. Although the relation between local myocardial contractility and regional deformation is complex and dependent on loading and geometry, it was shown that the deformation assessment (potentially combined with dobutamine stimulation) provides useful additional information, especially for the clinical assessment of coronary artery disease and hypertrophic hearts.

Chapter 3

Analysis of Doppler Ultrasound Outflow Profiles for the Detection of Changes in Cardiac Function*

3.1. Introduction

The detection of changes in myocardial contractility in the setting of coronary artery disease is a very important medical task. Besides a decrease in global systolic function, as detected by ejection fraction, and changes in regional deformation [1], it was suggested, from isolated myocytes research, that chronic ischemia decreases but prolongs contraction [49].

Ultrasonic imaging is a non-invasive medical imaging modality, which is routinely used in hospitals for the examination of cardiac patients. Doppler ultrasound imaging provides useful information about blood velocities through the cardiac valves [50]. From these, clinical information on LV inflow (mitral valve) and outflow (aortic valve) are obtained, which may be important for diagnosis. In current practice, CW Doppler outflow traces are mainly used to assess a potential pressure gradient across the aortic valve resulting from a narrowing of the valve. It was also shown that severe aortic stenosis shows not only higher but often also prolonged outflow velocities [51].

From these observations, we hypothesize that the profile of the aortic outflow velocities might provide information on global myocardial function [52]. Outflow velocities represent the pressure gradient between LV and aorta and are thus influenced by either of them. A dynamically increasing resistance in the vessel tree, as could be expected in the presence of pathology, reduces late velocities while a prolonged development of contractile force by the myocardium should show as an increase in late velocities. Thus, we assume a relationship between the morphology and duration of aortic outflow velocities and myocardial function.

To study this relation and its usefulness to provide diagnostic clinical information, we propose a novel method for Doppler signal analysis. To test the hypothesis, various features of the envelope of the aortic outflow were extracted. To study the potential of these features to discriminate normal cardiac function from changes induced by coronary artery disease, ROC curves have been calculated and the area under the ROC curves was used to obtain a quantitative measure of feature performance.

---

* With permission from: Kalinic H, Loncaric S, Cikes M, Baltabaeva A, Parsai C, Separovic J, Cikes I, Sutherland GR and Bijnens B. Analysis of Doppler Ultrasound Outflow Profiles for the Detection of changes in Cardiac Function. In *International Symposium on Image and Signal Processing and Analysis (ISPA)*, 2007, 326-331.

3.2. Method for ultrasound signal analysis

The proposed method for analysis of Doppler ultrasound signals consists of several steps. In the first step, an image acquired from the ultrasound scanner is automatically converted into a 1-D aortic outflow velocity signal. In the second step, manual signal segmentation of the time interval of interest of the 1-D velocity signal is performed by an expert cardiologist. In the third step, signal modelling is done in order to eliminate noise. In the final step, signal feature extraction is performed to enable quantification of the signal to analyse and compare signals from normal individuals and patients with ongoing coronary artery disease. The block-diagram of the proposed method is shown in Figure 3.1. Details are described in Sections 3.3-3.5. Experimental results are presented in Section 3.6.

3.3. Signal extraction

Continuous wave Doppler traces of the aortic outflow were acquired with a clinical echo-cardiographic scanner (Vivid 7, GE Healthcare) using an apical 5-chamber view. Images were digitally stored in 'raw' Dicom format, containing the spectral Doppler information in proprietary tags. These 'raw' Dicom images were converted into *Hierarchical Data Format* (HDF) using an Echopac workstation (GE Healthcare).

The image (Figure 3.2), containing information about aortic flow, was extracted from the input HDF file. In the obtained image, the intensities represent the Doppler shift of the beam, or the velocities of the objects in the direction of the scan line. The signal extraction from the image is divided in automated and manual steps. In the automated step of the procedure, the envelope of the Doppler ultrasound signal is detected. In the manual step, the expert selected the relevant portion of the blood flow trace.

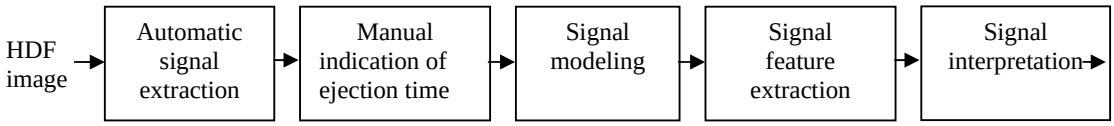

Figure 3.1: The block diagram of the proposed method for signal extraction

3.3.1. Automated extraction

The CW Doppler signal (Figure 3.2.) represents the time-change of velocities along a scan line in the 2-D ultrasound imaging plane. In this study, we are interested in the velocities in the narrowest part of the outflow (the atrium-ventricular connection). Thus, the relevant information is the instantaneous maximal velocity (i.e. the envelope) of the CW Doppler traces. Since the upper part of the Doppler signal (Figure 3.2.) represents negative velocities

and contains no relevant information for this study, the first problem was to detect the zero-level of the signal, and eliminate the irrelevant part. To detect the zero-level, the image was projected onto the y-axis. On the projection (Figure 3.3, left) the zero-level is recognized as the minimum between two peaks. To detect that minimum correctly, we performed a cross-correlation of the projection with a negative sine. The sine's width is defined by the number of dark pixels on the upper part of the image where the zero-level is expected. Figure 3.3, right, shows the result of the cross-correlation.

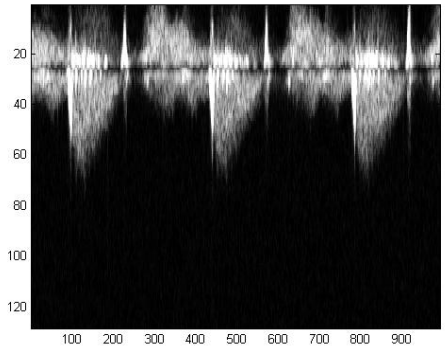

Figure 3.2: Image extracted out of HDF

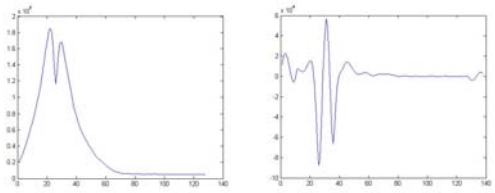

Figure 3.3: Results of y-axis projection and crosscorrelation

After the negative part of the signal is discarded, the procedure focuses on envelope detection. Figure 3.4. shows the Doppler trace together with the extracted envelope (left) and the resulting signal, corresponding to the instantaneous maximal velocity (right).

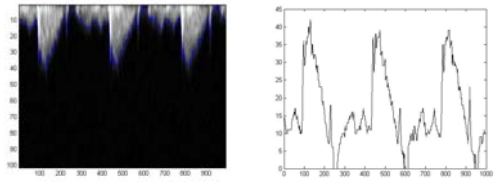

Figure 3.4.: Doppler trace and its envelope

3.3.2. Manual control and timing of the cycle

In the following step of the procedure, a cardiologist reviewed the result of the automated signal extraction and discarded the signals that could not be analysed due to excessive noise

or incorrect signal extraction. For the accepted cases, the region of interest (i.e. the ejection time) of the signal was manually defined by the cardiologist by indicating aortic valve opening and closure. To ease this work, an application was created that helped cardiologist to select the acceptable images and to mark aortic valve opening and closure. The graphical user interface of this application is shown in Figure 3.5, where two regions of interest are indicated by vertical lines. Figure 3.6. shows the resulting signal.

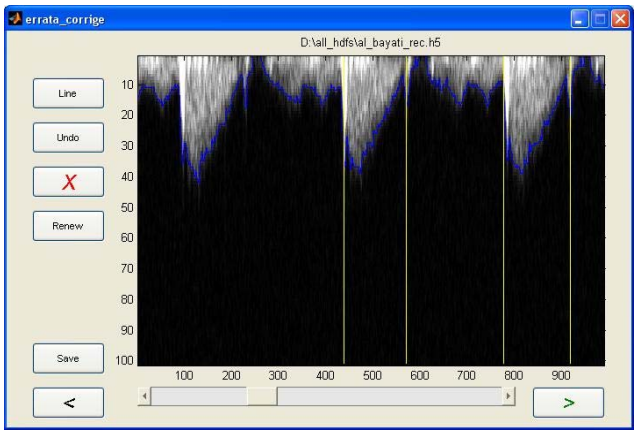

Figure 3.5: GUI of the application used for the manual control and timing of the cycle

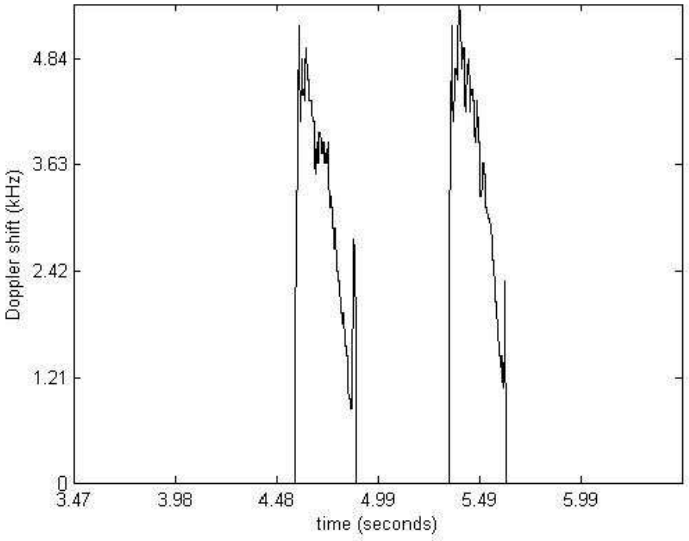

Figure 3.6: Region of interest

3.4. Signal modelling (interpolation)

The signal obtained in the previous step is usually very noisy and regularly contains artefacts, mainly corresponding to the 'valve clicks' (the broadband Doppler signal generated by the opening and closure of the aortic valve). These artefacts should be removed as they could interfere with the feature extraction in the next processing step. Since the noise on the signal is non-physiologically (the hart cannot produce high frequencies), it should be removed. We investigated two different approaches for eliminating signal noise. In the first approach, the noisy signal is filtered in the Fourier domain to remove the high frequencies that the human hart cannot produce. In the second approach, a polynomial approximation of the original noisy signal was used to obtain a smooth representation. In the assumption that the velocity is proportional to the remaining volume and the cardiac length is decreasing linearly, velocities would change with a third power. Following this idea we approximated the signal with two piecewise cubic polynomials.

Using both approaches, the noise was eliminated and the glitches at the beginning and the end of the signal were smoothed.

3.5. Signal feature extraction

From the signals, 14 features describing their shape were extracted, namely, peak value, time to peak, rise time, fall time, signal width at 10%, 50% and 90% of the peak, first harmonic, second harmonic, even harmonics, odd harmonics, an asymmetry factor, area under the curve and signal length. Rise and fall times are defined from 10% to 90% of the peak as illustrated in Figure 3.7. The asymmetry measure was defined as the difference between the areas of the right and left half (in the temporal dimension) of the signal. Out of these basic 14 features we derived 17 additional features by normalisation or combing two basic features.

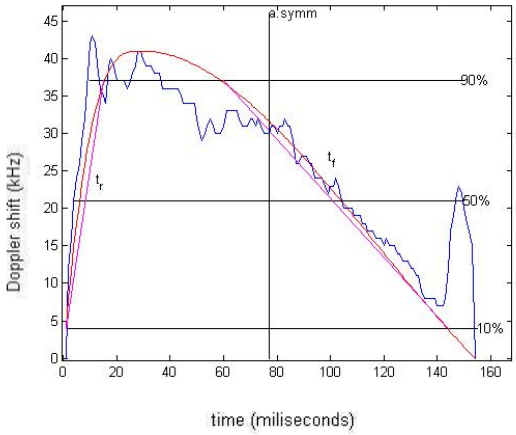

Figure 3.7: Signal rise and fall time

The feature set was selected based on the problem domain and the physical meaning of each attribute. The hypothesis is that some of these features are relevant for detecting changes in cardiac function so that their distributions could differ for normal individuals and abnormal patients. To detect the most useful features for diagnosis, we have calculated their ROC curves. The area under the ROC curve was used as a measure for the diagnostic potential of each feature.

3.6. Experimental results

In this study, we included 88 patients scheduled for a routine dobutamine stress echo study. Of these, 38/88 had signs of ongoing coronary artery disease at baseline, 40/88 showed normal cardiac function at baseline but had a positive response to the stress test and 10/88 showed no signs of ongoing coronary artery disease (normal contraction both at baseline and during the stress test). Additionally, 24 normal volunteers, with no evidence of coronary artery disease on clinical and echocardiographic examination, were included. For all these individuals, the CW Doppler traces of the aortic flow (at baseline) were acquired and analysed.

3.6.1. Signal extraction

For signal extraction we used the method described in Section 3. The Doppler images were first filtered using a Gaussian for noise reduction. Since blurring the image too much could cause loss of information, we choose to use a 3x3 Gaussian filter with $\sigma = 0.5$. After this, the zero-level was determined by cross-correlation, as described in Section 3.2. Since the negative part of a sine wave (which is real and symmetric) was used for this, convolution could be used instead of cross-correlation. After zero-level detection the irrelevant part was discarded and the image was smoothed once again. In the next step, a segmentation threshold was chosen defined by the mean value of the image increased by a parameter *p*. The value of *p* was experimentally determined, and, in our case, $p=20$ was chosen. In the resulting binary image, the edge was detected as the top-most pixel in the image with an intensity that corresponds to the signal. The procedure is shown in three steps in Figure 3.8.

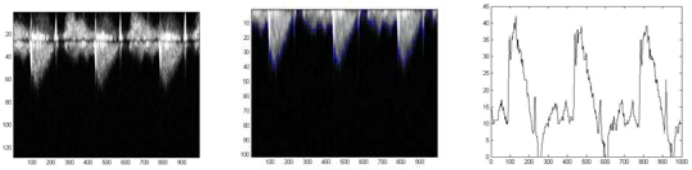

Image No-zero image Envelope

Figure 3.7: Three steps of automatic signal extraction

The signal quality was checked and the region of interest was indicated by a cardiologist, as described in Section 3.3 (Figure 3.5).

3.6.2. Signal modelling

Two approaches to signal conditioning were implemented. In the first approach, conventional filtering in the Fourier domain was used. Before the Fourier transform was calculated, the signal was anti-symmetrically extended (Figure 3.9). In this way, the harmonics of the Fourier transform corresponded to the harmonics of the extended signal. The signal conditioning was performed by filtering out all harmonics except the first ten. The filtered signal, overlaying its original, is shown in Figure 3.9.

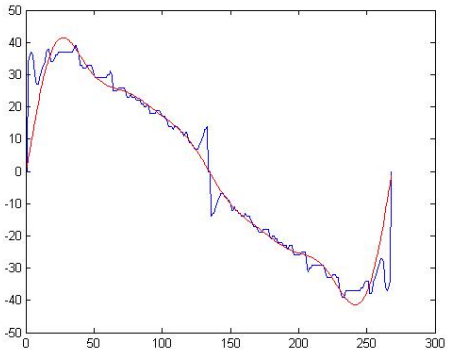

Figure 3.8: The asymmetrically extended original signal and overlaying filtered signal

In the second approach, a piecewise cubic polynomial approximation was used. Four fixed points were chosen for polynomial signal approximation: beginning, end, maximum and half way between the maximum and the end of the signal. These points were picked as fixed points for signal approximation (Equations (1) – (5)). With these points, the signal was divided in two portions joining at the signal maximum. The first portion was approximated with a cubic polynomial (Equation (9)) and the second portion with another cubic polynomial (Equation (10)). To achieve a smooth approximation, the first derivatives of both cubic polynomials at the maximum of the signal are forced to zero (Equations (6), (7)) and their second derivatives to be equal in that point (Equation 8). In this way we obtained a system of eight linear equations with eight unknowns. An example of a signal created using this approximation is shown in Figure 3.10, overlaying the original signal.

The system has been solved as shown below. The equations used in the cubic approximations were:

$f_1(0) = 0$ (1) $f_1(x_1) = y_1$ (2) $f_2(x_1) = y_1$ (3)

$f_2(x_2) = y_2$ (4) $f_2(x_3) = 0$ (5) $f_1'(x_1) = 0$ (6)

$f_2'(x_1) = 0$ (7) $f_1''(x_1) = f_2''(x_1)$ (8)

where f_1 and f_2 are:

$$f_1(x) = a_1 \cdot x^3 + b_1 \cdot x^2 + c_1 \cdot x + d_1 \quad (9) \qquad f_2(x) = a_2 \cdot x^3 + b_2 \cdot x^2 + c_2 \cdot x + d_2 \quad (10)$$

which, after a rewrite in matrix form leads to:

$$X*A=Y, \quad (11)$$

where A is an unknown column vector, X an 8x8 matrix, and Y the vector containing the values of the function and its derivatives.

$$A = X^{-1}*Y \quad (12)$$

The parameters of the cubic equations were calculated as shown in (Equation 12). The original signal and its approximation are shown in Figure 3.10.

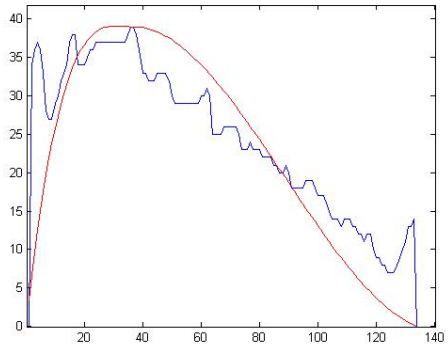

Figure 3.9: The original signal and its piecewise cubic approximation.

3.6.3. Signal interpretation

The smoothed signal approximation, obtained in the previous step, was used for feature extraction. The feature extraction procedure was applied to three different versions of the signal: i) the original signal, ii) the first ten harmonics of the Fourier transform, and iii) the piecewise cubic approximation of the signal. The features that were extracted are listed in

Table 3.1. An ROC analysis was performed for each feature to describe its performance to detect patients with signs of ongoing coronary artery disease (baseline abnormalities or a positive response to dobutamine stress). Table 3.1. lists the corresponding areas under the ROC curves for the features extracted from three different signal versions.

When studying the features, one can notice a significant difference between their distributions for normal individuals and patients. Figure 3.11. shows the histogram for the fall time, showing the difference between the mean values for normals and patients. This difference is quantified by the ROC curve of this feature. Picking a threshold and shifting it through the different values of the given feature results in different numbers of true positives and false positives. Sliding this threshold over the range of values, results in the ROC curve. The difference of change (derivate) between true positives and false positives describes how different the histograms of normals and patients are (at the given threshold). This can be quantified in the value of the area under ROC curve. The greater the area under ROC curve, the greater the capability for detecting more true positives with less true negatives, therefore the distance between the mean values of normals and patients is greater. This property was used as a measure of how much information about disease is present in each feature, or, in other words, how different normals and patients are with respect to this feature. The example of the ROC curve for the fall time is given in Figure 3.11. (right).

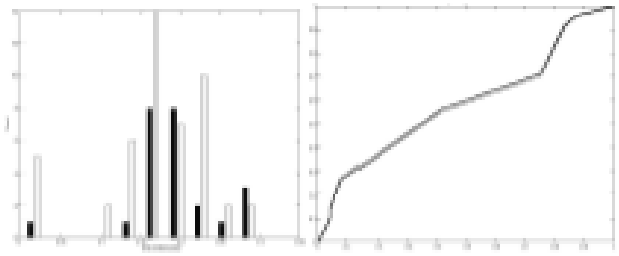

Figure 3.10: Histogram and ROC curve for fall time extracted out of original signal

Feature	Original signal	Fourier filtered	Cubic approximated
max	0,63108	0,66059	0,63021
tmax	0,57509	0,50391	0,53819
T_rise	0,6059	0,50521	0,53082
w10	0,57813	0,52604	0,53299
w50	0,53212	0,50347	0,5026
w90	0,5803	0,59983	0,50217
T_fall	0,59071	0,55859	0,55252
h1	0,61979	0,61979	0,64714
h2	0,59071	0,59071	0,625
hodd	0,61502	0,57726	0,53385
heven	0,51866	0,5612	0,55425
asymm	0,60981	0,58594	0,61589
A	0,63585	0,6428	0,65234
T	0,55295	0,55295	0,55295
max/T	0,64366	0,65451	0,64583
tmax/T	0,61979	0,52517	0,54253
Tmax/max	0,50087	0,58811	0,61979
t_rise/T	0,60286	0,50477	0,55469
T_rise/max	0,53776	0,55859	0,61979
W10/T	0,52734	0,58464	0,60851
W10/max	0,58854	0,61892	0,63064
W50/T	0,51042	0,56163	0,57986
W50/max	0,65061	0,60807	0,58984
W90/T	0,57856	0,61285	0,6033
W90/max	0,6046	0,55599	0,64366
T_fall/T	0,59071	0,60113	0,5842
T_fall/max	0,51953	0,51866	0,51215
h1/h2	0,5803	0,5803	0,54905
hodd/heven	0,59939	0,50825	0,52691
asymm/A	0,5803	0,55642	0,57161
A/max	0,53385	0,53168	0,51519

Table 3.1: Areas under ROC curves for extracted features

From Table 3.1. and the areas under the ROC curves, we can conclude that features describing the signal's symmetry or morphology contain information about disease. This includes features such as t_fall, t_max/T, asymm, t_fall/T, t_rise/T. Thus, this approach could be used to classify aortic flow patterns in being normal or abnormal, based on one individual feature or a combination of features, using a higher dimensional approach.

Figure 3.12. shows the scatter plot of 2 features related to the signal's morphology (fall time and asymmetry). It can be observed that the normal individuals cluster in the top right corner while in the group of patients with signs of ongoing coronary artery disease, there is a clear subgroup with a different aortic flow profile (more symmetric and overall broader). In figure 3.13, the patients scheduled for a stress test, but with a normal response to it, are plotted, together with an indication of the normal range that could be expected for this feature (mean ± 2 SD). It is clear that within these patients with apparently normal cardiac function, there is a subgroup which shows clearly altered aortic flow profiles, suggesting the presence of sub-clinical changes.

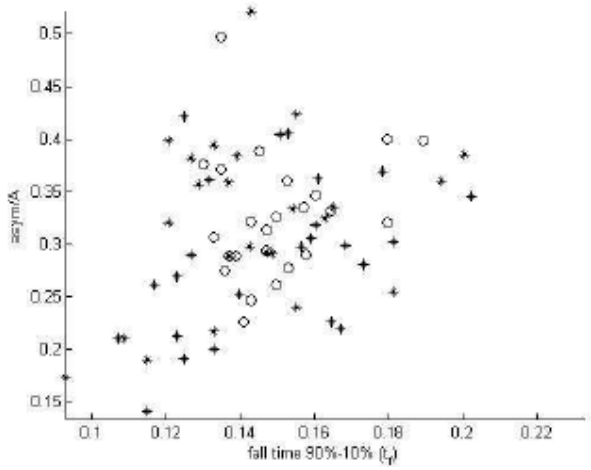

Figure 3.11: Patients (star) and normals (circle) distribution in fall time – asymmetry feature space

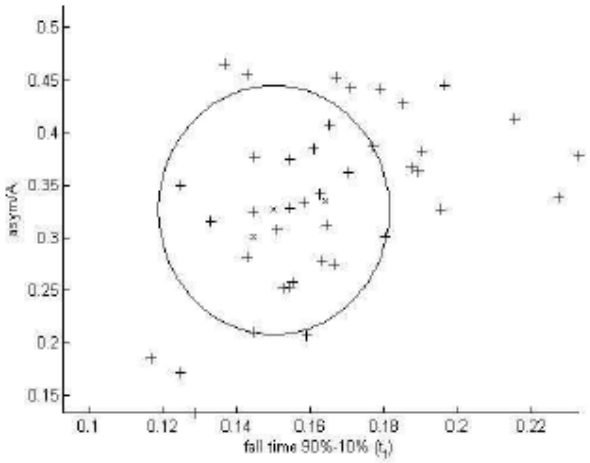

Figure 3.12: Distribution of patients with a normal response to stress

3.7. Conclusion

In this paper we presented a novel method for the analysis of aortic outflow velocity signals obtained from echocardiographic CW Doppler imaging. The extracted velocity profiles were modelled using two different approaches. Feature extraction was done on the original signal as well as on the two modelled versions. For each feature, the area under the ROC curve has been calculated to describe its ability to discriminate normal individuals from patients with signs of ongoing coronary artery disease. Thirty one different features were investigated.

The experimental results showed that all three signal representations yielded approximately the same quality of discrimination and the results provided a better insight regarding the choice of the best feature.

The signal analysis has shown that the probabilistic distributions of the various features are different for normals and patients. This shows its potential for diagnostic use in the presence of coronary artery disease

The features discriminating the best between normals and patients were related to the signal morphology with a wider signal in patients. This suggests that the broadening of the aortic valve profile contains information on changes in cardiac function in the presence of coronary artery disease and thus might be used as an additional diagnostic tool in clinical practice.

Chapter 4

The Shape of the Aortic Outflow Velocity Profile Revisited. Is there a Relation Between its Asymmetry and Ventricular Function in Coronary Artery Disease?*

4.1. Introduction

Blood pool Doppler echocardiography provides a method to measure blood velocities within the ventricles and blood vessels [51]. By measuring velocities through the cardiac valves, the amount of flow (cardiac output, filling) and the driving pressure gradient, causing the flow, can be quantified [51, 53-60], which can be clinically used to assess hemodynamic parameters and ventricular function [51, 53-57].

The profile of the aortic flow velocity curves can be described by the rate of increase (acceleration) in velocity, the peak and the time of peak velocity, the mean velocity during systole and the ejection duration [51]. Normal outflow shows an asymmetric, triangular shaped profile with a fast rise in velocities, peaking around 1/3 of the ejection duration [51]. Animal studies have shown that the flow acceleration is a sensitive indicator of the inotropic state [61], which was confirmed by clinical research [56, 62]. In LV failure, both a lower and a slower increase in velocities (a more rounded Doppler profile with a later peak velocity) was observed [51]. Similar changes can be present in normal function but decreased filling (i.e. severe mitral stenosis, atrial septal defect, pulmonary hypertension) [51]. Changes in aortic velocity curves have been reported in other conditions such as hypertrophic cardiomyopathy [63], mitral regurgitation [64] and shock [65]. Furthermore, flow remodelling is regularly seen in aortic stenosis where, besides an increasing gradient, the profile changes from a triangular shape with an early peak, to a much more rounded form with a later peak in higher grade stenoses [51, 59].

Additionally, it is known that active force development in the myocytes peaks around 1/3 of the ejection, after which it decreases rapidly [32]. This implies that the early flow acceleration is caused by the active contraction, while flow decelerates when force development declines. This explains why flow acceleration increases with increased contractility. Additionally, research on isolated myocytes suggested that chronic ischaemia decreases, but prolongs contraction [49].

---

* With permission from: Cikes M, Kalinic H, Baltabaeva A, Loncaric S, Parsai C, Milicic D, Cikes I, Sutherland GR, Bijnens B. The shape of the aortic outflow velocity profile revisited. Is there a relation between its asymmetry and ventricular function in coronary artery disease? Eur J Echocardiogr. 2009;10(7):847-57.

From this, we hypothesize that in the presence of coronary artery disease, in a subset of patients, the overall decrease in contractility caused by regional ischaemia and a slower contraction of chronic ischaemic myocytes, might be reflected in the aortic outflow profile, particularly in the timing and shape of the LV outflow curve and that these changes are related to the severity of contractile dysfunction. In order to study this relation and its usefulness in providing diagnostic clinical information, we propose a novel method for Doppler signal analysis where various properties of the envelope of the aortic outflow are quantified.

4.2. Materials and Methods

4.2.1. Patients

From a retrospective series of 109 patients which were referred for a routine dobutamine stress echo (DSE) at St. George's hospital (London, UK), 79 (37 male, 42 female, mean age 62.7±9.4 years) had sufficient visualization of all myocardial walls and interpretable continuous Doppler (CW) LV outflow traces and did not have increased outflow velocities at rest (baseline) due to either aortic stenosis or the presence of an intra-cavity gradient. Furthermore, none of these patients had significant valve disease or left bundle branch block. In patients prescribed with beta blocker therapy, it was discontinued three days prior to the study.

Based on the resting wall motion and the response to the dobutamine challenge, the patients were divided in 2 subgroups.

The **DSE negative group (DSE_{neg})** consisted of 35 patients without resting wall motion abnormalities and a (quantitative) DSE study without signs of inducible ischaemia (9 male, 26 female, 60.3±8.4 years).

The **DSE positive group (DSE_{pos})** consisted of 44 patients with a DSE study showing signs of ischaemic heart disease, either at baseline or during any of the stress levels (28 male, 16 female, 64.7±9.7 years).

Additionally, 32 healthy volunteers with no signs or symptoms of cardiovascular disease or arterial hypertension were studied at baseline (not undergoing an DSE study) and served as a **control group** (15 male, 17 female, 59.1±11.5 years). The investigation conforms with the principles outlined in the Declaration of Helsinki.

4.2.2. Echocardiographic Imaging

Standard cardiac ultrasound data (including Doppler myocardial imaging (DMI)) at baseline (healthy volunteers and patients) and during the DSE (patients) were acquired with a Vivid Seven ultrasound scanner equipped with a 2.5-MHz transducer (GE, Horten, Norway). Data

were obtained from the parasternal and apical views. For the 2D studies, parasternal long and short axis as well as apical two-, three-, four- and five-chamber views were used. Aortic outflow CW Doppler traces were acquired from the apical five-chamber view. The echocardiographic data were obtained for three complete cardiac cycles during a single end-expiratory breath hold.

For the DSE study, dobutamine was infused at rates of 5, 10, 15, 20, 30 and 40 mcg/kg/min and increased with 3 min steps until reaching 85% of age-predicted heart rate (HR) (target HR). The study was interrupted earlier in the presence of induced ischaemia, occurrence of severe symptoms, raised blood pressure (BP) or upon reaching target HR. Echocardiographic data, together with BP and a 12-lead ECG, were acquired at low (5 mcg/kg/min), intermediate (20 mcg/kg/min), peak dose (40 mcg/kg/min) and recovery. DMI data were simultaneously acquired for post-processing. At each stage, CW Doppler traces of aortic flow were additionally acquired.

The presence of echocardiographic signs of ongoing ischaemic heart disease was evaluated by two experienced cardiologists, both by assessment of regional wall motion abnormalities [66], as well as by analysis of the underlying DMI data [1].

Offline analysis was performed using dedicated software (Echopac, GE, Horten, Norway). Ejection fraction (EF) was measured by the Simpson biplane method [66]. LV size and mass (LVM) were measured [66, 67]; relative wall thickness (RWT) (the sum of posterior and septal wall thickness divided by the internal diameter) was calculated as an index of LV concentric remodelling [68]. 2D measurements of the basal interventricular septum as well as the basal lateral wall were obtained as an additional measure of LV hypertrophy in hypertensive heart disease [9].

4.2.3. Doppler Outflow Analysis

The baseline CW outflow Doppler traces were analyzed for the purpose of this study, both manually and semi-automatically. For the manual analysis, the time from onset of aortic flow to peak flow (T_{man}), as well as the ejection time (ET_{man}) and HR were measured. The ratio T_{man}/ET_{man} (indicating the position of the peak within the ejection period), as well as the ratio ET_{man}/HR (indicating the duration of ejection within the heart cycle), were calculated. The manual analysis was blinded to the DSE results as well as to the automatic analysis.

The automated quantification of the CW outflow Doppler traces was previously described [22]. Doppler traces were not calculated, but rather extracted from the ultrasound image. This was done using an image segmentation method. In the first step, the image is converted and pre-processed to obtain only the forward velocities. On these images, the velocity envelope is detected automatically using thresholding. Next, the onset and the end of the aortic flow were manually indicated, thus isolating the outflow profile. Since the Doppler trace has to be

continuous and smooth the constraint was implemented forcing the trace to be piecewise polynomial. This was done using two cubic polynomial (i.e functions of the form $f(x) = ax^3 + bx^2 + c + d$) with demands for the first derivatives to be zero at the beginning and end of the signal, as well as in the adjacent points where also the second derivative was forced to be equal for both of the adjacent polynomials to satisfy the smoothness criteria (Figure 4.1, right). From the modelled signals, several parameters describing their shape were extracted. Time to peak (T_{mod}), ejection time (ET_{mod}), rise time (t_{rise}) and fall time (t_{fall}) were quantified. Rise and fall times were defined from 10% to 90% of the peak (Figure 4.1, bottom). The ratio T_{mod}/ET_{mod} as well as the ratio ET_{mod}/HR were calculated. Additionally, an asymmetry index (asymm) was calculated as the difference of the area under the curve of left and right half of the spectrum normalized by the overall area. A value for asymm lower than 0.25 was considered an indicator of an abnormally symmetrical trace.

Additionally, the development of an intra-ventricular gradient during DSE was defined as a late-peaking LV Doppler velocity profile that exceeded the basal maximum velocity by at least 1 m/sec [70].

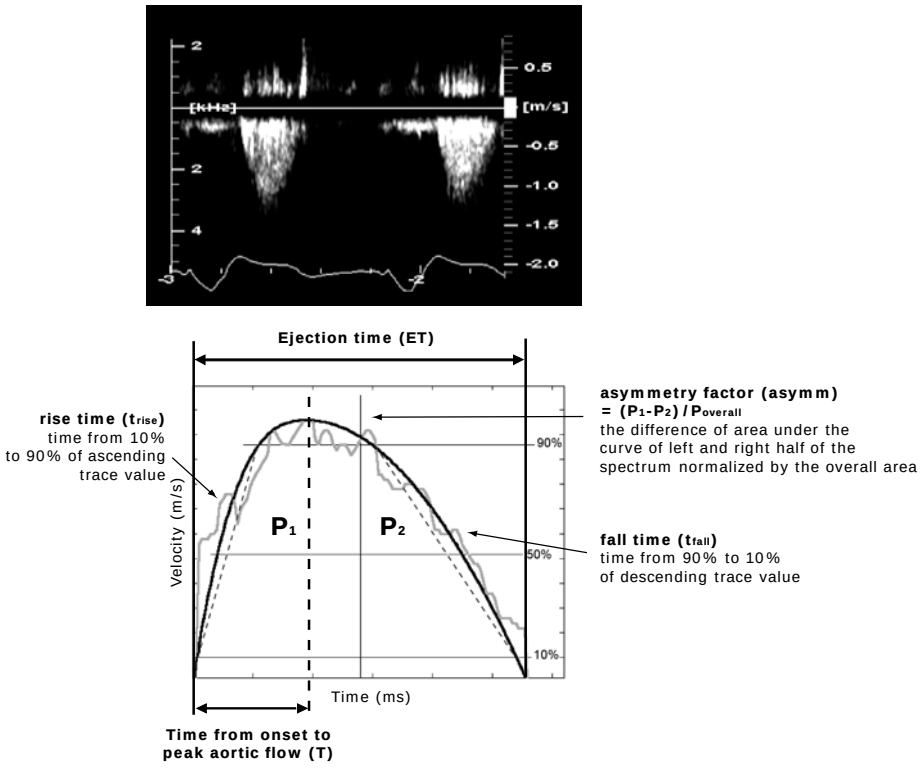

Figure 4.1. Raw aortic outflow CW Doppler trace (top). The piecewise cubic model fitted on the original trace and the properties extracted from it (bottom).

4.2.4. Statistical Analysis

Continuous variables' data are expressed as mean value ± SD and the unpaired two-tailed Student t-test was performed for comparative analysis. Categorical variables are expressed

as a percentage. For categorical variables, comparisons between groups were made using the chi-square test. Results were considered significant at $P<0.05$. A linear correlation was used to test the similarity between the manual and automated analysis.

4.3. Results

4.3.1. Patient Group Characteristics and Basic Echocardiography Data

The basic patient characteristics as well as coronary artery disease severity are provided in table 1. The values of both systolic and diastolic BP were significantly lower in controls while the values of systolic BP exceeded normal values in 66% of patients in DSE_{neg} and 71% of patients in DSE_{pos}. The heart rate was significantly higher in DSE_{pos}, compared to controls.

In 15/35 DSE_{neg} patients, a coronary angiogram was performed (which was diagnostically inconclusive, or performed due to recurrent chest pain symptoms after previous treatment). Five of the DSE_{neg} patients had undergone successful coronary revascularization (one by coronary artery bypass grafting - CABG), five had a (remaining) insignificant stenosis. Although they had normal rest and stress studies, in six patients, a significant stenosis was present at the time of the DSE study (single vessel disease in 1, double in 2, triple in 2 and multivessel in 1 patient).

In DSE_{pos}, significant, non revascularized, coronary artery stenoses were present in 16/44 patients (6 single vessel disease, 5 double vessel disease, while triple and multivessel disease were present in 3 and 2 patients, respectively). Overall, 27/44 patients had previous coronary revascularization (14/27 CABG), of these, 9 had a stenosis at time of investigation (2 in-stent restenoses and 2 bypass stenoses). 5/44 had an insignificant coronary artery stenosis and no angiography data were available for the remaining 5/44 patients.

The basic echocardiographic measurements are given in table 2. LV mass (ASE formula), was significantly higher in DSE_{pos} compared to DSE_{neg} and controls ($p=0.01$ and $p<0.00001$, respectively) mostly due to larger LV cavity measures. The size of the LV cavity was significantly smaller in DSE_{neg}, both in end systole as well as in end diastole. RWT, an indicator of concentric hypertrophy, was significantly larger in DSE_{neg}. Patients in DSE_{neg} and DSE_{pos} had a notable basal septal thickening/bulge, measuring in average 1.3±0.3 cm, while it was significantly smaller in the controls. Furthermore, EF was significantly higher in DSE_{neg} compared to the other two groups ($p<0.000001$ vs. controls and DSE_{pos}). Ejection fraction was preserved in all healthy volunteers and patients in DSE_{neg}, while it was reduced in 39% of the DSE_{pos} patients.

Notably, an LV dynamic intracavitary gradient was induced by DSE in 71.4% of DSE_{neg} patients and 18.2% of DSE_{pos}. In patients developing an intracavitary gradient, RWT ($p<0.004$ vs. no gradient, $p<0.000001$ vs. controls) and EF ($p<0.0001$ vs. controls,

p<0.00001 vs. no gradient) were significantly larger than in patients who did not develop an intracavitary gradient during DSE, or controls.

	control group (n=31)	DSE_{neg} (n=35)	DSE_{pos} (n=44)
Age (years)	59.0±11.5	60.3±8.4	64.7±9.7*
male/female	15/17	9/26	28/16
SBP rest (mmHg)	119.7±13.2	154.1±22.3†	146.3±16.7†
DBP rest (mmHg)	73.3±6.8	82.2±10.9‡	79.6±11.0§
HR rest (/min)	62.9±10.8	67.5±11.2	70.9±10.7§
CABG (pts)	-	1	14
PCI (pts)	-	4	15
Insignificant stenosis (pts)	-	5	5
single vessel (pts)	-	1	6
double vessel (pts)	-	2	5
triple vessel (pts)	-	2	3
multi vessel (pts)		1	2

Table 4.1. Basic patient characteristics

** $P<0.05$ vs. DSE_{neg}; †$P<0.0001$ vs. control, ‡ $P<0.001$ vs. control, § $P<0.05$ vs. control.*

	control group (n=31)	DSE_{neg} (n=35)	DSE_{pos} (n=44)
LVIDd (cm)	4.9±0.5	4.5±0.5*	5.3±0.9†‡
LVIDs (cm)	3.0±0.5	2.7±0.6§	3.5±0.9§‡
IVSd (cm)	0.9±0.2	1.1±0.2†	1.1±0.3†
LVPWd (cm)	0.8±0.2	1.0±0.3†	0.9±0.2†
IVS bulge (cm)	1.1±0.2	1.3±0.3†	1.2±0.3§
lateral wall (cm)	0.9±0.1	1.0±0.2§	0.9±0.2
RWT	0.35±0.06	0.47±0.08*	0.38±0.10‡
EF (%)	65.4±5.6	75.6±7.9*	57.5±13.9†‡
LV mass (g)	167.1±53.3	177.8±58.3	241.8±89.5*‖
LV mass ASE (g)	145.2±42.7	158.1±46.3	204.4±72,1*‖
inducible gradient (pts)	-	25	8

Table 4.2. Echocardiographic measurements

P<0.0001 vs. control, † P<0.005 vs. control, ‡P<0.0001 vs. DSE_{neg}, § P<0.05 vs. control, ‖P<0.001 vs. DSE_{neg}

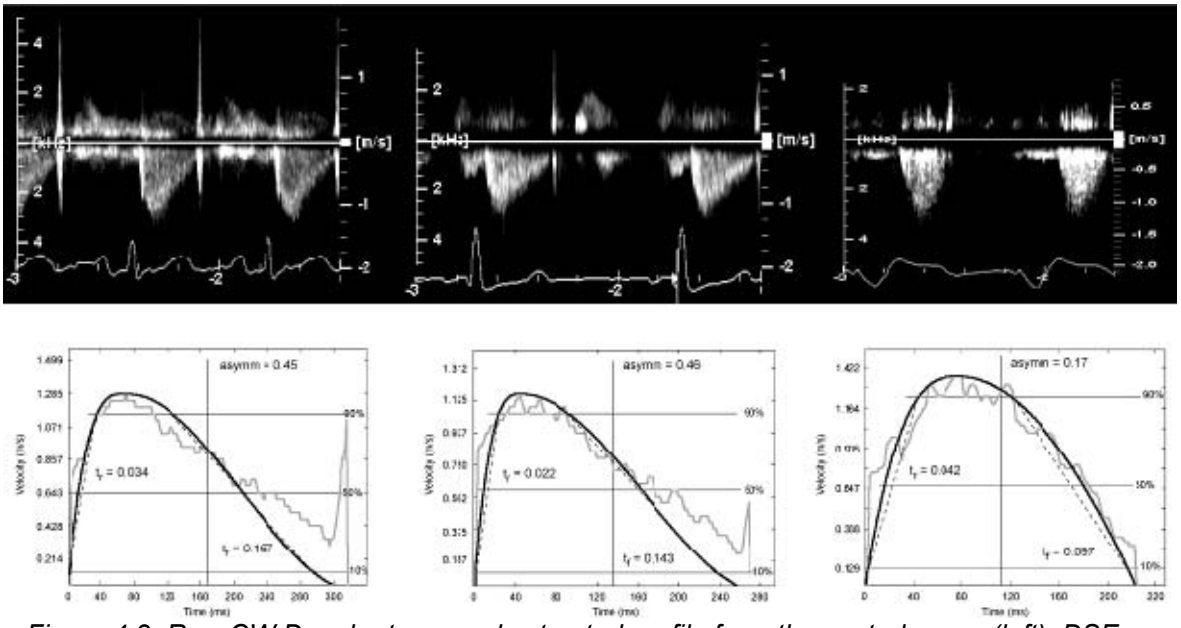

Figure 4.2. Raw CW Doppler trace and extracted profile from the control group (left), DSE negative group (middle) and DSE positive group (right).

	control group (n=31)	DSEneg (n=35)	DSEpos (n=44)
asymm	0.33±0.06	0.35±0.07	0.30±0.08*
asymm < 0.25 (%)	0.0	2.9	27.3
ET_{mod}	293.4±59.3	329.4±33.6†	305.3±37.7*
ET_{man}	296.0±19.4	324.8±40.5†	304.8±33.5‡
ET_{mod}/HR	4.55±1.30	5.12±1.11	4.62±1.22
ET_{man}/HR	4.59±0.90	5.06±1.27	4.60±1.16
T_{mod}	65.66±13.50	65.16±13.81	74.50±18.93 §‡
T_{man}	55.33±10.42	64.49±16.03§	68.73±15.97‖
T_{mod}/ET_{mod}	0.215±0.036	0.199±0.046§	0.244±0.055§*
T_{man}/ET_{man}	0.187±0.036	0.201±0.055	0.228±0.057†‡
T_{rise}	0.032±0.008	0.032±0.008	0.037±0.010§‡
T_{fall}	0.153±0.013	0.168±0.025†	0.146±0.026*

Table 4.3. Properties extracted from aortic Doppler traces

** P<0.005 vs. DSE_{neg}, † P<0.005 vs. control, ‡ P<0.05 vs. DSE_{neg}, § P<0.05 vs. control, ‖ P<0.0001 vs. control.*

4.3.2. Doppler Outflow Analysis

Figure 3.2 shows typical examples (both the raw Doppler trace and the extracted profile) from the 3 subgroups. The properties extracted from the aortic flow are shown in table 4.3.

Ejection time corrected by heart rate (ET_{man} or ET_{mod}) was not different among the three groups. The absolute time to peak (T_{mod}) was significantly higher in DSE_{pos}, followed by DSE_{neg} and the controls.

The relative time to peak T_{mod}/ET_{mod} was the longest in DSE_{pos}; notably, it was found to be shorter in DSE_{neg} compared to controls.

Rise time t_{rise} was longest in DSE_{pos} compared to DSE_{neg} ($p=0.01$) and controls ($p=0.02$). Fall time t_{fall} was shortest in DSE_{pos}, though it was the longest in DSE_{neg} ($p<0.005$ vs. controls and DSE_{pos}). Furthermore, t_{fall} was notably prolonged in the patients who developed an intracavitary gradient during DSE (0.17±0.03), compared to the ones without an inducible gradient (0.15±0.03, $p<0.01$) and controls (0.15±0.01, $p<0.03$).

Asymm was the lowest in DSE_{pos}, followed by controls and DSE_{neg} (Table 4.3). An abnormally symmetric profile (asymm<0.25) was found in 1/35 (2.9%) of the DSE_{neg} patients and in 12/44 (27.3%) of the DSE_{pos} patients, while in none of the controls.

The relations between the EF and asymm, T_{mod}/ET_{mod}, t_{rise} and t_{fall}, as well as LVIDd vs. asymm, T_{mod}/ET_{mod}, t_{rise} are shown in figure 4.4 and figure 4.5, respectively. No significant correlation was found between t_{rise} and t_{fall} (r=0.19). Moreover, neither asymm, nor t_{rise} or t_{fall} seemed to be influenced by systolic blood pressure (r=0.08).

The difference in values of asymm, T_{mod}/ET_{mod}, t_{rise} and t_{fall} among the three patient groups are shown in figure 6.

In the patients who developed an intracavitary gradient during DSE, t_{fall} was significantly prolonged while T_{mod}/ET_{mod} was significantly shorter compared to the group of patients without an inducible intracavitary gradient by DSE (figure 4.7).

In the subgroup of patients who underwent coronary angiography, the sensitivity of the DSE study in detecting CAD was 76%, while its specificity was 31%. In the same subgroup of patients, the sensitivity of the semi-automated method (using the asymmetry index) was 35%, while its specificity was 88%. A combined sensitivity of DSE and the semi-automated method (using the asymmetry index) was 58%, while the specificity was 67%. Within the DSE_{pos} and DSE_{neg} groups, the sensitivity of the asymmetry index in detecting the DSE study outcome was 27%, while the specificity was 97%.

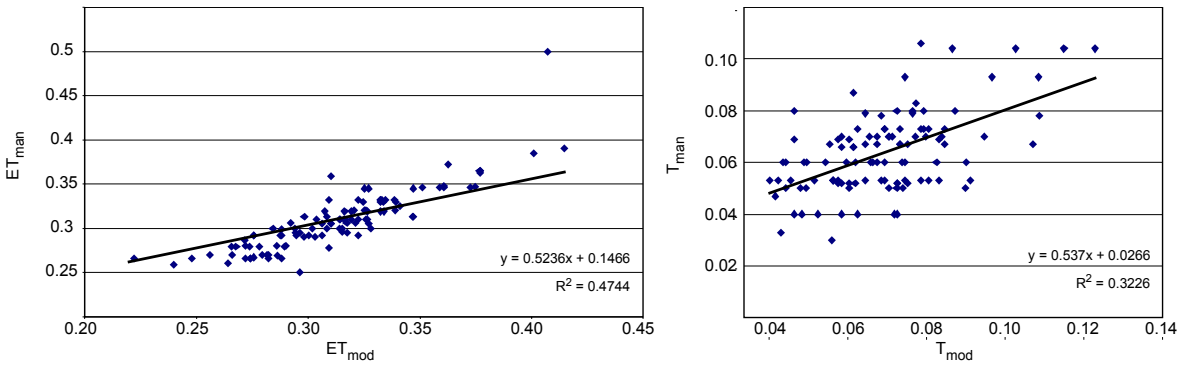

Figure 4.3. The correlation between the manual and automated measurements of ejection time and time to peak velocity.

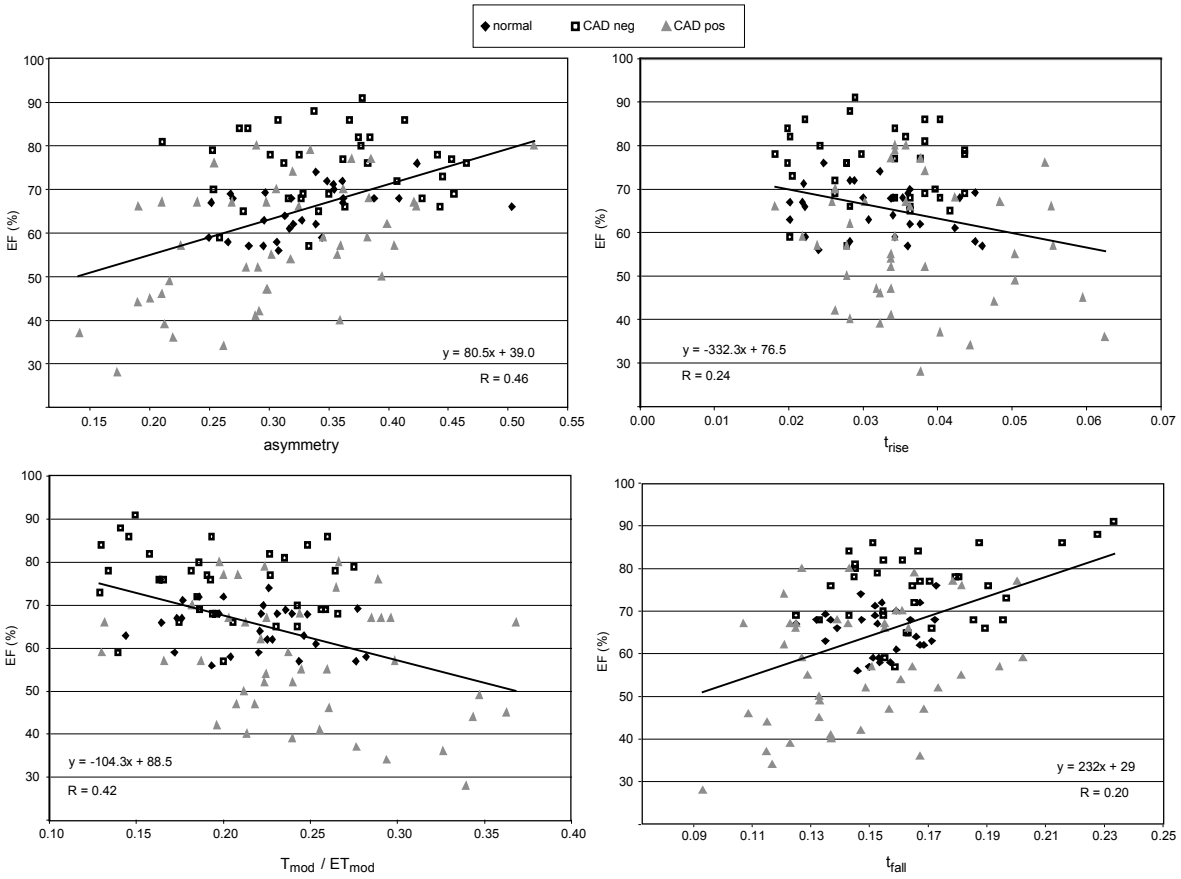

Figure 4.4. The correlation between EF and asymm, T_{mod}/ET_{mod}, t_{rise} and t_{fall}.

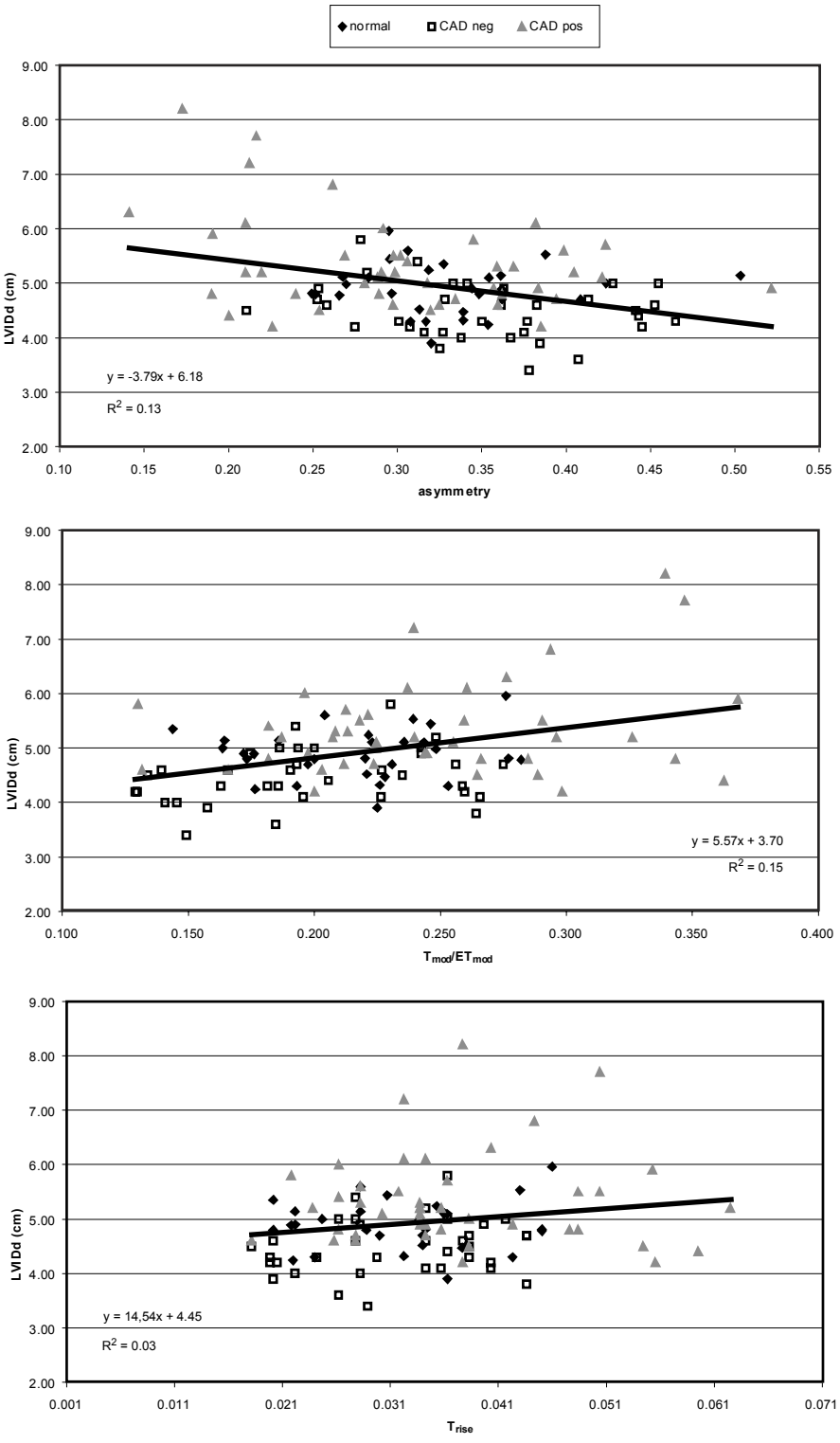

Figure 4.5. The correlation between LVIDd and asymm, T_{mod}/ET_{mod}, t_{rise}.

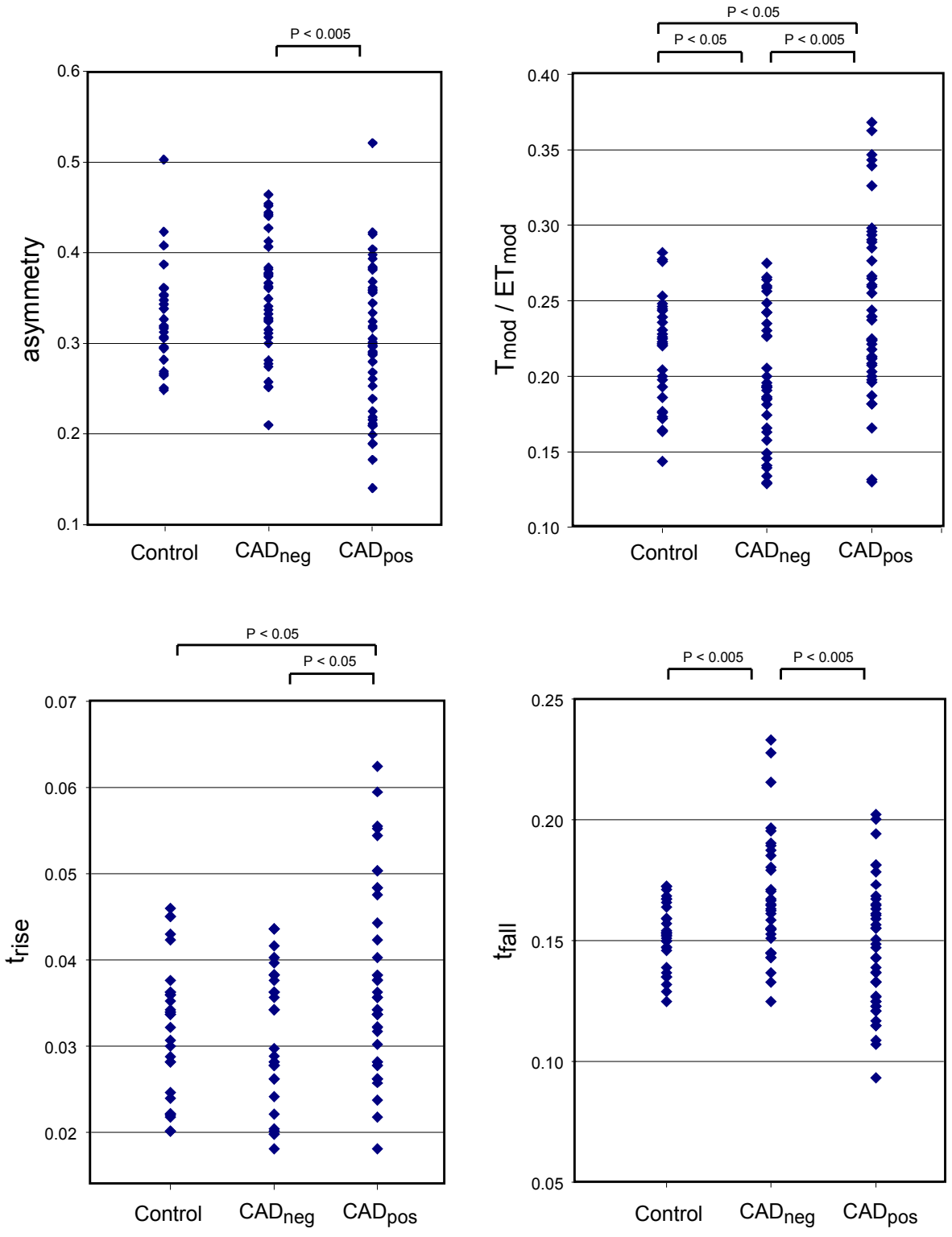

Figure 4.6. The values of asymm, T_{mod}/ET_{mod}, t_{rise} and t_{fall} among the three patient groups.

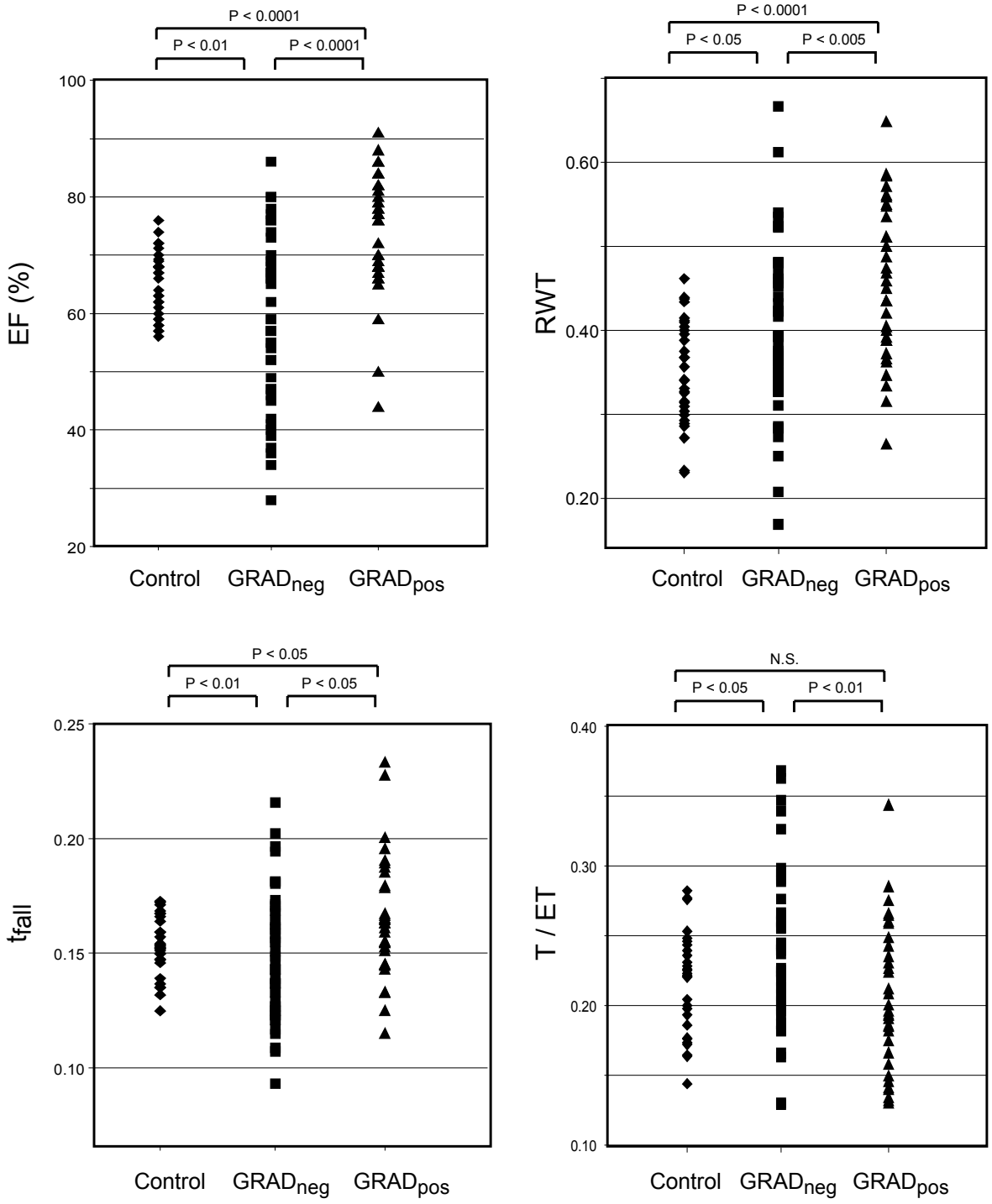

Figure 4.7. The values of EF, RWT, $t_{\_fall}$ and T_{mod}/ET_{mod} among the patients grouped in regard to inducible intracavity gradient.

4.4. Discussion

In this study, we have observed that the aortic outflow velocity profile is altered in the presence of coronary artery disease where in an import portion of patients the flow profile becomes much more symmetrical and rounded, whereas it is clearly asymmetrical and triangular in normal subjects. On average, in CAD, the rise time prolongs, the time to peak velocity is delayed and the fall time shortens.

Aortic outflow is the result of pressure development and deformation of the LV. Generation of pressure within the cavity of the LV is a direct consequence of active force development within the myofibres. Once initial force is developed by the contractile elements, the ventricle can increase its internal pressure up to the point high enough to open the aortic valve. From this moment, the shortening of the contractile elements will decrease the cavity size so that its internal blood content is ejected [1, 71]. The velocities with which the blood is ejected through the aortic valve depend on the pressure gradient. In the absence of an aortic stenosis, this gradient is determined by the developed LV pressure and the pressure in the aorta, which depends on the peripheral circulation and the aortic stiffness. In the absence of afterload changes, aortic outflow should directly reflect active force development and the resulting myocardial deformation. Sabbah et al. have shown that the peak acceleration of aortic blood flow assessed non-invasively in patients with a CW Doppler velocity meter is a useful indicator of global LV performance, as assessed by EF, while neither peak velocity nor the systolic velocity integral related as closely to EF [62]. This was also shown in experimental setups [61]. An analysis of aortic wave intensity and aortic velocities during a dobutamine infusion showed the increased acceleration of the velocity and a more asymmetrical profile with faster deceleration, mainly due to the interaction of the forward and backward waves in the aorta [72]. It was also shown that dobutamine provokes an increase in aortic acceleration, although the increase was significantly lower in patients with CAD. However, no difference in aortic acceleration was found between patients and controls at baseline [73].

Additionally, in a pig model of myocardial hibernation, Bito and co-authors demonstrated that isolated chronically ischaemic myocytes show a reduced and slowed contraction when compared to normal myocytes and that they show a significant reduction in active force development [49, 74]. Furthermore, several studies on long axis function have demonstrated that, in areas affected by CAD, the onset of contraction is delayed, the overall amplitude and velocity of contraction may be reduced and its duration prolonged [75-77]. Hatle and co-authors showed that the relative timing of the maximal aortic flow occurred later in LV heart failure [59]. The same study showed the lowest values of time to peak velocity in patients with hyperkinetic heart syndrome or with considerable aortic regurgitation.

In this study, we hypothesize that the presence of coronary artery disease can result in a global decrease in contractility such that the LV is not able to generate the required stroke volume anymore when developing (normal) short-lived active contraction force. In order to generate enough stroke volume the whole LV will prolong the development of contractile force, which, besides a slower increase in the blood velocities through the aortic valve, will also result in a longer duration of aortic acceleration and a more symmetrical profile of which the bulk of the flow shifts towards the later part of the ejection period.

This remodelling of the aortic velocity profile can be quantified based on the timing and the overall shape of the LV outflow curve. In this study we have analyzed CW Doppler traces in patients with and without signs of ischaemic heart disease, as assessed by quantitative DSE. We have implemented an automated analysis tool, using modelling of the velocity envelope, to measure the time intervals relevant for determining later peaking of the outflow traces in CAD.

Our results show that the shape of the aortic outflow trace may reflect decreased contractility: the traces of patients within DSE_{pos} show a tendency towards a more symmetrical, later peaking and faster falling curve than in DSE_{neg} patients and normals. There was a clearly positive correlation of the relative timing of the peak velocity (T_{mod}/mod_{mod}) with EF and a negative one with LVIDd, as a marker of LV dilatation. Furthermore, we observed that an asymm<0.25, indicating a markedly more symmetrical trace, was present in only 2.9% patients in DSE_{neg} and 27.3% of patients in DSE_{pos} while it was greater than 0.25 in all controls. Moreover, asymm proved to be a valid indicator of contractility: it correlated well with EF and had a somewhat weaker, negative correlation with LVIDd.

Although the acceleration of the aortic outflow was previously suggested as a marker of contractility [62], the aortic rise time t_{rise} showed a weaker correlation both with EF and LVIDd, compared to T_{mod}/mod_{mod} and our measure of curve symmetry (asymm), suggesting that not only the initial acceleration, but the whole velocity profile has to be considered to describe LV function.

While we hypothesize that a more symmetrical aortic outflow profile indicates decreased global contractility, surprisingly, we found that the patients within the DSE_{neg} group, on average, showed a more asymmetrical aortic flow pattern with a shorter T_{mod}/mod_{mod} and prolonged t_{fall} when compared to controls. This group of patients also had a significantly higher RWT and EF, as well as higher values of SBP and DBP, compared to the other two groups. Additionally, in this DSE_{neg} group, an LV dynamic intracavitary gradient was induced by DSE in as much as 71% of the patients while this was observed in only 18% in the DSE_{pos} group. This characteristic late and large increase in outflow velocities reflects the dynamic nature of an additional pressure gradient developed within the LV when the cavity size

decreases during ejection [78, 79]. This gradient was previously noted in 21% of patients in a series of 57 patients undergoing DSE and was associated with a significantly higher resting EF but no evidence of a significant difference in history of hypertension, LV hypertrophy, or signs of CAD was present [70]. In another series, the late increase in outflow tract velocities was associated with signs of basal septal hypertrophy and smaller LV cavities [80]. In a series of 394 patients, 17.5% developed a significant LV outflow gradient, which was associated with asymmetrical septal hypertrophy and a lower frequency of wall motion abnormalities [81]. Overall, in our group of patients, a significant prolongation of the duration of t_{fall} was present in patients who developed an intracavitary gradient compared to the ones which had no inducible gradient or controls. This, together with the increased hypertrophy and EF, would let us hypothesize that the patients who develop a dynamic gradient during the DSE have actually increased contractility at baseline and thus indeed show a more asymmetric outflow profile with an earlier peak. The hypertrophy and associated increased contractility in these patients might be caused by the transient, exercise induced, increased pressure overload due to the development of the gradient. The potential to develop a dynamic gradient might be triggered by the localized basal septal hypertrophy, induced by the presence of hypertension [9].

4.5. Clinical Perspective

The goal of this study was not to present another non-invasive parameter to be used in discrimination CAD patients, but rather to address flow remodelling as a consequence of cellular and force remodelling which occurs in ischaemic heart disease. We have shown that decreased overall contractility results in a more symmetrical outflow velocity profile. In clinical practice, the presence of an abnormally symmetrical profile in an individual patient would thus suggest that the global development of contractile force has been remodelled to cope with the decreased output resulting from decreased contractility. On the other hand, a very asymmetrical and early peaking profile implies increased contractility, which, in the presence of (regional) hypertrophy, might induce a dynamic intracavitary gradient. Additionally, these patients are prone to Tako-Tsubo cardiomyopathy [82].

Incorporating parameters describing the profile of the outflow trace, in the clinical echocardiographic measurements thus provides additional information on myocardial function

4.6. Limitations

Left ventricular outflow velocities represent the pressure gradient between the LV and aorta and are thus influenced by either of them. This implies that changes in the peripheral vessel tree could influence the flow profile. However, a dynamically increasing resistance in the vessel tree, associated with decreased compliance, as expected in CAD, would reduce late velocities while the presence of high late velocities should thus be related to prolonged LV pressure development. Changes in the isometric contraction duration in itself, would not change the measurements since we start quantifying from the opening of the valve. However, a lengthening of the isometric contraction time would also be expected with a decreased contractility, which would be reflected again in a slower rise time and later peaking, as we observe.

Although contractility was not measured directly, there is a strong body of evidence proving that DSE testing, especially including information on changes in local deformation, is indicative of increase in contractility. Furthermore, as this was a retrospective study on routine clinical data, catheterisation measurements of LV contractility were not available, nor was sufficient mitral regurgitation present in most of the patients in order to measure Dp/dt. Therefore, we have chosen to subgroup the patients based on the DSE response rather than angiographically proven CAD, which then served as an adjunctive marker of LV contractility,

Moreover, the current study was performed using CW Doppler, which is also influenced by velocities in the LV cavity (such as the development of a dynamic gradient). Finally, although dobutamine mimics exercise, its effects are quite different in terms of loading as it decreases preload and afterload. Therefore, identical effects should not be assumed for exercise echocardiography.

Chapter 5

The Symmetry of the Shape of the Instantaneous Peak Velocities in Aortic Stenosis: Does it Predict Functional Recovery after Aortic Valve Replacement?*

5.1. Introduction

Severe aortic stenosis (AS) is often masked in asymptomatic patients although subclinical systolic dysfunction with preserved ejection fraction may already be present [83]. It is a challenge to recognize patients with subclinical myocardial dysfunction in order to operate early enough to prevent irreversible myocardial damage, but not so early as to subject them to unnecessary risks. The optimal timing of valve replacement surgery is often unclear and mostly not obvious from regularly used measurements of ventricular function, suggesting the need for improved understanding and assessment of the potentially induced changes in ventricular function.

Forward flow across the aortic valve is determined by factors such as LV contractility, valve properties (valve area) as well as (systemic) afterload. Therefore, the Doppler trace of aortic outflow (instantaneous peak velocity) in AS should reflect not only stenosis severity, but potential LV functional damage as well. Although the *Doppler pressure gradient* measured over a stenotic valve is indicative of stenosis severity, it often does not relate to myocardial function or changes in contractility resulting from myocardial damage, as can be found in low gradient, severe AS. Furthermore, it has been shown that, despite preserved EF, paradoxical low-flow, low-gradient severe aortic stenosis is associated with higher afterload and reduced survival [84].

Beside data on blood flow velocities and pressure gradients, it has been suggested that the *profile of Doppler traces* of aortic outflow presents further insight into disease severity in patients with AS [51, 85]. The profile of the aortic flow velocity curves can be described by the rate of increase (acceleration) in velocity, the peak and the time of peak velocity, the mean velocity during systole and the ejection duration [51]. Normal outflow shows an asymmetric, triangular shaped profile with a fast rise in velocities and peaking around 1/3 of the ejection duration [51].

With mild AS and high flow, the peak velocity occurs early in systole, while in cases of severe stenosis the peak is reached in midsystole, presenting with a more symmetrical curve

---

* From: Cikes M, Kalinic H, Hermann S, Loncaric S, Milicic D, Beer M, Hatle L, Cikes I, Sutherland G, Weidemann F, Bijnens B. The Symmetry of the Shape of the Instantaneous Peak Velocities in Aortic Stenosis: Does it Predict Functional Recovery after Aortic Valve Replacement? Submitted for review.

[85]. Furthermore, it has been shown that in acute aortic constriction, the myocardium generates an active force of normal magnitude, but with a longer duration, while in chronic AS a bigger and longer force occurs [86]. Thus, to compensate for the obstruction to flow occurring in acute aortic constriction, the aortic instantaneous peak velocity curve will become more prolonged and increasingly symmetric in shape when the force development is prolonged.

The time in systole at which the peak pressure difference occurs is later with increasing obstruction, but is also influenced by the course of the LV pressure curve. It is known that active force development in the normal myocytes peaks around 1/3 of the ejection, after which it decreases rapidly [32]. This implies that the early flow acceleration is caused by active contraction, while flow decelerates when force development declines. This explains why flow acceleration increases with increased contractility [87]. There are some suggestions that the timing of myocyte contraction might be altered with a decrease in function [49]. This might be the reason why, with increasing severity of aortic stenosis, a concomitant change in the shape and duration of both the local deformation and the aortic outflow blood velocities can be observed. Therefore, in addition to the differences in the severity of obstruction, changes in the LV and aortic pressure curves as a consequence of changes in contractility and peripheral resistance may influence the pressure difference and thus the course of the maximal velocity curve [51].

Based on this, we hypothesize a relation between the shape of aortic instantaneous peak velocities and myocardial function in AS where myocardial contractility can be prolonged, resulting in a more symmetrical cardiac outflow as reflected from the Doppler signal.

5.2. Methods

5.2.1. Patients

We studied 34 patients undergoing aortic valve surgery for severe AS (as defined by the European Society of Cardiology guidelines) [88] preoperatively (PRE) and 9 months postoperatively (POST). This group consisted of 16 female and 18 male patients, mean age 69.4±9.3 years.

The control group consisted of 29 healthy volunteers with no signs or symptoms of cardiovascular disease or arterial hypertension (15 female, 14 male, mean age 63.1±10.5 years). All patients gave written consent for CMR and echocardiography studies including digital data storage and systematic analysis of the data. The study complies with the Declaration of Helsinki and was approved by the University Hospital Wuerzburg review committee.

5.2.2. Echocardiographic Imaging

Standard cardiac ultrasound data were acquired with a Vivid Seven ultrasound scanner equipped with a 2.5-MHz transducer (GE, Horten, Norway). Data were obtained from the parasternal and apical views. For the 2D studies, parasternal long and short axis as well as apical two-, three-, four- and five-chamber views were used. Aortic outflow CW and left ventricular outflow pulsed wave Doppler traces were acquired from the apical five-chamber view (LV outflow pulsed wave Doppler was acquired for AVA measurements, as described later). The echocardiographic data were obtained for three complete cardiac cycles during a single end-expiratory breath hold.

Offline analysis was performed using dedicated software (Echopac, GE, Horten, Norway). LV size and mass were measured from the M-mode images [66, 67]. EF was measured by the Simpson biplane method [66]. CW Doppler traces of the aortic outflow were analyzed by planimetry of the Doppler envelope in order to obtain the mean systolic transaortic pressure gradient (PG mean), which, as the maximal systolic transaortic pressure gradient, was calculated by the modified Bernoulli equation. Aortic valve area (AVA) was calculated from the continuity equation [89, 90]. The peak pulmonary artery pressure was measured from the pressure gradient calculated using the simplified Bernoulli equation of the tricuspid regurgitation jet peak velocity and adding the right atrial pressure as estimated from the inferior vena cava diameter and respiratory collapse, where available. The LV ejection time index was calculated as previously described [91].

5.2.3. Doppler Outflow Analysis

The aortic outflow CW Doppler traces were analyzed semi-automatically. The approach was previously described [69]. Figure 5.1 (left) shows the original Doppler image. In the first step, the image was converted and pre-processed to obtain only the forward velocities. On these images, the velocity envelope was detected automatically using thresholding. Next, the onset and the end of the aortic flow were manually indicated, thus isolating the instantaneous peak velocity profile. In order to eliminate the non-physiological noise and artefacts (mainly corresponding to the “valve clicks”) a piecewise cubic model was fitted to the trace. From the modelled signals, several parameters describing their shape were extracted. Time to peak (T_{mod}), ejection time (mod_{mod}), rise time (T_rise) and fall time (T_fall) were quantified. Rise and fall times were defined from 10% to 90% of the peak (Figure 5.1, right). The ratios T_{mod}/ET_{mod} as well as ET_{mod}/R-R were calculated. Additionally, an asymmetry index (asymm) was calculated as the difference of the area under the maximum velocity curve contained in the first and second half of the ejection period normalized by the overall area.

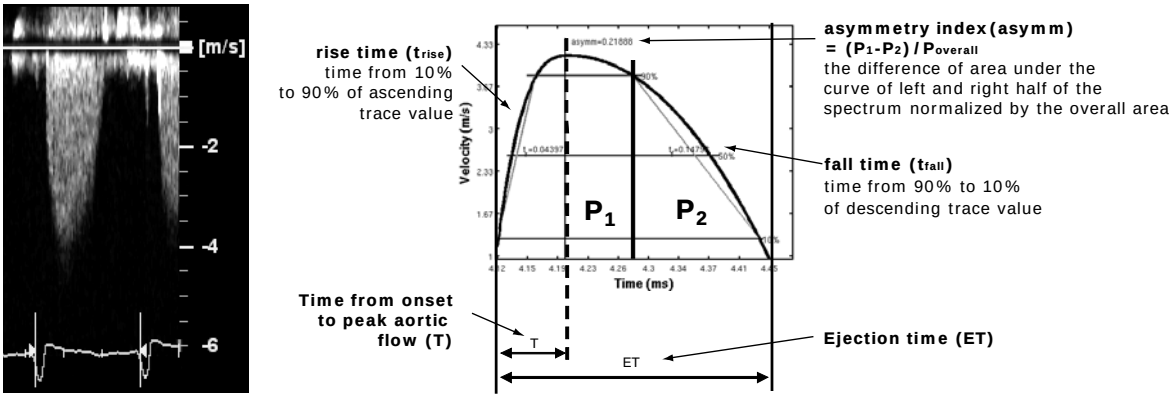

Figure 5.1. Aortic outflow Doppler image (left), the piecewise cubic model fitted on the original trace and the parameters extracted from it (right).

5.2.4. Cardiac Magnetic Resonance Imaging

CMR was performed on Siemens Sonata – Avanto (Erlangen, Germany) or Phillips Gyroscan ACS-NT (Best, The Netherlands) 1.5 T whole-body scanners with dedicated cardiac coils. Breath-hold cine images were acquired in multiple short-axis and three long-axis slices with steady-state free precession sequences. Ventricular coverage was achieved with contiguous 10 mm-thick slices or 7 mm slices (2–3 mm gap). Images for late enhancement (LE) diagnostics were acquired 15 min after the injection of gadopentetate dimeglumine (Magnevist; Schering, Berlin, Germany; 0.2 mmol per kilogram of body weight) with a breath-hold segmented inversion-recovery sequence (inversion time 240–300 ms) acquired in the same views.

5.2.5. Statistical Analysis

Continuous variables' data are expressed as mean value ± SD. For comparative analysis, an unpaired two-tailed Student t-test was performed between groups with unequal distribution, while a paired test was performed between the PRE and POST groups. Categorical variables are expressed as a percentage. For categorical variables, comparisons between groups were made using the chi-square test. Results were considered significant at $p<0.05$. A linear correlation was used to test the similarity between the relevant parameters. Comparisons of the areas under the receiver operating characteristic (ROC) curves for patients with postoperative improvement of EF as well as those with postoperative stagnation or deterioration in EF were performed to assess diagnostic accuracy of asymm, AVA and PG mean.

5.3. Results

5.3.1. Patient Group Characteristics and Basic Echocardiography Data

The basic patient characteristics are given in table 5.1. The preoperative age of the patients did not differ significantly from the control group. SBP, DBP and HR values POST were significantly higher compared to the control group. The NYHA class was improved in most patients after AVR. Most of the patients suffered from arterial hypertension (94%), less from diabetes (24%). In the PRE group, signs of CMR LE were demonstrated in 72% of the patients in which such a study was performed. Table 5.2 shows the obtained echocardiographic measurements. No significant difference was found in LV cavity size between the three groups, although a tendency toward reduction in LV cavity size was present postoperatively. The patients presented with marked concentric hypertrophy preoperatively, which was significantly reduced postoperatively, although LV wall thickness was still significantly higher, compared to the control group ($p<10^{-8}$), as was the LV mass ($p<0.00001$) (Table 2). EF was significantly lower in the PRE and POST groups ($p<0.05$, compared to the controls), tending to normalize after AV surgery ($p<0.05$ POST vs. PRE). Notably, only 8.8% of the patients had EF PRE values ≤45% (Table 5.2). The values of AVA, PG mean, maximal systolic transaortic PG and Vmax have significantly improved after AVR, compared to the PRE values ($p<10^{-8}$ for all parameters). No significant change was noted in PAP POST compared to PRE (Table 5.2). No significant correlation was found between EF PRE and EF POST-PRE (r=-0.44)

	control group (n=29)	Aortic stenosis PRE (n=34)	Aortic stenosis POST (n=34)
Age (years)	63.1±10.5	69.4±9.3	71.4±9.2*
male/female	14/15	18/16	18/16
SBP rest (mmHg)	121.0±11.9	128.3±15.8	131.9±13.9*
DBP rest (mmHg)	72.7±6.2	79.9±8.4†	77.6±9.4*
NYHA	1.0±0.0	3.0±0.6	2.0±0.9‡
MI (no pts/%)	0/0	3/34=8.8%	3/34=8.8%
DM (no pts/%)	0/0	8/34=24%	8/34=24%
HTN (no pts/%)	0/0	32/34=94%	32/34=94%
CMR LE (no pts/%)	-/-	13/18=72%	14/19=74%

Table 5.1. Basic patient characteristics

** P<0.05 vs. control; † P<0.002 vs. control, ‡ P=0.00001 vs. PRE.*

	control group (n=29)	Aortic stenosis PRE (n=34)	Aortic stenosis POST (n=34)
LVIDd (cm)	4.9±0.5	4.9±0.9	4.7±0.7
LVIDs (cm)	3.0±0.5	3.3±0.9	3.3±0.7
IVSd (cm)	0.9±0.2	1.4±0.2†	1.2±0.1†‡
LVPWd (cm)	0.8±0.2	1.4±0.2†	1.1±0.1†‡
LV mass ASE (g)	141.8±43.1	292.0±97.2†	205.4±58.9§#
EF (%)	65±6	59±9‖	61±8‖#
LV EF ≤45% (%)	0	8.8	3.4
AVA	3.54±0.66	0.80±0.17§	1.93±0.45‖‡
PG max (mmHg)	6.08±1.32	78.74±21.75†	23.94±8.11†‡
PG mean (mmHg)	3.14±0.53	48.74±13.27†	13.58±5.04†‡
AV Vmax (m/s)	1.02±0.32	4.26±0.70†	2.32±0.45‖‡
PAP (mmHg)	13.73±3.16	33.65±10.74‖	31.65±8.39‖

Table 5.2. Echocardiographic measurements

** P<0.0000002 vs. control, † P<0.00000001 vs. control, ‡ P<0.00000001 vs. PRE, § P<0.00005 vs. control, ‖ P<0.05 vs control, # P<0.05 vs. PRE*

5.3.2. Doppler Outflow Analysis

Figure 5.2 shows typical examples of the extracted PRE and POST profiles in patients with and without postoperative EF recovery.

Table 5.3 shows the parameters extracted from the aortic flow traces. Asymm was the lowest in the preoperative patient group indicating the most symmetrical traces, while its values have risen significantly after AVR. Asymm was the highest within the control group. Notably, 91.2 % of the AS patients had an abnormally symmetric trace (asymm <0.25) before aortic valve surgery, while only 34.5% of the AS patients retained such symmetric traces after AVR. None of the control group patients had such abnormal traces.

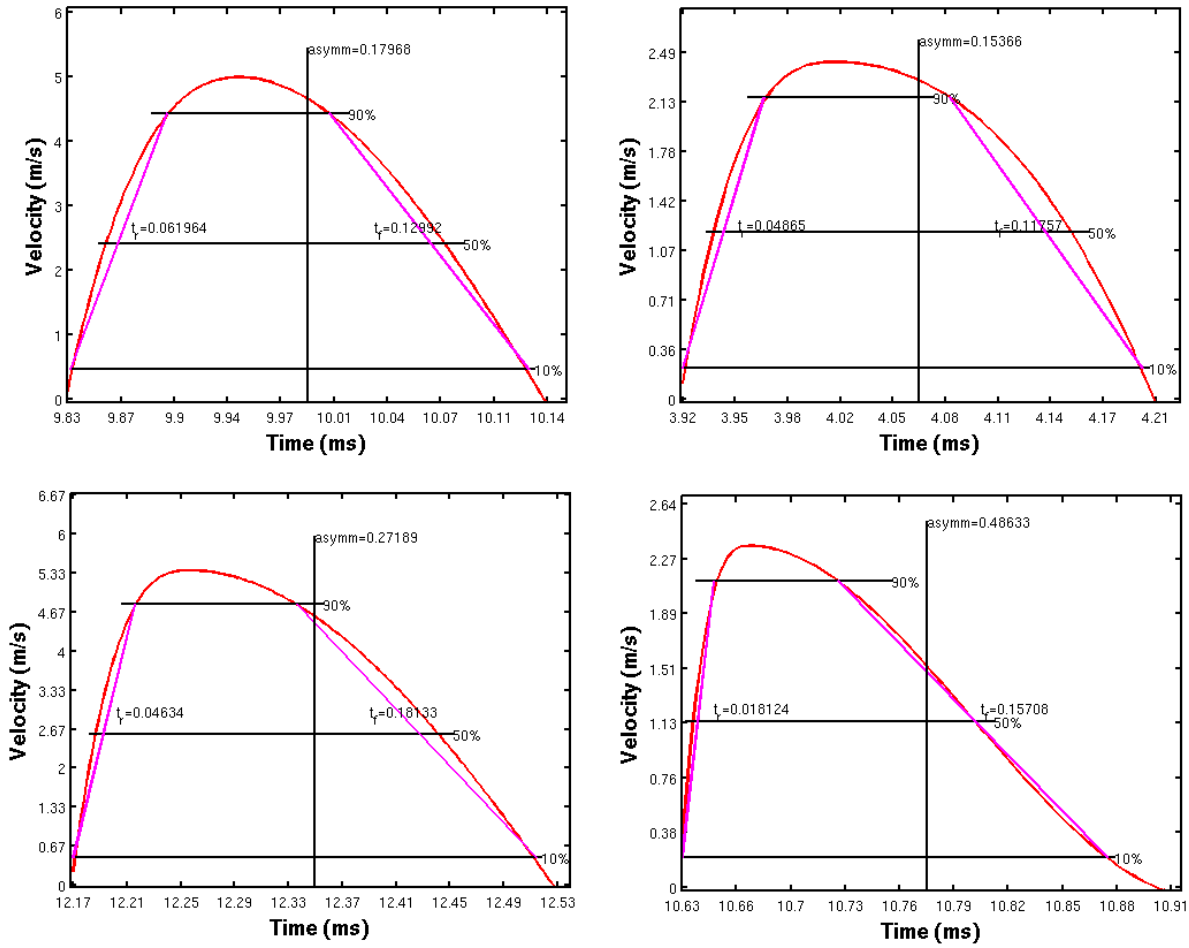

Figure 5.2. The piecewise cubic model of aortic outflow. A typical symmetric aortic outflow trace in a patient with AS showing no ejection fraction recovery postoperatively (top; preoperative trace – left, postoperative trace - right) and an asymmetric aortic outflow trace in a patient with AS showing ejection fraction recovery postoperatively (bottom; preoperative trace – left, postoperative trace - right).

	control group (n=29)	Aortic stenosis PRE (n=34)	Aortic stenosis POST (n=34)
asymm	0.33±0.06	0.16±0.06*	0.28±0.08†‡
asymm < 0.25 (%)	0.0%	91.2%	34.5%
T_rise	0.032±0.008	0.054±0.013*	0.035±0.011§
T_fall	0.153±0.013	0.127±0.026‖	0.138±0.019†#
T_{mod}	65.7±13.5	103.2±21.5*	68.5±18.3‡
ET_{mod}	303.5±21.5	315.7±40.3	284.6±33.3†#
ET_{mod}/ R-R	0.316±0.044	0.381±0.078†	0.328±0.051#
T_{mod}/ET_{mod}	0.22±0.04	0.32±0.06*	0.12±0.03*‡
LVETI	410.5±17.1	432.1±43.1†s	402.7±32.2#
HR (/min)	62.9±10.8	73.2±15.2†	69.5±10.4†

Table 5.3. Properties extracted from aortic Doppler traces and time intervals
** P<0.00000001 vs. control, † P<0.05 vs. control, ‡ P<0.00000001 vs.PRE, § P<0.00001 vs. PRE, ‖P<0.00001 vs. control, # P<0.05 vs. PRE*

T_rise was the longest in the PRE group, with a significant shortening in the POST group, while it was the shortest in the control group. Similarly, T was the longest in patients before surgery and became much shorter after AVR. T_fall, on the contrary, was the shortest in the PRE group, rising significantly in the POST group while it was the longest within the control group (Figure 5.3).

Relative ejection time mod_{mod}/R-R was the most prolonged in the PRE group, showing normalization in the POST group. Finally, the relative time to peak T_{mod}/ET_{mod} and LVETI were the longest before AVR, shortening after surgery to values lower than within the control group.

Notably, within the PRE group of patients, a significant correlation was found between asymm PRE and change in EF POST-PRE (r=0.65, P<0.05, figure 5.4) while no correlations were found between neither AVA nor PG mean and the change in EF POST-PRE (r=0.05 and r=0.04, respectively, p>0.05). Figure 5.5. demonstrates the ROC curves for asymm, AVA and PG mean in relation to EF POST-PRE. Asymm PRE values ≥ 0.15 demonstrated 95.2 %

specificity in detecting improvement in EF after surgery. Conversely, all patients showing no improvement or deterioration of EF after surgery had asymm PRE < 0.15 (100% sensitivity).

Finally, asymm PRE did not correlate significantly with PG mean PRE (r=0.20), while the patients with higher values of asymm PRE all showed improvement in EF POST-PRE (positive delta EF), regardless of PG_mean PRE (figure 5.6). A positive correlation was present between asymm PRE and AVA PRE within the subgroup of patients which had an improvement in EF POST-PRE (r=0.62), while such a correlation was not found in the patients with an EF POST-PRE stagnation or deterioration (figure 5.7).

In the subgroup of patients with asymm PRE ≥ 0.15 (which all improved EF postoperatively), CMR LE was present in 50% of these patients. Conversely, in the subgroup of patients with asymm PRE < 0.15, CMR detected LE in 90.9% of these patients. Finally, after AVR, values of asymm had increased to ≥ 0.15 in all patients. Nevertheless, 10 patients retained asymm < 0.25. Preoperative CMR data were available in 6/10 patients and all of these patients showed signs of LE detectable on CMR imaging.

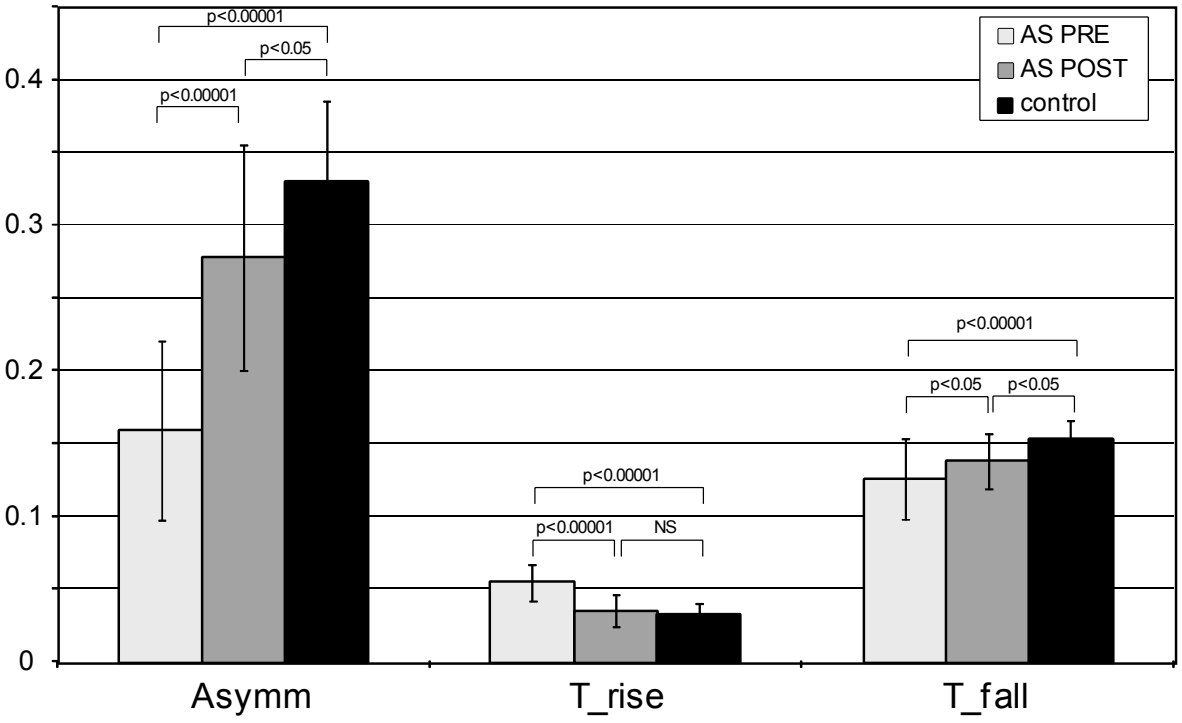

Figure 5.3. Values of properties extracted from the aortic flow traces.

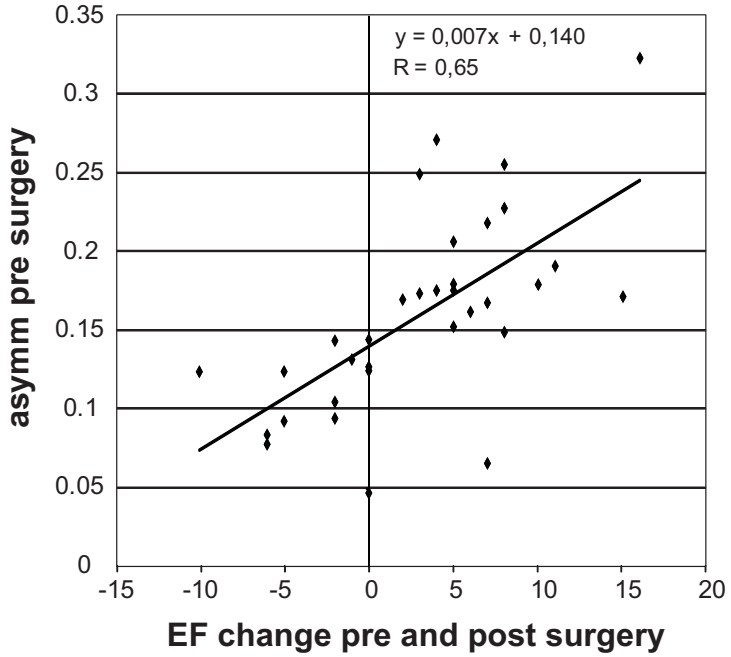

Figure 5.4. Positive correlation between asymm values PRE compared to EF POST-PRE.

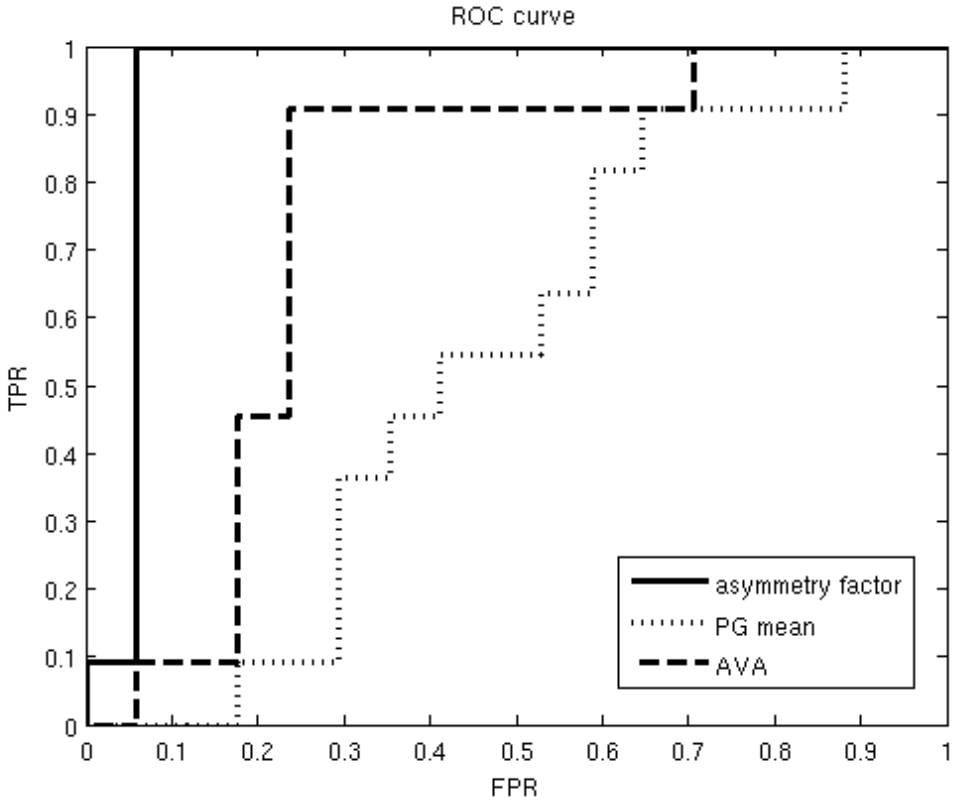

Figure 5.5. Receiver-operating characteristic analysis for the asymmetry index, PG mean and AVA comparing AS patients with postoperative improvement of EF and AS patients with postoperative stagnation or deterioration of EF.

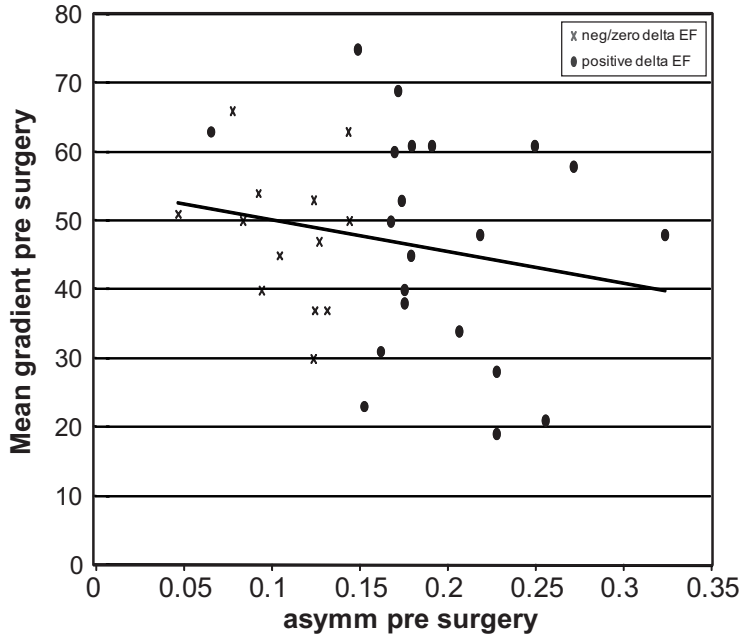

Figure 5.6. Absence of significant correlation between the asymm values and PG mean PRE. Notably, the patients with higher asymm PRE all showed improvement in EF POST (circles - positive delta EF), while the patients with lower asymm demonstrated no change or even a decrease in EF POST (x sign – neg/zero delta EF), both regardless of PG mean PRE.

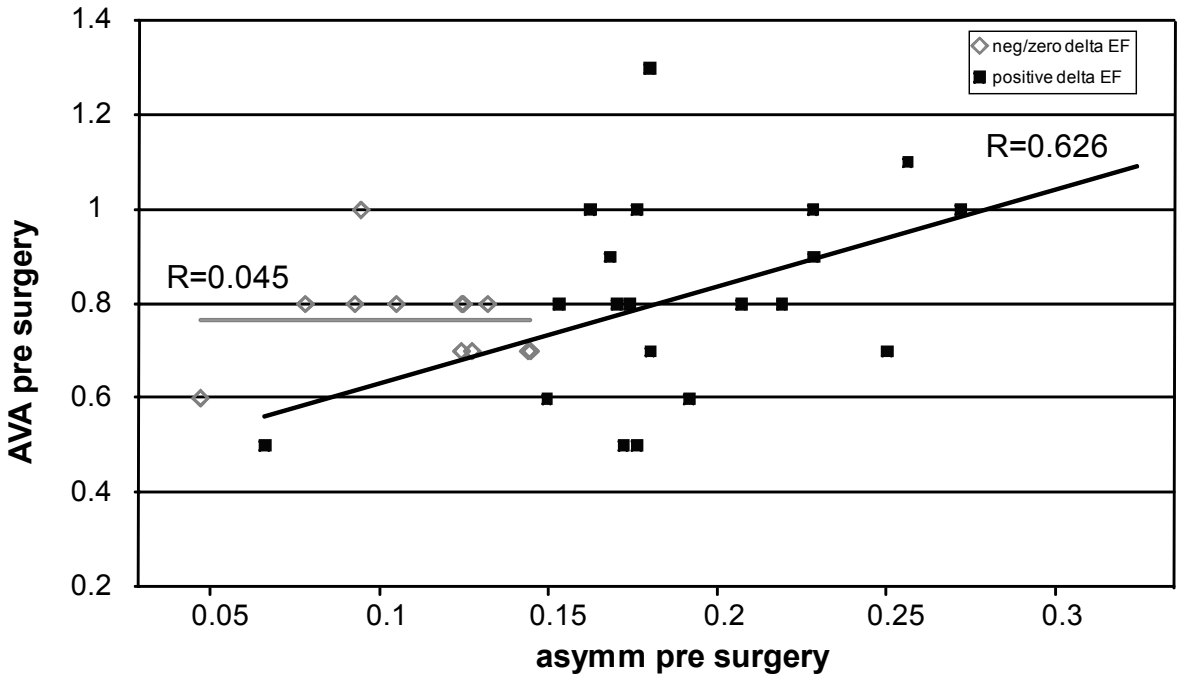

Figure 5.7. A positive correlation between the preoperative values of the asymmetry index and the preoperative aortic valve area within the subgroup of patients showing an improvement in postoperative EF. Such a correlation was not found in the patients with a postoperative EF stagnation or deterioration.

5.4. Discussion

In the present study, we have shown that the aortic instantaneous peak velocity Doppler traces in aortic stenosis vary in the degree of symmetry and that this is predictive of functional recovery after AVR. The current study has shown that: I) the shape of the aortic instantaneous peak velocity in patients with AS is markedly more symmetric than in the control group; II) an increase in trace symmetry before AVR is predictive of poorer EF recovery 9 months after surgery: all patients with asymm PRE <0.15 showed no improvement or even deterioration of EF postoperatively. Interestingly, no significant correlations were found between classical indices of stenosis severity such as PG mean nor AVA and change in EF pre- and postoperatively, neither did the preoperative values of EF influence postoperative EF recovery.

Current guidelines on AS are largely based on Doppler measurements of transaortic gradients, being an easily quantifiable measure of stenosis severity [88]. Nevertheless, due to their flow dependency, pressure gradients are a suboptimal measure of stenosis severity. Therefore, as demonstrated by multiple studies, measurements of aortic valve area would theoretically be an ideal way of AS severity quantification, although they are less robust and have potential inaccuracies as well [90, 92, 93]. Having such potential setbacks in mind, the current guidelines suggest combining several different echocardiographic parameters in the assessment of AS severity, as well as in the prediction of disease progression and outcome. Owing to the lack of a haemodynamic gold standard, it has been recognized that clinical outcome is the only end point available for defining stenosis severity [94], as well as that poor outcome can be independently predicted by multiple factors such as age, chronic renal failure, aortic valve velocity as well as significant valve calcifications in the case of mild /moderate AS [70, 95].

In the absence of afterload changes, instantaneous peak velocities should directly reflect active force development and the resulting myocardial deformation, while in severe AS it is influenced by the pressure gradient across the stenotic valve as well. Therefore, the shape of the instantaneous peak velocities in AS reflects both stenosis severity, as well as LV functional changes and myocardial damage. The relation between the late peaking features of aortic outflow and AS has been recognized some time ago. Bonner et al have found that a higher ejection time index, decreased maximum rate of carotid pulse rise and later timing of the peak of the systolic murmur were highly suggestive of severe AS [96], while Wranne et al described midsystolic peaking of the aortic Doppler signal in cases of severe stenosis [85]. Apart from demonstrating that the maximum aortic velocity occurred later in ejection in patients with severe AS, a temporal discrepancy of maximum left ventricular outflow tract velocity and aortic velocity was shown by Beauchesne et al, such that the left ventricular outflow tract velocity occurred later during ejection, while they occurred simultaneously in

control patients [97]. In another study, Agatston and co-workers have studied the relation between the modified time to peak/modified LV ejection time derived by Doppler and the peak to peak catheterization gradient. They have found that a ratio of 0.3 distinguished patients with a peak-to-peak gradient of <50 mmHg from those with a larger gradient in all but one patient which also had poor LV function. This patient actually had a symmetric trace (higher modified time to peak/modified LV ET than expected), which indeed might have been related to reduced LV function [98].

In pressure overload due to AS, reactive hypertrophy will cope with the increased afterload until wall stress becomes so high that irreversible damage occurs [99]. Although most patients with advanced AS have preserved EF, myocardial dysfunction occurs through reactive fibrosis [100, 101]. In a previously performed study, addressing flow remodelling as a consequence of cellular and force remodelling occurring in ischemic heart disease, we have shown that decreased overall contractility results in a more symmetrical outflow velocity profile [52]. A study performed by Bermejo and co-workers analyzed in vivo the effects of flow interventions on instantaneous valvular dynamics of stenotic valves for which a custom algorithm for signal processing of Doppler spectrograms was developed. By plotting instantaneous AVA against normalized ejection time, two types of curves were obtained: those of rapid, early opening of the aortic valve (represented in 80% of the control group) and those of slow, end-systolic opening (80% of AS patients). When given a dobutamine infusion, the patients increased and anticipated the peak AVA, which was explained by acceleration of valve opening. Furthermore, the ones in which a more rapid valve opening pattern developed after dobutamine, demonstrated a more favourable 3-year outcome. The changes of AVA over time demonstrated in this study might reflect the changes in LV contractility, i.e. force generation and deformation of the myocardium as well. The fact that administration of dobutamine induced a transformation of the curve toward the early peaking type in some AS patients provides an additional argument to support this hypothesis [102]. Furthermore, in pressure overloaded rats with normal usual indices of systolic (dys)function, Derumeaux et al. demonstrated early abnormal LV systolic deformation. Recovery in regional deformation occurred after early, but not after late debanding [103]. In humans, acute improvement in global and regional LV systolic function was shown shortly after percutaneous AVR [100, 103]. In a study performed in patients with AS before and promptly after balloon aortic valvuloplasty, Shim et al. have shown that the ejection pressure gradient and velocity traces tended to become less symmetric with steeper upstrokes and downstrokes, aside form the decrease in their values after the intervention. Furthermore, the time to peak ejection gradient and peak ejection velocity shortened after valvuloplasty [104].

Using Doppler myocardial imaging, it has been shown that abnormal LV systolic function in AS starts at an early age of the disease with reduction of regional deformation despite

preserved EF [1]. In a study by Kowalski and co-authors, end-systolic strain and peak strain correlated with AVA, peak gradient and stroke volume [22]. Moreover, regional differences in deformation parameters were noted: longitudinal deformation was inhomogeneous between the base and apex with basal segments having significantly lower strain/strain rate values than apical segments. In another study, patients with severe AS showed longer time to peak strain and peak strain rate before AVR when compared to normal subjects, while after AVR these parameters tended to normalize [101]. A recent study measuring pre-and postoperative systolic strain-rate in patients with AS and preserved EF showed a flattened and delayed systolic strain-rate profile in these patients when compared to patients with arterial hypertension or normals, thus implying a close relation between the systolic strain rate curves and LV contractility [105].

In the current study we have hypothesized a relation between the instantaneous peak velocity profiles and impaired myocardial function in aortic stenosis which results in prolonged myocardial contractility, leading to a more symmetrical cardiac outflow, as reflected by the Doppler signal. Our data have shown that instantaneous peak velocity symmetry occurs in >90% of patients with severe AS before AVR and persists in only 35% of patients after surgery, while Doppler trace symmetry was absent from the control group population. By analyzing aortic CW Doppler traces we have distinguished several trace properties, among which the asymmetry index, showing very low values (indicative of very symmetric traces) within the AS preoperative group and tending to normalize during a one year follow-up period after aortic valve replacement. Furthermore, the preoperative traces were characterized by a significantly prolonged rise time and shortened fall time which both improved after valve replacement. Finally, the relative ejection time (ET/R-R) and relative time to peak (T/ET) were much longer before surgery and normalized postoperatively, demonstrating a prolonged ejection phase as well as its delayed peak in severe AS.

Moreover, we have shown that the values of asymmetry before surgery are predictive of the change in EF pre- and postoperatively in these patients: all of the patients with markedly symmetric preoperative traces (asymm <0.15) showed stagnation or deterioration of EF postoperatively. Thus, preoperative asymmetry values ≥ 0.15 showed 95 % specificity and 100 % sensitivity in detecting patients with an improvement in ejection fraction after aortic valve replacement surgery, regardless of the preoperative mean aortic gradient values. Furthermore, we were unable to show a correlation between classical indices of stenosis severity such as aortic valve area or mean aortic gradient before surgery nor preoperative EF and the change in EF pre- and postoperatively. When looking at a subgroup of patients with severe AS with a low preoperative mean aortic gradient and low EF POST-PRE in which it is

usually difficult to assess AS severity and recovery according to the current guidelines, we have found that all of them had preoperative asymmetry <0.15.

Moreover, preoperative asymmetry did not correlate significantly with preoperative mean aortic gradient, while within the subgroup of patients which showed an postoperative improvement in EF, a positive correlation was present between preoperative asymmetry values and preoperative aortic valve area (patients with lower AVA had lower asymmetry values – more symmetric traces). Such a correlation was not found in the patients with a poor postoperative EF recovery outcome. This suggests that there is a direct impact of stenosis severity on the instantaneous peak velocity symmetry in patients with severe AS without LV dysfunction, while in the ones with poor LV function trace symmetry is mostly due to functional impairment and myocardial damage.

Finally, CMR data showed that signs of LE were present in half of the patients with preoperative asymmetry ≥ 0.15 and occurred in most of the patients with highly symmetrical traces (asymm < 0.15). In all patients which postoperatively retained asymm <0.25 and had CMR data available, evidence of LE was detected, indicating the finding of replacement fibrosis. This severe fibrosis affects the subendocardium, thus influencing longitudinal LV function which is likely to be reflected in the retained symmetry of the postoperative instantaneous peak velocities.

Therefore, we can conclude that aortic Doppler trace symmetry proves to be a more reliable predictor of functional improvement after the valve replacement procedure as compared to mean aortic gradient and aortic valve area which are widely used in preoperative assessment of patients with aortic stenosis.

Chapter 6

Detecting Volume Responders prior to Implantation of a Cardiac Resynchronization Therapy Device via Minithoracotomy: The Septal Flash as a Predictor of Immediate Left Ventricular Reverse Remodeling*

6.1. Introduction

Although cardiac resynchronization therapy (CRT) is well established as adjunctive heart failure treatment, a 30% rate of non-responders poses a challenge to better define the potential candidates before device implantation [106]. Several echocardiographic parameters of predicting CRT responders have been proposed, mostly based on measurements of time intervals between velocities of the segments of the left ventricular (LV) walls, but were shown to add no further benefit in predicting CRT response [44]. A mechanism based approach to patient selection has been recently proposed, based on multiple independent mechanisms, correction of which leads to CRT response [108, 109]. Along with atrioventricular and interventricular dyssynchrony, the septal flash has been defined as an echocardiographic sign of LV intraventricular dyssynchrony, occurring as a mechanical consequence of left bundle branch block (LBBB) induced activation of the LV. Furthermore, it has been shown that disappearal of the septal flash after CRT implantation, which occurred in almost 90% of the patients at a median follow up of 6 months, provides high sensitivity and specificity in detecting response to CRT.

We hypothesized that immediate response to CRT implantation observed from the point of LV intraventricular dyssynchrony can be detected/predicted by resolution of the septal flash (immediately following device activation), thus demonstrating that the presence of a septal flash prior to CRT pacing is a direct consequence of early septal activation in LBBB, correctable by biventricular pacing.

6.2. Methods

6.2.1. Patients

In this pilot study, we have studied 5 consecutive patents referred for CRT-P implantation by means of a left anterior mini thoracotomy. These patients underwent a preoperative

* By permission from: Čikeš M, Bijnens B, Đurić Ž, Lovrić Benčič M, Gošev I, Velagić V, Gašparović H, Miličić D, Biočina B. Detecting Volume Responders prior to Implantation of a Cardiac Resynchronization Therapy Device via Minithoracotomy: The Septal Flash as a Predictor of Immediate Left Ventricular Reverse Remodeling. Heart Surg Forum 2009;12(6):in press

echocardiography dyssynchrony screening study, as routinely performed in our centre, in which they were all identified as potential CRT responders based on the presence of the septal flash. The group consisted of 3 male and 2 female patients, mean age 62 ± 9 years. All patients fulfilled the current guidelines criteria for CRT implantation (EF<35%, QRS duration >120 ms, NYHA class III-IV, being under optimal pharmacotherapy) [110]. All patients underwent coronary angiography prior to CRT device implantation to exclude significant obstructive coronary artery disease.

Informed, signed consent was obtained from all patients and the study was in accordance to the ethical guidelines of the hospital.

6.2.2. Echocardiographic Imaging

Standard cardiac ultrasound data were acquired intraoperatively pre- and post- CRT device implantation with a Vivid Seven ultrasound scanner equipped with a 2.5-MHz phased – array transducer (GE, Horten, Norway). The post-activation echocardiography sequences were obtained after the below mentioned atrio-ventricular (A-V) interval optimization was performed.

Standard 2D data, spectral Doppler flows and myocardial velocity data were obtained from the parasternal and apical views. The echocardiographic data were obtained for three complete cardiac cycles. In patients with lower quality transthoracic views, the intraoperative study was extended by a transesophageal echocardiography (TEE) study (6 MHz transducer, GE, Horten, Norway), using the mid-esophageal and transgastric views.

Offline analysis was performed using dedicated software (Echopac, GE, Horten, Norway). LV size was measured from the M-mode images [66, 67]. Left ventricular EF and LV volumes were measured by the Simpson biplane method from the apical 4- and 2-chamber views [66]. PW Doppler traces of the LV outflow acquired from the 5-chamber view were analyzed by planimetry of the Doppler envelope in order to obtain the stroke volume, which was calculated by multiplying the LV outflow tract (LVOT) velocity time integral by the LVOT area (the LVOT diameter was measured from the 2D image of the parasternal long axis). Cardiac output was further calculated as the product of the stroke volume and heart rate. Transmitral flow velocities were obtained by positioning the PW sample volume at the tips of the mitral leaflets in the 4-chamber view. dP/dt was measured from the CW traces of mitral regurgitation, from which the pre-systolic mitral regurgitation was assessed as well (where available) [44, 111].

DMI velocity data were acquired as data superimposed on the underlying 2-D gray-scale image. To obtain the necessary high frame rate, the angle of insonation and depth of imaging were optimized, as previously described [112]. Special attention was paid to avoid aliasing within the image by adjusting the values of pulse repetition frequency (between 2.0-2.5 kHz).

The early septal fast inward/outward motion (thickening/thinning), i.e. the septal flash was visualized on the parasternal short or long axis views using either gray scale or tissue Doppler colour M-mode, where it was imaged as a rapid change of colour during the isovolumic contraction time (Figure 6.1, left). The amplitude of this septal motion was measured as the maximal excursion in the parasternal (or transgastric, in cases of TEE imaging) short or long axis views, or a transverse M-mode in an apical 4-chamber view. Furthermore, the septal flash was identified on the DMI radial velocity data as an early, fast, short lived negative declination shortly after the QRS onset where its peak velocity was measured [108, 109].

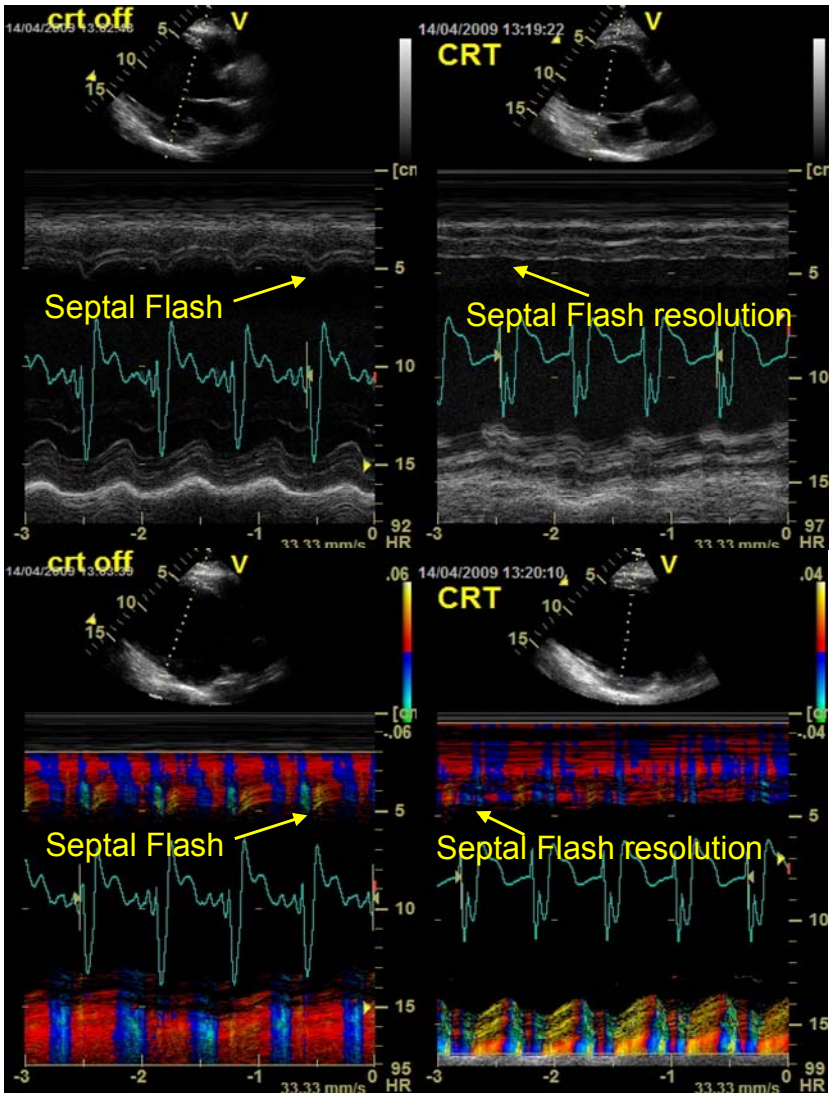

Figure 6.1. The septal flash i.e. the early septal thickening/thinning (occurring within the duration of the QRS complex), visualized on the parasternal long axis view using gray scale (top, left) or tissue Doppler color M-mode (bottom, left), imaged as a rapid change of color during the isovolumic contraction time. The resolution of the septal flash as seen immediately after CRT device implantation (top and bottom, right).

6.2.3. Mini Thoracotomy and CRT Device Optimization

The right atrial and ventricular leads were placed transvenously. The actual LV lead placement was performed through a left anterior mini thoracotomy, positioning the LV screw-in lead epicardially on the LV lateral wall.

Immediately following the CRT device activation, a simplified A-V delay screening was performed. In cases of a truncated or absent transmitral A wave (indicating a too short A-V delay) or a merged E and A wave (indicating a too long A-V delay), initial A-V optimization was performed using the iterative method.

6.2.4. Statistical Analysis

Continuous variables' data are expressed as mean value ± SD. For comparative analysis, a paired test was performed between the pre- and post-implantation groups. Categorical variables are expressed as percentages. For categorical variables, comparisons between groups were made using the chi-square test. Results were considered significant at $p<0.05$.

6.3. Results

6.3.1. Patient Group Characteristics

During an extensive diagnostic investigation for the aetiology of heart failure, significant coronary artery disease was detected by coronary angiography in only 1/5 patients, for which this patient underwent a percutaneous coronary intervention. Therefore, at least one year prior to CRT, coronary artery disease was absent/resolved in all patients. The remaining patients (80%) were diagnosed with idiopathic dilated cardiomyopathy. The values of neither systolic and diastolic blood pressure nor heart rate differed significantly before and after CRT device implantation (Table 6.1). All patients were in sinus rhythm before and after the procedure. The duration of the QRS interval decreased significantly after CRT (182±36 ms vs. 136±22 ms, respectively; $p=0.05$). The average duration of the PR interval reduced by biventricular pacing as well (184±43 vs. 138±17 ms, respectively; ns).

6.3.2. Echocardiographic Imaging

The obtained echocardiographic measurements are summarized in table 6.1. A significant reduction of LV end-diastolic dimension (7.6±1.3 cm vs. 7.2±1.2 cm, $p=0.01$), end-systolic (248±99 ml vs.180±89 ml, $p=0.01$) and end-diastolic volume (302±109 ml vs. 247±107 ml, $p=0.01$) were noted immediately after CRT device activation. Reverse remodelling, defined as a reduction of end-systolic volume (LVESV) ≥10% [113], was found in all patients (mean LVESV reduction after CRT activation being 27±13%, range16-46%). An immediate increase of EF was noted in all patients as well (mean delta EF 9±6%, range 4-19%). Furthermore,

dP/dt obtained noninvasively from the mitral regurgitation trace (obtainable from 4/5 patients) showed immediate improvement after CRT activation in all of these patients (mean delta dP/dt 303.2±64.2 mmHg/s, range 213-363.2 mmHg/s) (Figure 6.2). Increase in stroke volume and cardiac output have been noted after CRT activation, although without statistical significance. 3/5 patients (60%) had moderate or severe mitral regurgitation preoperatively which was immediately reduced with at least one grade.

The septal flash was detected before CRT activation in all patients and has diminished immediately after onset of biventricular pacing with an average of 80%, measured from the amplitude of this early, rapid septal motion imaged by gray scale or tissue Doppler colour M-mode, leading to normalization of septal motion (Figure 6.1). Likewise, its peak velocity measured from the DMI radial velocity datasets was decreased in the entire study group as well, with an average of 70% (Table 6.1, Figure 6.3).

Significant interventricular dyssynchrony (expressed as a ≥40 ms delay between left and right ventricular pre-ejection periods measured from the aortic and pulmonary outflow Doppler velocity traces, respectively) was present in 60% (3/5) patients and was resolved by biventricular pacing in all cases.

A significantly prolonged isovolumic contraction time (IVCT) was found before CRT device activation, which was significantly reduced by CRT (181±23 ms vs, 61±51 ms, respectively, $p<0.001$). The isovolumic relaxation time (IVRT) was generally shorter than the IVCT before pacing, by which it was somewhat prolonged, though without significance.

Assessment of the transmitral traces before the onset of biventricular pacing showed absence of significant atrioventricular dyssynchrony in two patients, while a filling pattern correspondent to a prolonged A-V delay was revealed in two other patients (fusion of the transmitral E and A wave and presence of pre-systolic mitral regurgitation). This was resolved by CRT in one of these patients, while the other had persistent sinus tachycardia intraoperatively, presumably causing the ongoing E and A wave fusion after CRT activation (regardless of attempts to optimize the A-V delay). Finally, one patient had signs of restrictive filling prior to biventricular pacing which reverted to pseudonormal filling after CRT activation.

	Pre CRT implantation	Post CRT implantation	p-value
SBP (mmHg)	111±7	115±13	Ns
DBP (mmHg)	67±8	66±9	Ns
HR (/min)	67±8	74±13	Ns
LVIDd (cm)	7.6±1.3	7.2±1.2	0.01
LVIDs (cm)	6.6±1.4	6.2±1.1	0.05
LVESV (ml)	248±99	180±89	0.01
LVEDV(ml)	302±109	247±107	0.01
EF (%)	19±5	28±5	0.01
MR dP/dt	299±58	602±111	0.001
Septal flash (mm)	10.2±6.9	1.5±0.7	0.02
Septal flash (cm/s)	4.8±2.3	1.4±0.2	0.01
IVCT (ms)	181±23	61±51	0.001
IVRT (ms)	147±109	109±75	Ns
IVD (ms)	60±39	29±11	Ns
SV (ml)	59.0±6.2	66.8±14.1	Ns
CO (ml)	4.5±0.8	4.7±1.0	Ns

Table 6.1. Basic clinical and echocardiographic measurements

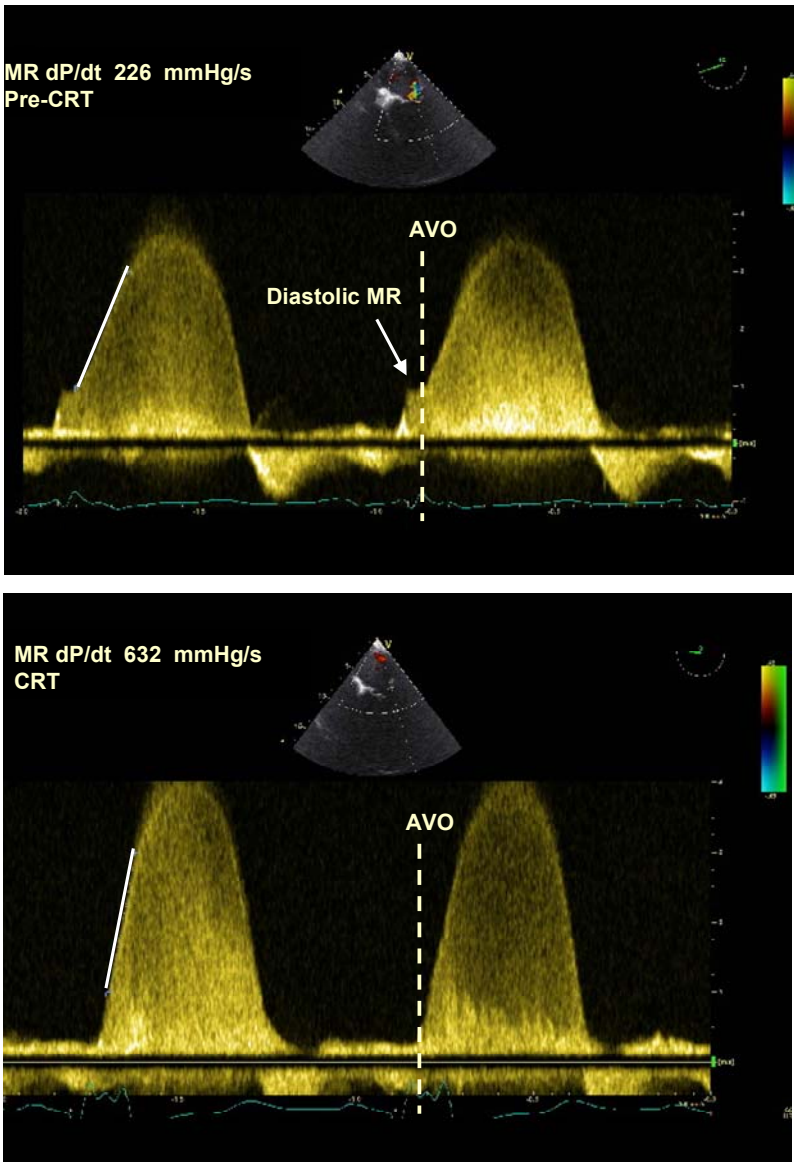

Figure 6.2. Significant improvement of dP/dt values derived form the mitral regurgitation trace (MR) before (top) and immediately after CRT device implantation, obtained by transesophageal echocardiography. Furthermore, pre-systolic MR present before biventricular pacing as a consequence of a long atrioventricular delay (top, arrow) is resolved by CRT (bottom).

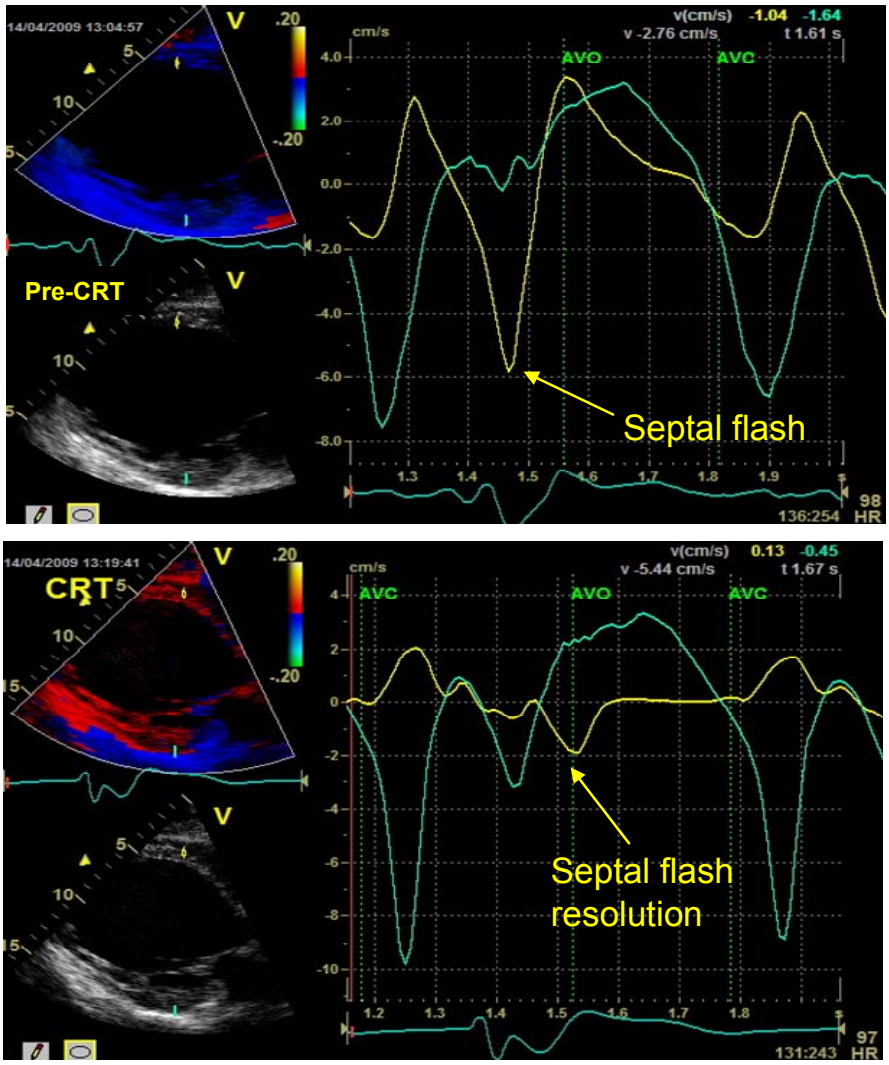

Figure 6.3. The septal flash seen on the pre-implantation DMI radial velocity data as an early, fast, short lived negative declination shortly after the QRS onset (top) which is immediately resolved by CRT, normalizing the radial velocities which become mirrored (bottom).

6.4. Discussion

In this study, we have shown that patients who fulfilled guidelines criteria for CRT implantation, presenting with a septal flash as a marker of intraventricular dyssynchrony, show an acute volume response as well as contractility recruitment immediately following CRT device activation.

Ventricular remodelling is in the first instance a response to either an inherent problem within the myocardium or the environment in which it has to work and is a compensatory attempt to preserve the heart's function. In the long term, within this abnormal situation,

imminent mechanical disadvantages will lead to irreversible myocardial damage, leading to ventricular dysfunction and heart failure [71]. With new treatment concepts available for heart failure patients, reverse remodelling is emerging as a new entity in patients where progressive LV dilatation and deterioration in contractile function show partial reversibility, instead of stagnation [114].

A substantial number of studies assessing survival and clinical response (change in NYHA class, exercise capacity and quality of life) have acknowledged the benefits of CRT, while the current knowledge on the mechanisms and effects of volume response is far less evident.

Generally, CRT leads to a significant decrease in LV size (optimally assessed by measuring LV volumes), as well as an increase in LV EF [106, 115-117]. Various time periods have been chosen for patient follow up, at which signs of reverse remodelling have been documented, ranging from as early as 1 month to 18 months at which LV reverse remodelling and associated clinical improvement are sustained [106, 115, 116, 118]. Recently, long-term results from the Cardiac Resynchronization in Heart Failure (CARE-HF) trial have been published, reporting on the long-term effects of CRT on LV reverse remodelling [119]. After an average study period of 29 months after CRT implantation, it has been demonstrated that CRT induces sustained LV reverse remodelling, with the most marked effects occurring within the first 3-9 months (the earliest follow up being 3 months after device implantation) and further improving at following assessments.

However, the onset of reverse remodelling induced by CRT is not well documented. In this study, we have demonstrated that in patients with true, LBBB induced intraventricular dyssynchrony (as defined by the septal flash), it occurs immediately after the activation of biventricular pacing. All patients within this group had preoperative evidence of the septal flash, deemed as a marker of intraventricular dyssynchrony, which was promptly abolished by biventricular pacing.

The preoperative presence of the septal flash was appreciated as a direct mechanical consequence of LBBB-induced early septal activation which develops force and shortens against the opposite lateral wall which is still latent. Because it is contracting against a reduced load, it will move faster than normally, resulting in the septal flash. The septum thus pulls the lateral wall until the latter becomes electrically activated, at which point the lateral wall starts to contract and will start in turn to influence the septum, resulting in a “rocking” apical motion in the ejection phase [108].

Beside a prompt, significant decrease in LV volumes and concomitant increase in EF, a marked increase in noninvasively obtained dP/dt was observed as well in this study, reflecting a direct, positive influence of CRT on LV contractility.

6.5. Conclusion

In this group of patients with overt heart failure and LBBB, immediate reverse remodelling (volume response) to biventricular pacing occurred in all patients after CRT activation and appears to be a direct effect of correcting the underlying conduction abnormality and its mechanical consequence, which can readily be imaged by echocardiography as the septal flash.

Chapter 7

Early Stage Acromegalic Cardiomyopathy: Evidence of LV Hypertrophy without Increased Afterload and Increased Contractility Associated with Increased Cardiac Output *

7.1. Introduction

The excess of growth hormone (GH) occurring in acromegaly stimulates the growth of various tissues [120]. Cardiac myocytes carry receptors for both GH and its tissue effector, insulin-like growth factor-I (IGF-I) [121]. In experimental studies, it has been shown that IGF-I causes hypertrophy of cultured rat cardiomyocytes [122] and delays cardiac apoptosis [123]. In patients with acromegaly, cardiac morphology and performance are affected due to chronic GH and IGF-I excess which lead to a specific acromegalic cardiomyopathy [124-126]. The first stage of acromegalic cardiomyopathy found in young patients with short disease duration is characterized by a hyperkinetic left ventricle (LV), increase in contractility and cardiac output and reduced peripheral vascular resistance [127, 128]. The second stage, at which the diagnosis is made in most adult patients, comprises concentric or eccentric LV hypertrophy, diastolic filling abnormalities at rest and impaired cardiac performance during physical exercise. If untreated or undiagnosed, acromegaly may lead to the final stage of heart involvement: valve disease and impaired systolic and diastolic function with low cardiac output occurring even at rest, occasionally leading to congestive heart failure [129 130]. Interstitial fibrosis, increased extracellular collagen deposition, myofibrillar derangement and areas of monocyte necrosis and lymphomononuclear infiltration, gradually impair the entire organ architecture as seen at histology [131]. Beside the specific cardiomyopathy, accompanying risk factors of acromegaly such as arterial hypertension, dyslipoproteinaemia, diabetes mellitus and peripheral insulin resistance [132, 133], lead to the fact that cardiovascular abnormalities are among the major causes of increased morbidity and mortality rates in acromegaly [134, 135].

Blood pool Doppler echocardiography provides a method to measure the blood velocities within the ventricles and blood vessels [51]. By measuring velocities through the cardiac valves, the amount of flow (cardiac output, filling) and the driving pressure gradient, causing

* From: Cikes M, Separovic Hanzevacki J, Kastelan D, Dusek T, Lovric Bencic M, Ernst A, Korsic M, Bijnens B. Early Stage Acromegalic Cardiomyopathy: Evidence of Left Ventricular Hypertrophy without Increased Afterload and Increased Contractility Associated with Increased Cardiac Output. Submitted for review.

the flow, can be quantified [51, 53-60], which can be clinically used to assess hemodynamic parameters and ventricular function [51, 53-57].

The profile of the aortic flow velocity curves can be described by the rate of increase (acceleration) in velocity, the peak and the time of peak velocity, the mean velocity during systole and the ejection duration [51]. Normal outflow shows an asymmetric, triangular shaped profile with a fast rise in velocities and peaking around 1/3 of the ejection duration [51]. Animal studies have shown that the flow acceleration is a sensitive indicator of the inotropic state [61], which was confirmed by clinical research [56, 62]. In LV failure, both a lower and a slower increase in velocities (a more rounded Doppler profile with a later peak velocity) were observed [51].

The most common feature of early stage acromegalic cardiomyopathy is biventricular hypertrophy which is initiated in the absence of any increase in wall stress [136]. Consequently, unlike in other forms of hypertrophy, wall stress may be reduced [137]. We hypothesize that the visually hyperkinetic LV which occurs in the earlier stages of disease is associated with Doppler signs of increased contractility in acromegaly patients, while commonly used indices of systolic function such as EF still remain unchanged.

Additionally, an increase in aortic root diameter has previously been demonstrated in patients with acromegaly [138], which was shown not to be related to increased afterload. However, this finding has not been related to an increase in LV contractility,

7.2. Methods

7.2.1. Patients

37 patients with acromegaly (20 female, 17 male, mean age 50.1 ± 10.5 years) were included to this study. The diagnosis of acromegaly was based on specific clinical characteristics, failure to suppress serum GH level bellow 2 mIU/L after a glucose tolerance test and a high serum IGF1 level for age. The patients who were successfully treated by pituitary tumor surgery, had normal IGF-1 level for age and adequate suppression of GH after glucose load were considered to be in disease remission. The disease duration was defined as the time interval between the clinical onset of disease (based on patient history and comparison of old photographs) and the echocardiographic exam date (in the active acromegaly subgroup), or the interval between clinical onset and successful pituitary tumor surgery (in the remission group). Patients were divided into two subgroups based on disease activity. 25 patients (13 female, 12 male, mean age 52.4±10.9 years) had active disease, i.e. they were included in the study before any therapeutic regimen was applied. Other 12 patients (7 female, 5 male, mean age 45.3±8.3 years) were included in the study after the

successful neurosurgical treatment and were considered to be in disease remission. Mean disease duration was 6.6 ± 6.0 years.

The acromegalic patients were compared to 15 patients with arterial hypertension (7 female, 8 male, 52.7±16.6 years, normal EF), which was defined as blood pressure > 140/90 mmHg [139].

32 healthy volunteers (15 female, 17 male, mean age 44.9 ± 15.2 years) with no signs or symptoms of arterial hypertension, diabetes mellitus or heart disease served as a control group.

7.2.2. Echocardiographic Imaging

All participants underwent a complete standard echocardiographic study (2D, M-mode, pulsed, and continuous Doppler). During the examination, the participants were lying in the left lateral decubitus position. The echocardiographic data for three complete cardiac cycles during a single end-expiratory breath holding were acquired with a Vivid Seven ultrasound scanner equipped with a 2.5-MHz transducer (GE, Horten, Norway). Data were obtained from the parasternal and apical views. For the 2D studies, parasternal long and short axis as well as apical two-, three-, four- and five-chamber views were used. Aortic outflow continuous (CW) and pulsed (PW) wave Doppler traces were acquired from the apical five-chamber view. The echocardiographic data were obtained for three complete cardiac cycles during a single end-expiratory breath hold. Offline analysis was performed using dedicated software (Echopac, GE, Horten, Norway). EF was measured by the Simpson biplane method [66]. LV size and mass (LVM) were measured [66] and indexed to body surface area in order to obtain the LV mass index (LVMI) [18]. The aortic root diameters were measured by M-mode, guided by a parasternal long axis image. The velocity time integral (VTI) was measured by tracing the signal of transaortic flow from pulsed-wave Doppler traces. Ejection time (ET) was measured as the time difference between the clicks of aortic valve opening and closure detected from pulsed-wave Doppler traces of the transaortic flow. ET was indexed by heart cycle duration (R-R) to obtain relative ET duration (ET/R-R). LV stroke volume (SV) and cardiac output (CO) were calculated pertaining to previously described formulae [54].

The study was performed according to the regulations of the Ethics Committee of the Zagreb University Hospital Centre and informed consent was obtained from all volunteers and patients.

7.2.3. Hormone Essays

Serum IGF-1 was measured by enzyme-linked immunosorbent assay (ELISA; Biocode-Hycel, Belgium) and GH level was assayed by radioimmunoassay (RIA; IBL Germany).

7.2.4. Statistical Analysis

Continuous variables' data are expressed as mean value ± SD and the unpaired two-tailed Student t-test was performed for comparative analysis. Categorical variables are expressed as a percentage. For categorical variables, comparisons between groups were made using the chi-square test. Results were considered significant at $P<0.05$.

7.3. Results

7.3.1. Patient Group Characteristics

The clinical characteristics of the studied patients and the control group are provided in Table 7.1. None of the three study groups differed significantly in age. Interestingly, the BSA did not differ significantly between the hypertensive and acromegalic patients, mostly due to concomitant adiposity of the hypertensive patients. The values of systolic (SBP) and diastolic blood pressure (DBP) were significantly higher in the hypertension group than the other two groups, while SBP and DBP were significantly higher in the acromegaly group compared to the control group. Arterial hypertension was present in 40% of the acromegalic patients. The serum levels of GH and IGF-I were, as expected, significantly higher in patients with active disease, when compared to those in remission (Table 7.3).

	Control (n=32)	Hypertension (n=15)	Acromegaly (n=37)
Age (years)	44.9±15.2	52.7±16.6	50.1±10.5
gender (male/female)	15/17	8/7	17/20
BSA (m^2)	1.87±0.22	2.00±0.15*	2.01±0.26*
Acromegaly duration (years)	-	-	6.5±6.0
Remission (%/no)	-	-	68/25
Active disease (%/no)	-	-	32/12
Systolic BP (mmHg)	121.0±9.2	159.5±16.7†	134.6±19.4†‡
Diastolic BP (mmHg)	71.0±5.5	100.0±10.0†	84.6±9.4†‡
heart rate (bpm)	73.0±11.6	72.1±7.4	74.2±11.2
Hypertension (%/no)	-	100/15	40/15

Table 7.1. Clinical Patient Characteristics

** P<0.05 vs. control; †P<0.0005 vs. control, ‡ P<0.002 vs. hypertension.*

7.3.2. Basic Echocardiography Data and Doppler Outflow Analysis

Echocardiographic measurements revealed that the group of acromegalic patients had the largest LV with the highest LVM (P<0.005 vs. control) (Table 7.2). Notably, the size of the aortic root was the largest in the acromegaly group, followed by the group of hypertensive patients (P<0.005 acromegaly vs. control, P<0.05 hypertension vs. control). The ET and ET/R-R were the shortest in the acromegaly group (P<0.05 vs. control, P<0.005 vs. hypertension and P<0.05 vs. control, P<0.05 vs. hypertension, respectively), while these time intervals were the longest in the group of patients with hypertension (Figure 7.1.). Inversely, T/ET was the longest in acromegalic patients (P<0.05 vs. control and HTN), while it was the shortest in the control group. Furthermore, SV and CO had by far the largest values in the acromegaly group (P<10^{-6} vs. control, P<20^{-6} vs. hypertension). No significant difference was noted among the three groups in respect to EF (Table 7.2).

	Control (n=32)	Hypertension (n=15)	Acromegaly (n=37)
LVIDd (cm)	4.97±0.41	5.07±0.42	5.35±0.51*
IVS (cm)	0.93±0.15	1.06±0.15	1.05±0.21†
LVPW (cm)	0.87±0.17	0.99±0.19	0.97±0.14†
LVM ASE (g)	143.2±29.1	179.1±22.1*	189.8±51.3*
LVMI (g/m^2)	76.5±11.9	93.1±13.1*	94.5±24.2*
EF (%)	67.1±7.5	68.3±9.9	65.7±10.1
ET (ms)	284.7±23.3	300.1±26.5	267.4±27.3†‡
ET/R-R	0.34±0.04	0.36±0.03	0.33±0.03†§
T/ET	0.22±0.04	0.24±0.05	0.25±0.05†§
AV SV (mL)	84.1±20.4	87.3±16.0	158.3±60.1‖¶
AV CO (L/min)	6.0±1.3	6.0±1.0	11.8±4.5‖¶

Table 7.2. Echocardiography Measurements

** P<0.005 vs. control; †P<0.05 vs. control, ‡ P<0.005 vs. hypertension, § P<0.05 vs. hypertension, ‖P<0.000001 vs. control, ¶ P<0.000002 vs. hypertension*

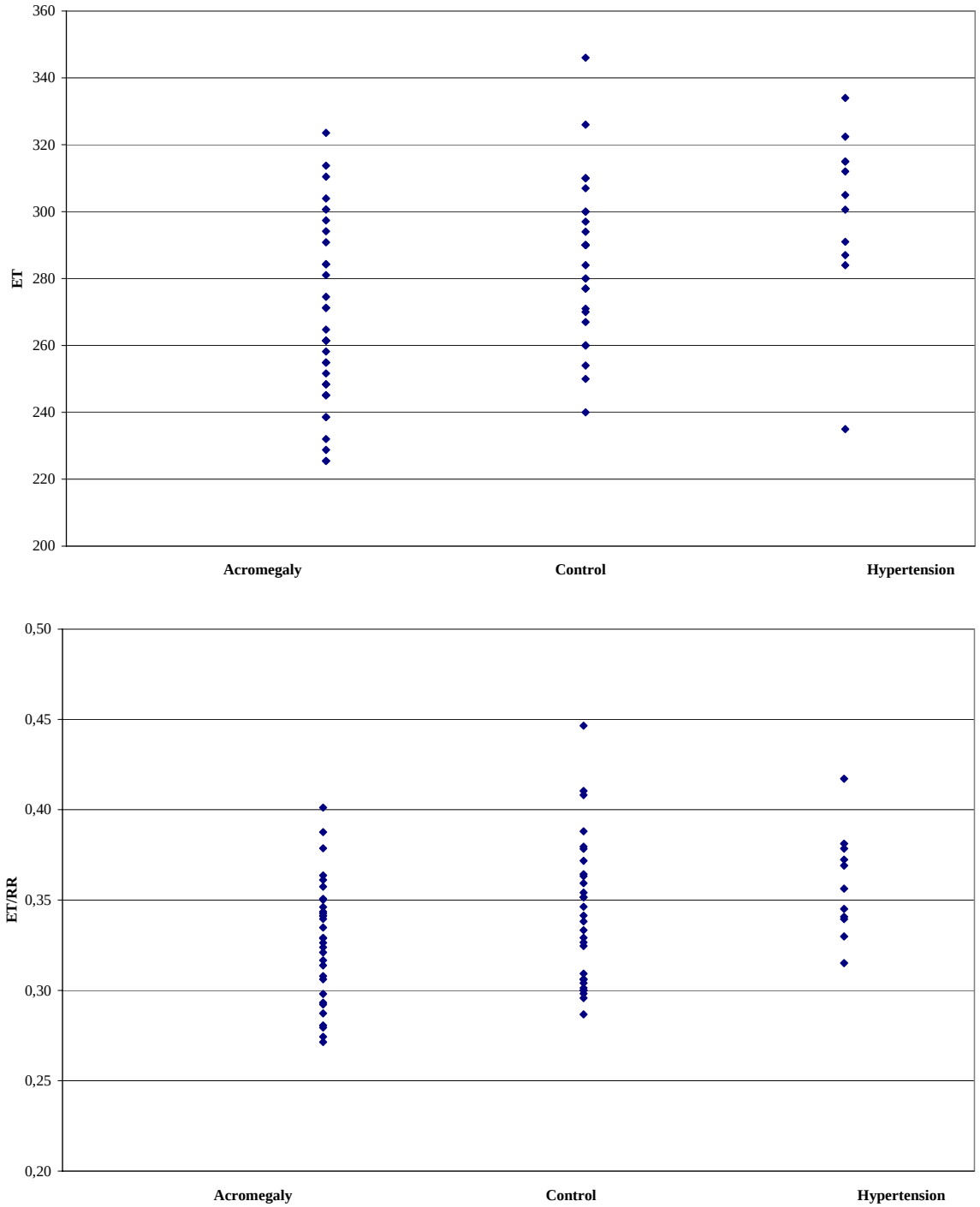

Figure 7.1. Values of ET and ET/R-R among the three patient groups.

7.3.3. Acromegaly Patient Subgroups and Echocardiography Measurements

Within the acromegaly group, the patients with active disease were the eldest, had the longest disease duration and the highest SBP values (P<0.03 vs. remission) (Table 7.3.). Furthermore, the group of patients with active disease had the highest LV mass, EF, VTI, SV

and CO, longest T/ET and shortest ET, although all non-significant. Notably, ET/R-R was the shortest in this group (P<0.03 vs. remission).

Although the patients with acromegaly had significantly higher BP values than the control group, they showed no significant correlation between LVMI and SBP values (r=0.43) (Figure 7.2.). Within the control group, no significant correlation was found between LVMI and ET/R-R nor LVMI and VTI (r=0.13 and r=0.37, respectively) (Figure 7.3. left). A significant correlation was absent between these parameters within the arterial hypertension group as well (r=0.15 for both correlations). Conversely, the acromegalic patients presented a negative correlation between LVMI and ET/R-R (r=0.34) and a positive correlation between LVMI and VTI (r=0.58) (Figure 7.3. right).

	Remission (n=12)	Active disease (n=25)	Acromegaly all (n=37)
Age (years)	45.3±8.3	52.4±10.9*	50.1±10.5
gender (male/female)	5/7	13/12	17/20
Disease duration (years)	3.5±2.8	8.0±6.6*	6.5±6.0*
GH (mIU/L)	1.7±3.0	27.5±46.5*	18.4±39.2*
IGF-I (nmol/L)	41.3±20.2	108.5±41.9†	86.1±48.1†
EF (%)	63.3±8.3	66.9±10.9	65.7±10.1
SBP (mmHg)	126.0±10.5	138.1±21.1*	134.6±19.4
LVM ASE (g)	176.8±72.4	196.6±36,1	189.8±51.3
LVMI (g/m^2)	87.9±28.2	97.9±21.6	94.5±24.2
LVH (pts/%)	2/17	4/16	6/16
ET (ms)	273,4±28.2	264,1±26,9	267.4±27.3
ET/R-R	0.34±0.03	0.32±0.03*	0.33±0.03
T/ET	0.24±0.06	0.26±0.05	0.25±0.05
AV VTI (cm)	21.8±4.5	24.8±5.0	23.8±5.0
AV SV (mL)	150.7±51.2	162.5±65.5	158.3±60.1
AV CO (L/min)	10.7±4.3	12.4±4.6	11.8±4.5

Table 7.3. Acromegaly Patient Characteristics and Echocardiography Measurements

** P<0.03 vs. remission, † P<0.00005 vs. remission*

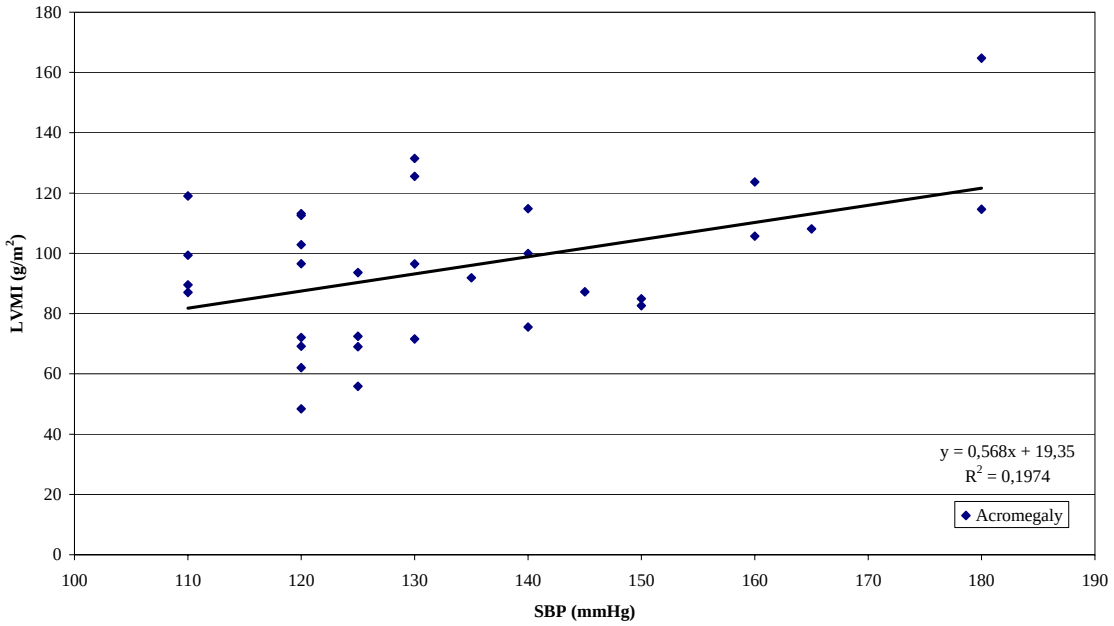

Figure 7.2. The correlation between SBP and LVMI in acromegaly patients.

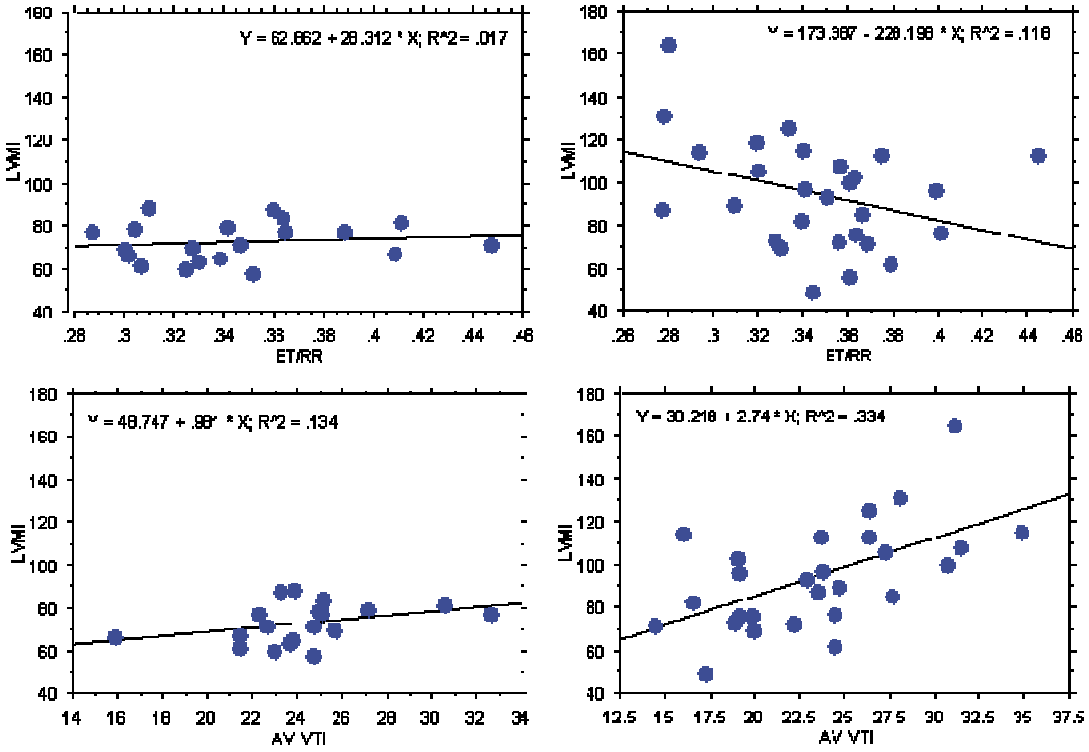

Figure 7.3. The correlation between ET/RR and VTI vs. LVMI in the control group (left) and acromegaly patients (right).

7.4. Discussion

In this study we have demonstrated that the visually hyperkinetic LV with normal EF, before the onset of functional impairment, is associated with Doppler signs of increased contractility in acromegalic patients. The values of stroke volume and cardiac output are substantially greater than in patients with hypertension or the control group, while a significantly shorter ET/R-R in acromegalic patients implies increased LV contractility, leading to a more rapid outflow phase. Notably, the values of EF did not differ between the three groups. In acromegalics, a shorter ET/R-R as well as an increased VTI (indicating increased outflow) correlated with an increase in LV mass.

An increase in the ejection phase indices has been demonstrated in normal subjects after short term GH administration [140]. Previous research has shown that IGF-I increases the intracellular calcium content and enhances the calcium sensitivity of myocyte myofilaments [141], which is found to be the most likely mechanism of increased myocardial contractility in animal models of chronic GH excess [32, 129]. Furthermore, it is known that active force development in the myocytes peaks around 1/3 of the ejection, after which it decreases rapidly [52]. This implies that the early LV outflow acceleration is caused by active myocyte contraction, while flow decelerates when force development declines, explaining why flow acceleration increases with increased contractility. Sabbah et al. have demonstrated that the peak acceleration of aortic blood flow assessed non-invasively with a CW Doppler velocity meter is a useful indicator of global LV performance [62], thus confirming data from experimental setups as well [61]. Hatle et al showed that the relative timing of the maximal aortic flow occurred later in LV heart failure, while the lowest values of time to peak velocity were found in patients with hyperkinetic heart syndrome or with considerable aortic regurgitation [59]. In a previous study, we have observed that the aortic outflow velocity profile is altered in the presence of coronary artery disease in which the flow profile becomes more symmetrical and rounded with a delayed time to peak velocity, whereas it is asymmetrical and triangular in normal subjects [142]. Additionally, a very asymmetrical and early peaking profile implied increased contractility in patients prone to the development of a dynamic intracavitary gradient during dobutamine stress echocardiography.

While diastolic dysfunction may be present in early acromegalic cardiomyopathy, normal parameters of systolic function at rest have been previously described in patients early after onset of disease [143]. Nevertheless, radionuclide studies have demonstrated an impairment of EF on effort, revealing functional alterations in the majority of the studied patients, although more pronounced in higher patient age and longer disease duration [144].

Although 40% of our patients with acromegaly had concomitant hypertension, their BP values were significantly lower than within the arterial hypertension group. Moreover, a significant correlation was not found between the values of SBP and LVMI within the

acromegaly group, allowing us to consider that LVH in these patients is not a consequence of pressure overload remodelling. Additionally, an increase in pressure overload due to hypertension would lead to prolonged ET/R-R which is obviously not the case in our acromegaly group. Nevertheless, Fazio et al. have shown that systemic vascular resistance is reduced in acromegaly patients [136], which might additionally contribute to the shortened ET/R-R interval in these patients.

In this study, the values of LV mass were significantly higher within the acromegaly and hypertension patient groups than in the control group, while they were comparable among the first two groups. Nevertheless, the underlying mechanism of hypertrophic remodelling differs in acromegaly and hypertensive heart disease. Remodelling is in the first instance a response to a problem with either the muscle itself or the environment in which it has to work and is an attempt to keep on fulfilling the heart's task - circulating the blood [145]. Hypertrophic remodelling in hypertension is an adaptive process to an increase in wall stress occurring in pressure overload [9]. Wall stress is directly related to the intracavity pressure and the radius of curvature of the ventricle while it is inversely related to wall thickness. Therefore, as a response to increased wall stress, an increase in wall thickness i.e. ventricular hypertrophy will be induced, being an adaptive process which leads to a reduction of wall stress. Conversely, early stage acromegalic cardiomyopathy comprises biventricular hypertrophy, which is, unlike hypertensive heart disease, initiated in the absence of an increase in wall stress [136] and is predominantly induced by the direct effects of chronic GH and IGF-I excess, inducing myocyte hypertrophy.

Although the values of LVMI were significantly higher in our group of acromegalic patients compared to the control group, only mild, initial LVH was present in most of our patients. Compared to data from Fazio et al. studying a group of young patients with short term (<5 years) acromegaly [146], although older in age and with longer disease duration, our group of patients had lower values of LVMI and signs of (supra)normal systolic function, thus being representative of early stage acromegaly.

The stroke volume and cardiac output were significantly increased in the acromegaly group, in the absence of any valve regurgitation, shunt or anemia. Although GH has been shown to induce sodium retention and volume expansion [147-149], which might additionally explain the increased LVIDd measurements in the context of volume overload, the only explanation for the increased SV is the increase in contractility due the hypertrophy in the absence of increased pressure loading. The increase in volume flow in the aorta results in an increase in wall shear stress, which in itself will induce vessel dilatation [150]. This can explain the observed increase in the aortic root size.

Thus, the increase in aortic root diameter in acromegaly is likely to be secondary to the increase in contractility and SV occurring in the early course of the disease.

Unlike other forms of hypertrophic remodelling which often lead to early signs of myocardial fibrosis detectable by late gadolinium enhancement imaging, CMR performed in patients with acromegaly has not shown signs of myocardial fibrosis [151]. Therefore, before the onset of disease progression and development of heart failure, acromegalic cardiomyopathy may be considered as a model for LV hypertrophy and increased contractility without an alteration in loading conditions.

7.5. Conclusion

A significantly higher degree of LVH in patients with acromegaly compared to normals and hypertensive patients is associated with a shorter ET/R-R suggesting the presence of increased contractility in the acromegalic hearts, resulting in an increase in outflow, both of which are not induced by changes in loading. Additionally, the aortic diameter is increased, most likely due to the increased wall shear stress induced by the volume increase. Thus acromegalic heart disease, at an early stage, shows evidence of hypertrophy and hypercontractility without an additional change in afterload resulting in increased cardiac output and inducing additional signs of vascular remodelling.

Chapter 8

The New Role of Echocardiography in the Diagnosis and Assessment of Hypertrophic Myopathies *

8.1. Introduction

Echocardiography plays a leading role in the assessment and diagnosis of hypertrophic ventricles in daily clinical practice. However, since the current clinical assessment of the hypertrophically remodelled myocardium is mostly performed using M-mode based geometric measurements and global measurements of left ventricular function, it is traditionally assumed that diastolic properties are primarily impaired, while systolic function is preserved until late in the course of the disease. Furthermore, as opposed to ischaemic heart disease, hypertrophic myopathies are considered to globally affect the myocardium.

Unlike physiologic hypertrophic remodelling which may be seen in athletes, examples of cardiac conditions leading to myocardial hypertrophy are:

- Reactive hypertrophy due to pressure overload in hypertension or aortic stenosis: hypertrophy will compensate the increase in afterload until high values of wall stress induce irreversible damage.
- Hypertrophic cardiomyopathy (HCM), amyloidosis, Fabry's disease, Friedreich's ataxia: if undiagnosed and untreated, the final stage of heart involvement results in impaired systolic and diastolic function with low cardiac output leading to congestive heart failure.

In all of these diseases, a better insight in the pathways of adaptive changes in cardiac function together with better and more specific evaluation, might help to improve patient management, where for the long-term prognosis, it would seem preferable to prevent the occurrence of myocardial fibrosis and irreversible myocyte degeneration, prevent arrhythmias and optimise diastolic function. Thus, it is of high clinical importance to detect and treat myocardial dysfunction at an early stage, preferably prior to the onset of irreversible myocite injury.

Recent advances in echocardiography have provided insight in regional myocardial motion and deformation. Ultrasound deformation imaging (through Doppler myocardial imaging (DMI) or speckle tracking) provides more sensitive markers of early myocardial dysfunction, compared to standard echocardiographic parameters [1]. Both basic and clinical

* From: Cikes M, Bijnens B, Anderson L, Sutherland G. The New Role of Echocardiography in the Diagnosis and Assessment of Hypertrophic Myopathies. Submitted for review.

research, applying deformation analysis tools, has put a focus on the regional level in hypertrophic ventricles, revealing early, often subclinical impairment in systolic (longitudinal) function and providing better insight to understanding the pathophysiological mechanisms underlying the progression of disease. From this, it has become clear that each of the different etiologies leading to (regional) hypertrophy have a specific signature in regional changes in deformation. Therefore, these specific markers can be used to discriminate the hypertrophic processes and to improve the assessment and follow-up of treatment.

8.2. Ventricular Remodelling

Ventricular remodelling is a mechanism by which the ventricle reacts and tries to adapt to a problem, either intrinsic to the myocardium or related to the environment it has to interact with, intended to generate an adequate cardiac output as required by the peripheral organs (figure 8.1.). However, such an adaptation implies inherent disadvantages and may induce irreversible myocardial damage, potentially evolving into cardiac dysfunction and heart failure.

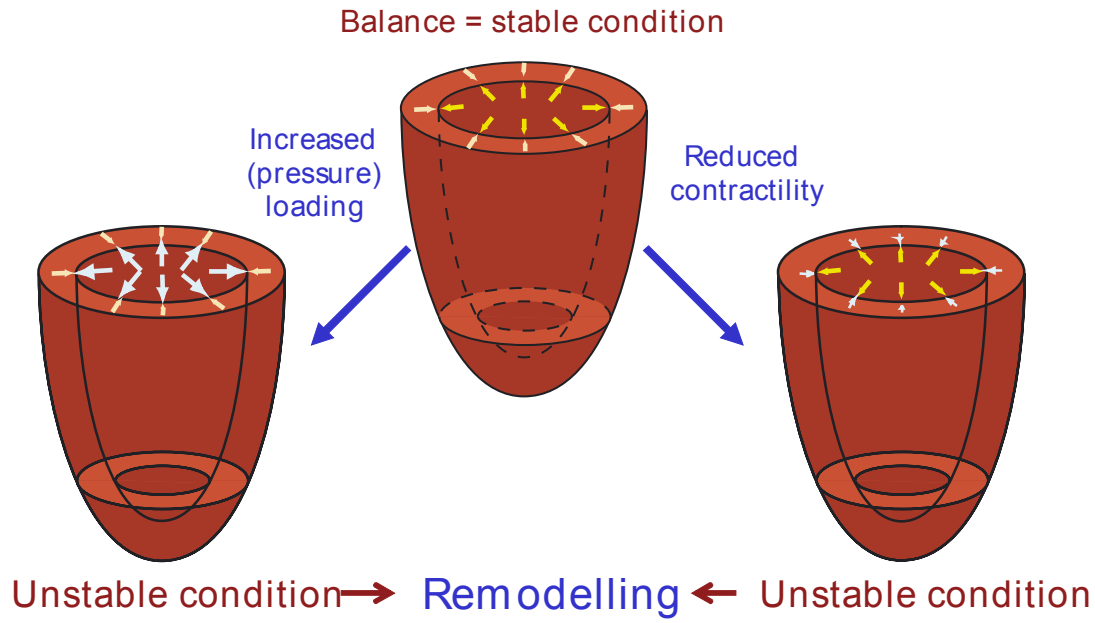

Figure 8.1. Balance of cardiac contractility and loading.

Remodelling is triggered by the average local myocardial wall stress. Wall stress is dependent on the ventricular pressure, which is transferred to the myocardium depending on the local geometry (radius of curvature and wall thickness) (figure 8.2.). Grossman et al. have suggested that increased peak systolic wall stress (as seen in pressure overload)

stimulates the formation of hypertrophy by parallel replication of contractile material within the myocyte (figure 8.3.) [33, 152]. Conversely, the trigger for ventricular dilatation is the increase in end-diastolic wall stress (typically seen in volume overload), releasing factors within the myocardium that will stimulate the serial lengthening/replication of the sarcomeres, effectively resulting in the enlargement of the cavity. However, it has to be kept in mind that dilatation itself will change the geometry of the cavity and by increasing the local radius of curvature will increase wall stress (and potentially trigger the development of local hypertrophy, as well).

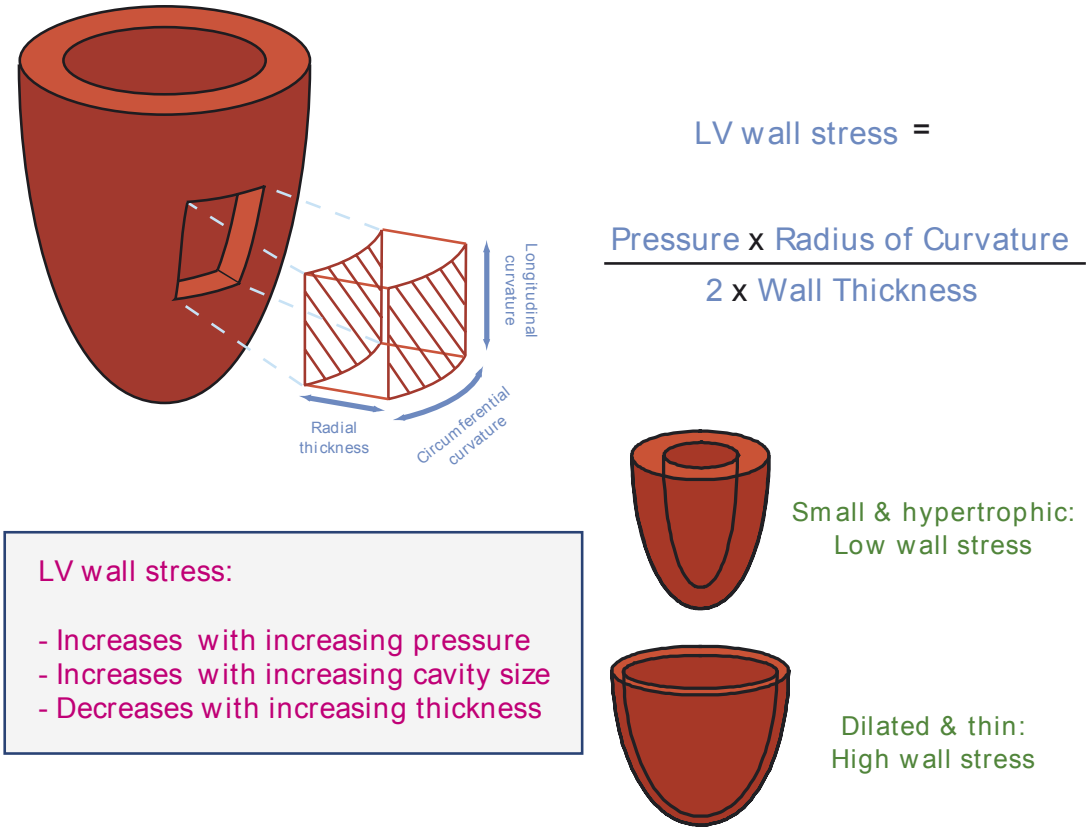

Figure 8.2. Myocardial wall stress and its determining factors.

Most non-ischemic remodelling, like left ventricular hypertrophy (LVH), has classically been considered as a substrate affecting the ventricle *globally*. However, it has been shown that e.g. arterial hypertension results in localized LVH [9] due to regional differences in wall stress, suggesting that *regional* phenomena might play a more important role than previously assumed in clinical practice. This implies that enhanced understanding of LV remodelling might still lead to improved treatment of these patients.

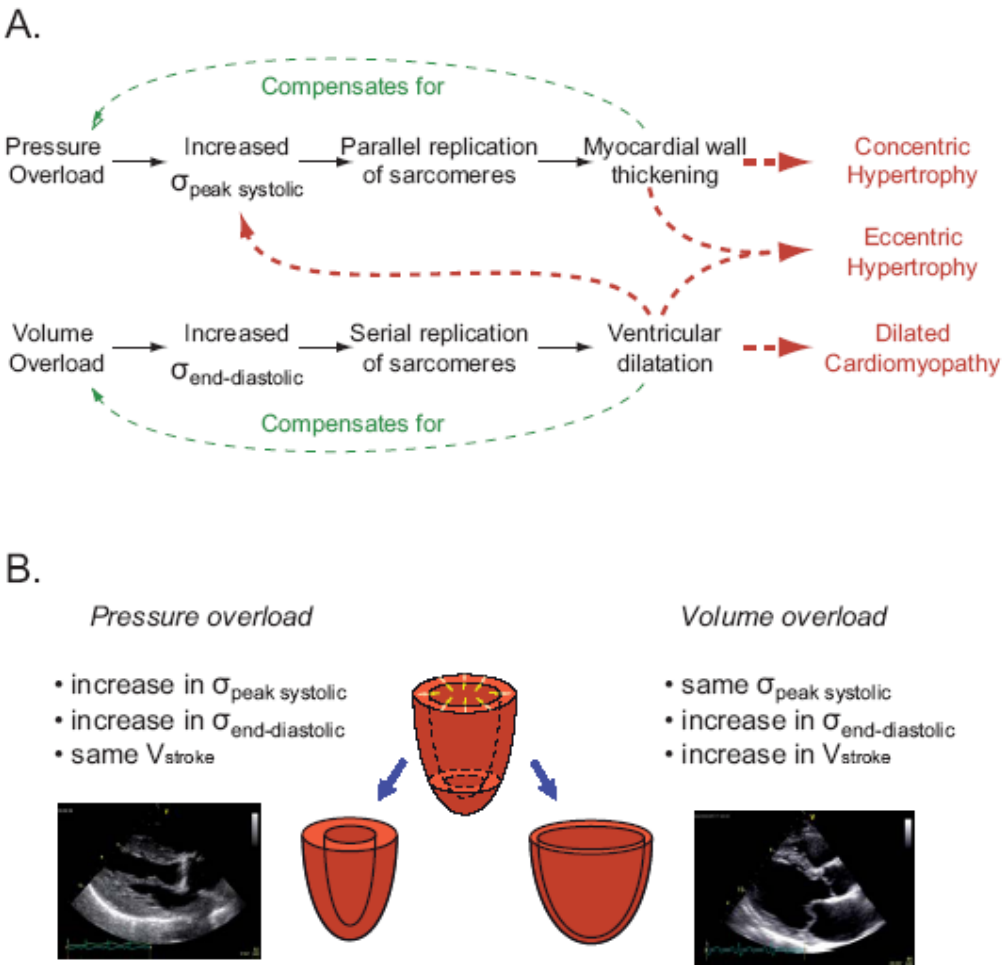

Figure 8.3. A. Mechanisms for ventricular remodelling (adapted from [33]). B. Pressure versus volume overload.

For the clinical evaluation of patients with signs of ventricular remodelling, a good method which can evaluate and track the evolution of intrinsic cardiac function is necessary. However, this is influenced by abnormal loading conditions and altered ventricular geometry, which can be found in several of these heart diseases, importantly affecting the current methods used to evaluate cardiac function.

8.3. Normal Myocardial Motion and Deformation

Two-dimensional (2D) echocardiography allows the assessment of the heart's geometry and the presence of ventricular hypertrophy by quantifying cavity sizes, wall thickness and calculating the myocardial mass (index) [18], while Doppler echocardiography provides direct insight to cardiac haemodynamics. In the evaluation of (systolic) myocardial function, the intrinsic fibre and myocyte properties are of utmost importance, since they determine

whether a chronic condition has affected the myocardium and thus when irreversible injury has been induced. Currently, in everyday clinical practice, only indirect measurements of contractility and volume ejection are being used, mainly derived from non-invasive cardiac imaging techniques such as echocardiography, computed tomography (CT) and cardiac magnetic resonance imaging (CMR), using indices as ejection fraction (EF) or fractional shortening. These volume-derived parameters are associated with significant limitations in the event of altered loading conditions: (I) the evaluation of intrinsic myocardial function based on volume-derived indices, i.e. EF or fractional shortening, relies on geometric assumptions. The influence of ventricular shape and wall thickness on these indices is not well known. In hypertrophic ventricles, 'supranormal' values of EF are frequently measured - it is not well known whether these values are reflective of true contractility changes [17]. (II) Another limitation of all volume derived indices is important load dependency. During the progression of the disease, alterations in loading conditions or geometry will influence the (global) functional evaluation. (III) Furthermore, conventional imaging indices assess only global cardiac function while the evaluation of regional cardiac function is relevant in most conditions affecting myocardial contractility. Moreover, some of the methods evaluating global function focus entirely on radial indices, omitting longitudinal function that is affected prior to the changes in radial function in most cases of cardiac pathology [19]. An increase in radial function often compensates for the impairment of global longitudinal function. (IV) Finally, measurements of global function do not consider segment interactions which may only result in regional wall deformation, not contributing to pressure increase or a reduction in overall ventricular volume to contribute to stroke volume [20, 145].

In the context of these limitations, new echocardiographic methods focusing on regional ventricular function have been proposed. Doppler myocardial imaging (also known as Myocardial Velocity Imaging or Tissue Doppler Imaging) as well as greyscale (2D) speckle tracking are recent echocardiographic techniques that allow to quantify myocardial segmental motion [1]. Post-processing of velocity data or image-processing of greyscale data, allow the calculation of regional myocardial deformation. Myocardial deformation can be quantified by strain rate or the speed of deformation, as well as by strain or the amount of deformation. When using myocardial velocities, strain rate is calculated as the spatial derivative of local (neighbouring segment) myocardial velocities, while strain is derived as a temporal integral of strain rate. Tracking the motion of the speckle patterns of greyscale images provides potentially similar information. Unlike a normal base-apex gradient occurring in myocardial velocities (with the highest velocities at the base of the heart), a relatively homogenous distribution of peak systolic strain(-rate) values appears within the LV walls, Furthermore, the main limitation of velocity data is the influence of myocardial segment interaction (tethering of adjacent segments) and overall heart motion. This limitation has

been resolved by deformation imaging, as it measures local changes of deformation within a myocardial segment and should thus better reflect intrinsic contractile function [1].

The longitudinal motion/deformation (describing the basal LV displacement towards a stationary apex) can be evaluated from an apical view. From a parasternal (short- and/or long-axis) view, the inward radial deformation (best with Doppler based techniques) as well as the circumferential shortening (best with speckle tracking approaches) can be measured [145].

The deformation of a myocardial region throughout the cardiac cycle [10] (Figure 4 A) consists of normal deformation (i.e. longitudinal lengthening/shortening, radial thinning/thickening as well as circumferential lengthening/shortening) and shear (i.e. base-apex twist, epi-endocardial circumferential shear and epi-endocardial longitudinal shear) [1, 25, 26].

Figure 8.4. B shows a typical longitudinal deformation (strain) and speed of deformation (strain-rate) trace from a normal adult (obtained by high frame-rate DMI). Deformation is relatively homogenous in the normal myocardial wall while its patterns will be distorted in different cardiac pathologies. When applying Doppler based approaches, radial and longitudinal motion and deformation are mostly studied, since circumferential motion is difficult to align with the ultrasound beam, which is required by this method. It has been shown that speckle tracking is more reproducible and is less dependent on user expertise, while it inherently requires more temporal and spatial averaging of the obtained traces, which results in significantly lower measured values than DMI and less sensitivity to detect smaller abnormal myocardial segments [28, 30, 31, 145].

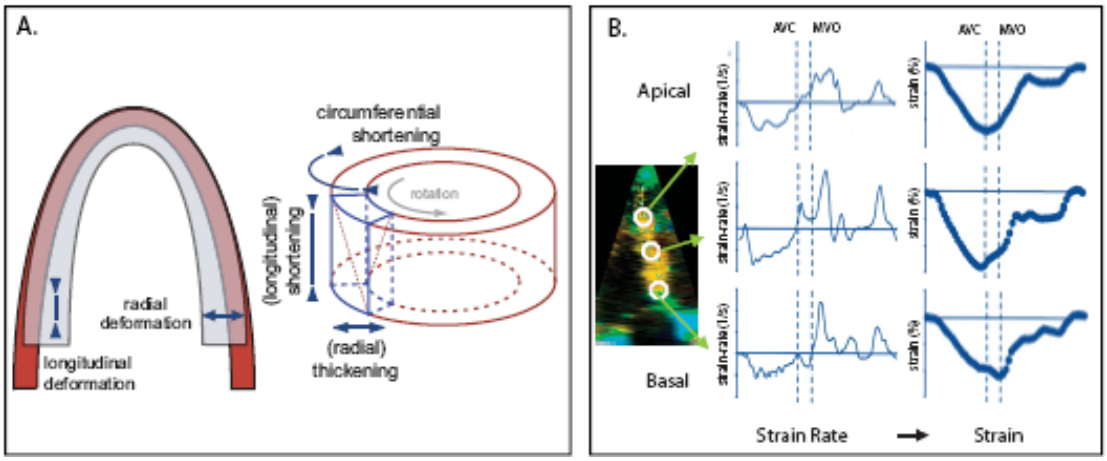

Figure 8.4. A. Normal myocardial motion and deformation and its three major components: longitudinal, radial and circumferential motion/deformation;
B. Typical profiles of strain-rate and strain traces (adapted from [145]).

8.4. The Athlete's Heart

The "athlete's heart" is a form of physiologic hypertrophic remodelling which may occur as a consequence of long-term exercise training [153]. Magnetic resonance spectroscopy studies have supported that ventricular hypertrophy in athletes is associated with a normal cardiac energy metabolism, both at rest and during atropine-dobutamine stress [154, 155]. However, long term LV adaptation in very high-level endurance athletes may also lead to LV cavity dilatation [156]. Morganroth et al. were the first to demonstrate that different hypertrophic remodelling patterns are associated with two basic training substrates: isotonic exercise (such as swimming or running) leads to an increase in LV mass and mean LV end-diastolic volumes, similar to chronic volume overload, while isometric exercise (wrestling, shot putting) induces an increase in LV mass as well, although with normal values of mean LV end-diastolic volumes, mimicking chronic pressure overload, which was supported by further research [157, 158]. Similarly to humans, exercise induced remodelling has been described in animals as well [159]. As opposed to pathological LVH, which is characterized by structural changes and collagen accumulation along with myocyte hypertrophy, physiological LVH results in an increase in ventricular mass with underlying normal cardiac structural organization and no collagen increase [103, 160, 161]. In an animal study performed by Derumeaux et al. it has been demonstrated that both exercise and aortic banding lead to similar and significant LVH. Nevertheless, systolic and diastolic myocardial velocity gradients (i.e. strain-rates) were similar in sedentary and exercising rats (indicating that exercise leads to physiologic hypertrophy, not influencing myocardial function), while the gradients were significantly reduced in rats with aortic banding (pathologic hypertrophy occurring due to an increase in afterload, reducing systolic function) [103].

In a study comparing patients with HCM, systemic hypertension and athletes, Vinereanu et al. have demonstrated a decrease in long-axis systolic and early diastolic velocities in patients with pathologic hypertrophy, while these parameters were preserved in athletes. [10].

It has also been shown that athletes with LVH have enhanced global and long-axis diastolic function, compared to sedentary normals [10, 162]. Another study of athletes' regional myocardial function has shown higher systolic and diastolic velocities in several LV regions, while deformation parameters (strain and strain rate) showed normal values of these parameters in athletes when compared to the control group, although with a tendency to somewhat higher mean values [163]. Myocardial deformation studied in athletes with LVH demonstrated an overall normal myocardial deformation [164]. Finally, a "supranormal" LV velocity pattern (including both systole and diastole), as well as "supranormal" values of systolic strain rate have been described in several studies on athletes with LVH [165-167]. This was supported by 2D strain data demonstrating higher values of transverse and radial

strains in athletes (compared to patients with HCM and normals), while in pathologically hypertrophic segments longitudinal strain was lower in patients with HCM than in athletes [168].

8.5. Pressure Overload (Hypertensive Heart Disease and Aortic Stenosis)

Typical examples of hypertrophic remodelling induced by pressure overload are hypertensive heart disease and aortic stenosis. Hypertensive LVH is characterized by increased LV mass and relative wall thickness [68] and may be associated with reduced global systolic function, due to longstanding pressure overload. Nevertheless, due to increased radial systolic performance associated with hypertrophy, standard indices of global systolic function such as EF and short axis endocardial shortening may be supranormal in early stages of the disease [19, 169, 170]. Beside increased radial systolic function, an increase in circumferential systolic function and systolic torsion, measured by 2D speckle tracking echocardiography, were demonstrated in hypertensive patients [171, 172], while the LV radial and circumferential systolic impairment appears in patients with heart failure symptoms NYHA III and IV class [173]. Conversely, reduced longitudinal systolic function has been well documented at early stages in patients with hypertension, both by conventional echocardiography, velocity and deformation imaging, as well as CMR tagging [9, 10, 174]. Although hypertensive left ventricular hypertrophy is mostly considered to be a global myocardial disease, resulting in concentric (symmetrical) LVH and overall reduction of deformation parameters, it has been shown that the distribution of LV wall stress on different LV segments is not homogenous, being significantly greater upon the septal wall [175]. Further studies have shown that the basal septal segment, being under increased wall stress associated with a greater local radius of curvature, is the first to show changes under the influence of pressure overload: both a decrease in deformation parameters (strain, strain-rate) as well as the development of post-systolic deformation and localized hypertrophy occur (figure 8.5.) [9, 176]. The initiation and localization of functional abnormalities in the basal septum has been confirmed by 2D speckle tracking as well [172]. With increasing overload, the entire ventricle becomes hypertrophic and shows less deformation.

Strotmann et al. have compared patients with preserved EF and the same extent of LVH induced by arterial hypertension or aortic stenosis [105]. Generally, the systolic segment of the strain-rate profile was more flattened in patients with aortic stenosis. Radial and longitudinal systolic strain rates were depressed in patients with aortic stenosis, compared with those with arterial hypertension and controls. This was contributed to higher wall stress due to higher LV end-systolic pressures as well as a higher amount of perimyocytic fibrosis, which was previously demonstrated in patients with aortic stenosis, compared to those with

hypertension [177]. Furthermore, regional differences in deformation parameters were noted in a study on patients with aortic stenosis by Kowalski et al: longitudinal deformation was inhomogeneous between the base and apex, with basal segments having significantly lower strain/strain rate values than apical segments [22]. A prospective follow-up study by Weidemann et al, investigating the effect of myocardial fibrosis on myocardial performance in symptomatic severe aortic stenosis, demonstrated the development of myocardial fibrosis, typically located subendocardially at the basal segments of the LV. This type of fibrosis, demonstrated by CMR LE, was found to have a profound impact on long-term clinical outcome in these patients. Nevertheless, such fibrosis remains undetected by standard echocardiography until the terminal disease stages, but its functional consequences can be detected by longitudinal mitral ring displacement which predicts functional improvement after valve repair [178].These findings suggest that remodelling in aortic stenosis may be seen as a continuation of the adaptation to pressure overload (systolic wall stress), underlying regional remodelling in hypertension.

A discrimination between hypertensive LVH and non-obstructive HCM has been suggested by Kato et al, based on the septum/posterior wall thickness ratio and averaged longitudinal systolic strain values of eight myocardial segments [179]. A systolic strain cutoff value of -10.6% discriminated between HCM and hypertensive LVH with a sensitivity of 85%, specificity of 100% and predictive accuracy of 91.2%, with lower values in the HCM group of patients. This is supported by the finding that, while decreased deformation is present in the basal septum in hypertensive heart disease, it is never as low as showing almost absence of deformation, as observed in HCM [176]. Thus, an average value of systolic strain in several myocardial segments will be lower in HCM. Therefore, basal septal deformation is the most sensitive to changes in pressure overload pathology, emphasizing the regional nature of initial remodelling. Finally, with increasing overload, hypertrophy is induced over the entire ventricle, but reactive hypertrophy will cope with the increased afterload until wall stress becomes so high that irreversible damage (fibrosis) occurs [99].

8.6. Hypertrophic Cardiomyopathy

Hypertrophic cardiomyopathy is a disease with autosomal dominant transmission, caused by mutations in the genes encoding protein components of the cardiac sarcomere, occurring in 1:500 of the general population [180-182]. Due to the fact that the defective genes encode contractile proteins such as myosin - binding protein C, β – myosin heavy chain, Troponin T and I, it leads to a *disorder of force generation* within the myocardium [180].

In the recent years, molecular genetic and clinical research have demonstrated that there is not a minimum LV wall thickness required to be compatible with the presence of one of the

HCM mutant genes [183-188]. In combination with age-related penetrance and delayed appearance of LVH on echocardiography in adulthood (most often associated with myosin – binding protein C defects [183, 184, 189], these novel findings make it no longer possible to exclude the diagnosis of HCM in family members solely based on a normal echocardiogram.

The clinical diagnosis of HCM is most often established with echocardiography, which was traditionally found to demonstrate non-dilated LVH in the absence of hemodynamic stresses (arterial hypertension, aortic stenosis) or systemic disease (amyloidosis or storage diseases) capable of inducing such hypertrophy, regardless of the presence of LV outflow tract obstruction [181, 182, 190-195]. However, a substantial overlap is present between echocardiographic findings in patients with HCM and those with hypertensive LVH [196-200]. Furthermore, it is considered that HCM predominantly affects the heart's diastolic function [201-204], while the systolic properties remain intact (at least in the initial disease period). This is mostly due to the assessment of intrinsic function based on volume parameters, such as fractional shortening and EF, which often yield 'supra-normal' values of EF in hypertrophied ventricles [19, 145, 174, 205-207]. Moreover, these conventional parameters only assess global function and concentrate only on radial function, ignoring longitudinal function, which in most cardiac pathology is altered before changes occur in radial indices [19]. Increased radial function often acts as a compensation for the reduction in global longitudinal function [145].

In a mouse model of familial HCM, cardiac dysfunction (reduced myofibrillar shortening) was shown to precede histopathologic changes [209]. Transgenic mice models of HCM have shown decreased sarcomere length, systolic shortening and shear strain in segments with more pronounced hypertrophy. Myofiber disarray was associated with reduced septal torsion and reduced surface shortening [210]. Using regional deformation analysis, these areas of histological abnormalities can be easily localized since they do not show any systolic deformation, while the rest of the (hypertrophic) segments still deform (although mostly much reduced compared to normal) [168, 179, 211-214]. Studies performed to quantify deformation in HCM have found a decrease in regional deformation in such patients when compared to the control group. However, the localization of fiber disarray areas can vary in localization and size among patients with HCM [215, 216]. Recently, it has been shown in children with HCM that, despite normal echocardiographic indices of global LV systolic function, longitudinal and radial deformation are reduced, where the reduction in deformation is inhomogeneous and correlates with the regional pattern of hypertrophy. Furthermore, increased post – systolic shortening/lengthening (often found in ischaemic myocardium) and delayed mechanical activation were associated with decreased peak systolic deformation in the hypertrophic segments, emphasizing the regional nature of myocardial involvement [20, 217]. A similar pattern of regional deformation was found in a study by Weidemann et al.

which describes the “double peak sign” (the second strain – rate peak resulting from post – systolic deformation) as a typical deformation pattern seen in hypertrophic segments with fibrosis, which was confirmed by CMR LE [218]. Moreover, it has been demonstrated that the detection of non-deforming regions, using ultrasonic strain (-rate) imaging allows for easy and accurate discrimination between patients with HCM and other forms of hypertrophy (hypertension), where the non-deforming regions were most often found in the anterior septum and anterior wall (figure 8.5.) [176]. Similar segmental abnormalities were demonstrated by circumferential, radial and longitudinal 2D-strain in the septal, anterior septal and anterior walls as well [219]. Regional impairment of systolic deformation indices was also demonstrated in a DMI study employing strain(-rate) imaging by Kato et al. which has shown a correlation between regional systolic strain/strain rate and LV wall thickness in patients with HCM, unlike in patients with hypertensive LVH, demonstrating that heterogeneity of regional LV systolic function detected by deformation imaging is partly attributable to heterogeneity of LVH, suggesting the link to impaired global LV relaxation in HCM [220].

Finally, CMR studies have confirmed the regional pattern of myocardial involvement in HCM: CMR tagging data suggest a heterogeneous reduction in shortening and thickening of the myocardium which is inversely correlated with end-diastolic wall thickness (reduced thickening occurring in HCM patients), while regions of delayed enhancement which correspond to tissue with reduced circumferential deformation can be found, such that focal nodular enhancement is particularly related with regional dysfunction in patients with HCM [221-223].

Unlike strain/strain–rate indices, which can demonstrate reduced deformation before the occurrence of apparent LVH, a study performed in patients with mutations in TNNI3, focal fibrosis was not detected by late gadolinium enhancement CMR before LVH and ECG abnormalities were present [224].

8.7. Amyloidosis

Amyloid cardiomyopathy can occur within several known forms of systemic diseases – amyloidoses [225, 226]. **Primary amyloidosis (AL)**, associated with plasma – cell dyscrasia, is the commonest form in which the heart is involved in around 50% of the cases with rapidly progressive signs and symptoms of predominantly right heart failure (occurrence of which is the worst prognostic factor in this group of patients) [227, 228]. **Secondary amyloidosis (AA)** is increasingly uncommon and typically clinically insignificant [225, 229, 230], while **hereditary (familial) amyloidosis** involves the myocardium, but not as common as AL amyloidosis. Hereditary amyloidosis is transmitted as an autosomal dominant disease with

an onset predominantly after the age of 40 [225]. It occurs mostly due to transthyretin protein mutation which then produces amyloid [231]. Thus, the pattern of cardiac involvement varies according to the mutation, while it is generally less aggressive than the AL type. **Senile systemic amyloidosis** results from the deposition of amyloid derived form the wild – type transthyretin, invariably presents as congestive heart failure and is linked to a longer median survival than the AL type [225, 232, 233]. **Isolated atrial amyloidosis** is a common finding at autopsy, being the only non systemic deposition, limited to the atrium [225, 235, 236].

Due to widespread amyloid deposits throughout the heart, endomyocardial biopsy is virtually 100% sensitive in detecting amyloid cardiomyopathy [236, 237]. Regardless of the type of amyloidosis, *extracellular deposition* of amyloid throughout the heart results in biventricular wall *thickening* (rather then hypertrophy), associated with a restrictive pattern detected by Doppler echocardiography [225]. Although these findings are typical of end - stage disease, diastolic dysfunction can be mildly impaired while its progression suggests progressive myocardial infiltration [238].

It has been shown that amyloid deposits induce oxidant stress that depresses myocyte contractile function [239, 240]. Furthermore, amyloid infiltration of the myocardium interrupts contractile function which, with progression, can lead to myocyte necrosis and interstitial fibrosis, resulting in systolic dysfunction. Conversely, LV ejection fraction assessed by conventional echocardiography is considered to remain normal until the late stages of the disease. Initial DMI studies were based on pulsed DMI and have demonstrated accuracy in detecting the presence of diastolic dysfunction as well as the ability to detect impairment in longitudinal systolic function which occurs prior to abnormal LV EF [241, 242]. More recent studies implementing strain/strain – rate imaging have confirmed the diffuse pattern of the disease (primarily affecting longitudinal function), as well as showing superiority of the technique in early detection of impaired LV systolic function: a reduction of longitudinal systolic strain in all 16 myocardial segments was shown in patients with systemic AL without echocardiographic or Doppler evidence of cardiac involvement. This was reflected in the mean systolic strain values of the 6 or even 3 relevant basal segments (basal inferoseptal, anteroseptal and posterior segments) as well which were demonstrated as the most accurate DMI measurements to differentiate patients with AL with normal echocardiograms from the controls [243].

In line with pathological findings as well as with DMI studies demonstrating diffuse myocardial involvement in amyloid cardiomyopathy, **CMR studies** have shown global subendocardial late gadolinium enhancement as well as abnormal myocardial and blood-pool gadolinium kinetics [244]. The subendocardial/subepicardial involvement leads to a severe reduction of the contractility of the longitudinally oriented fibers and results in the virtual absence of longitudinal deformation in amyloid cardiomyopathy (figure 8.5.), especially

in the basal segments. This is compensated by radial/circumferential shortening, being the only deformation generating the cardiac output.

8.8. Systemic Diseases

Although heart involvement in systemic diseases is variable, the evaluation of myocardial involvement is important in the initial diagnosis of the disease as well as in disease progression monitoring. In diseases for which a specific therapy is available, follow up data on the impact of therapy is of high importance [245-247]. However, in subclinical disease stages, commonly applied echocardiographic parameters (such as EF calculations) are often insensitive to subtle functional impairment [248-250]. Moreover, a later onset of global changes which can be detected by routine echocardiography can be anticipated by detecting preceding regional changes. Traditionally, metabolic disorders are most often linked with concentric hypertrophy [180].

Recent research within this group of diseases provides evidence of regional LV involvement, detectable by deformation imaging. Even in early stages of disease, signs of similar remodelling of the basal “free” LV wall are detectable by reduced systolic deformation which may be associated with post-systolic deformation.

Fabry’s disease is an X-linked genetic storage disorder leading to deficient activity of a lysosomal enzyme α – galactosidase A, resulting in intracellular, lysosomal accumulation of globotriaosylceramide [251]. Despite the severe course of the disease, its rare occurrence (estimated incidence of 1:40.000-117. 000 newborn males) and various manifestations often lead to misdiagnoses and lengthy inadequate treatment strategies [252]. In these patients, cardiac symptoms account for 50-60% of the presenting symptoms, while heart failure is among the leading causes of death at an earlier age [253]. This lysosomal storage disorder affects the myocytes, leading to LVH (most often concentric hypertrophy in 50% of the patients, followed by concentric remodelling in 37%, mostly in younger patients) with subsequent systolic and diastolic dysfunction [254, 255]. Deformation imaging data have shown a correlation between radial strain rate and myocardial wall thickness, with lower strain rate values measured in thicker walls [250]. Furthermore, it has been shown that functional abnormalities occur prior to morphologic changes, initially involving the lateral LV wall with an impairment of longitudinal systolic function preceding radial dysfunction, thus demonstrating a regional (rather than global) nature of myocardial involvement [250]. This has been supported by CMR data which demonstrate that fibrosis is initiated in the mid-myocardial layers of the basal inferolateral wall, combined with reduced strain/strain rate values in the involved regions, in which the “double-peak sign” has been described, as a

marker of post-systolic thickening [218, 256, 257]. In the end-stage of heart involvement, Fabry's disease is characterized by LVH, myocardial fibrosis (as seen on myocardial biopsy) and severely reduced regional LV function [250, 255].

In the last several years, the availability of specific enzyme replacement treatment has focused myocardial imaging studies on the follow up of these patients after enzyme replacement therapy, demonstrating both a regression of LVH and an increase of strain rate values after one year of therapy [247, 258]. Nevertheless, myocardial segments demonstrating LE as seen by CMR have shown no functional improvement during enzyme replacement therapy, suggesting that early disease detection and initiation of treatment is crucial within this patient population [259].

Friedreich's ataxia is an autosomal recessive neurodegenerative disease caused by an intron GAA triplet repeat expansion, which leads to a gene defect encoding for a mitochondrial protein (frataxin), resulting in mitochondrial dysfunction [260]. As a consequence, cellular hypertrophy, diffuse fibrosis and focal myocardial necrosis occur [261]. Myocardial involvement most often includes concentric or asymmetrical LVH, not affecting the right ventricle [248, 262, 263]. An initial DMI study performed by Dutka et al. demonstrated reduced systolic and diastolic myocardial velocity gradients in patients with Friedreich's ataxia free of cardiac symptoms [248]. Additionally, an inverse relation between the age corrected myocardial velocity gradients and the size of the GAA triple repeat expansion was demonstrated in this study, suggesting that abnormal myocardial velocity gradients might reflect myocardial involvement as a consequence of the specific genetic defect. These findings were followed by a study demonstrating marked reduction of myocardial deformation parameters in patients with Friedreich's ataxia – a marked reduction of end-systolic strain and peak systolic strain rate within the hypertrophied myocardium. Moreover, impaired systolic and diastolic deformation parameters were present in patients with Friedreich's ataxia without evidence of LVH, as well as in the non-hypertrophied segments of patients with regional LVH, suggesting that regional myocardial dysfunction precedes changes in LV geometry [255, 263]. Interestingly, the lowest values of systolic deformation properties were noted in the basal anterior and lateral LV walls, suggesting a similar pattern of regional abnormalities as seen in other systemic diseases as well [263].

Recently, it has been shown that an antioxidant drug Idebenone protects mitochondrial respiratory dysfunction [264]. In regards to the myocardium, this was confirmed in an initial study on eight patients undergoing one year of treatment in which an early linear increase in strain rate imaging parameters, reflecting an improvement in cardiac function, was demonstrated to precede the reduction of LVH [246].

Duchenne muscular dystrophy is an X-linked recessive disease caused by a mutation in the dystrophin gene on chromosome Xp21.1,2, resulting in a deficiency of the subsarcolemmal protein dystrophin, which is critical for muscle membrane stability [265, 266]. This disease is clinically associated with skeletal myopathy and dilated cardiomyopathy, leading to congestive heart failure and causing death in 30% of these patients [267]. A study by Mertens et al employing velocity and deformation analysis, performed in young patients with Duchenne muscular dystrophy and normal global systolic function, has demonstrated reductions in systolic deformation parameters in the anterolateral and inferolateral LV walls [267], thus confirming similar, regional distribution of the affected regions in different systemic diseases (figure 8.5.)

8.9. Summary

Regional deformation analysis in hypertrophic myopathies provides insight to the various underlying pathophysiological mechanisms and reveals early, often subclinical impairment in systolic function. The combination of detecting the affected myocardial region in conjunction with the deformation pattern analysis provides an indicator toward the disease underlying hypertrophic remodelling of the ventricle (figure 8.5.).

The athlete's heart often comprises hypertrophic remodelling, which in this case, is a physiologic form of ventricular adaptation. In such hearts, deformation analysis demonstrates normal or even "supranormal" ventricular systolic function.

In *hypertensive heart disease* LVH is predominantly localized in the basal septal region, where wall stress is highest, resulting in reduced systolic strain values with post-systolic shortening. With increasing pressure overload (e.g. *aortic stenosis*), the neighboring LV segments will be affected as well, until irreversible myocyte damage - fibrosis occurs.

The clinical importance of myocardial involvement in *systemic diseases* is emphasized by the availability of specific therapies. Hypertrophic remodeling is frequently seen in *Fabry's disease, Friedreich's ataxia and Duchenne cardiomyopathy,* in which a specific region - the basal (infero)lateral segment is most often affected, and which is detectable by reduced systolic deformation associated with post-systolic deformation.

Hypertrophic cardiomyopathy, is associated with regions of local fibre disarray, in which no myocardial deformation is present at all, while in the surrounding segments (often showing similar thickness), deformation is reduced, but almost normal compared to normal hearts. The absence of deformation is mostly associated with the thickest segments. Depending on the individual patient, these regions can be located anywhere within the ventricles, but are

most often localized in the interventricular septum where the basal-mid segment reveals total absence of longitudinal deformation, while radial function is still preserved.

Unlike the aforementioned diseases in which myocardial involvement is regional, amyloidosis seems to provide an exception in which the impairment of systolic function affects the myocardium globally (although with slightly more involvement in the basal regions compared to the apical). *Amyloid cardiomyopathy* presents with global LVH and diffuse, severe reduction (and even absence) of longitudinal strain, while the radial strain is still preserved, but of low values.

Figure 8.5. provides a schematic overview of basic substrates of hypertrophic remodelling as well as the pertaining longitudinal strain curves, as described above. Note that the longitudinal strain y-scale is equally set in all examples, thus providing more consistent information on the scale of deformation abnormalities.

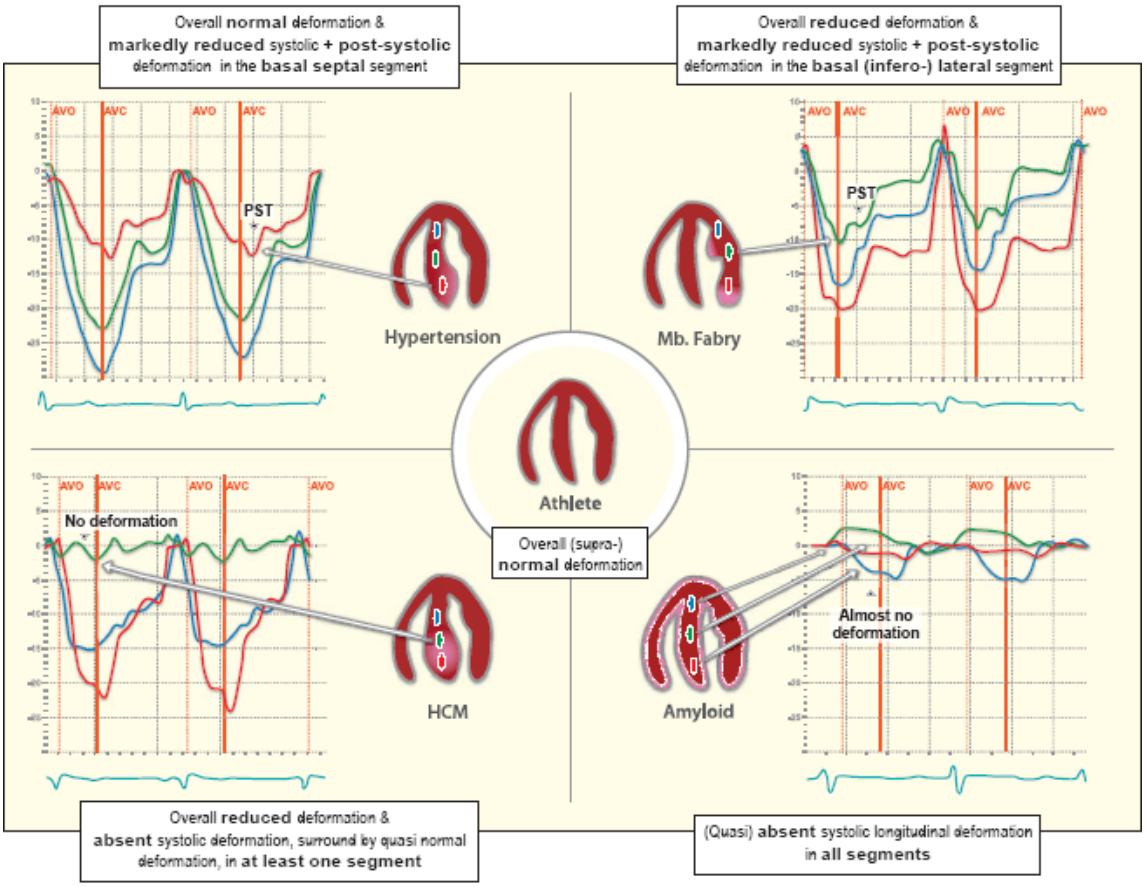

Figure 8.5. Schematic overview of basic substrates of hypertrophic remodelling and the pertaining longitudinal strain curves.

8.10. Conclusion

While all hypertrophic myopathies show thickening of the myocardial walls, they clearly represent a heterogeneous group of diseases with a wide spectrum of myocardial involvement. This heterogeneity can be appreciated from the microscopic level, to specific myocardial regions affected by the underlying disease (Table 8.1, figure 8.5.).

By the introduction of deformation imaging in clinical practice, a novel insight to regional myocardial function has been provided; since then, multiple studies provided clinical data which support the regional nature of these myopathies, frequently emphasizing the significance of induced abnormal systolic function. Furthermore, the assessment of longitudinal myocardial function proves to be of high importance: the assessment of radial function, which is routinely performed, might mask the early onset of functional impairment which most often primarily affects the longitudinal myocardial fibers. Moreover, regional phenomena such as post-systolic thickening/shortening may occur in several of these diseases (arterial hypertension, Fabry's disease), in which case the localization of the affected segment might point toward the underlying substrate.

Therefore, the assessment of systolic function in hypertrophic myopathies must not be deemed secondary to the assessment of diastolic (dys)function, these data should rather be integrated in a comprehensive approach to hypertrophic remodelling and early detection of myocardial functional impairment.

	Biopsy	**Regional/ global**	**Affected region**	**Deformation**	**Longitudinal/ Radial dysfunction**	**Diastolic function**
Athletes	Normal	Global	Diffuse	(Supra)normal	-	(Supra)normal
Pressure overload	Cellular hypertrophy	Regional	Basal septum	Reduced + PST	Longitudinal	Impaired
HCM	Myocyte disarray	Regional	Basal septum	Absent	Longitudinal	Impaired
Amyloidosis	Extracellular amyloid deposit	Global	Diffuse	Severely reduced	Longitudinal, less radial	Impaired – pseudonormal
Systemic diseases	Cellular hypertrophy	Regional	Basal inferolateral	PST	Longitudinal, less radial	Impaired

Table 8.1. Typical biopsy findings and characteristics of deformation parameters and diastolic function in the early stages of different types of hypertrophic remodelling.

Chapter 9

Summary

In contemporary clinical cardiology practice, echocardiography plays a leading role in the diagnosis and management guidance of various forms of myocardial remodelling. Furthermore, it is the most commonly used diagnostic technique in the elucidation of the underlying substrates and pathophysiologic mechanisms of heart failure as a consequence of ventricular remodelling. Due to its widespread availability, non-invasiveness, user-friendliness and relatively low cost, echocardiography is still irreplaceable by other cardiac imaging methods which should rather be seen as complementary diagnostic tools.

This thesis sought to study several types of ventricular remodelling and their consequences on regional and global myocardial function, employing different echocardiographic tools and dedicated signal and image analysis algorithms in the detection of ventricular dysfunction.

Recent echocardiographic techniques based on Myocardial Velocity Imaging have provided the possibility of a more detailed and integrated insight to cardiac (dys-) function. Based on novel understandings, we first gave an original integrated overview on 'cardiac function', distinguishing *intrinsic myocyte function* (often referred to as *contractility*) and *ventricular pump function* as well as the main components of function, namely force development and deformation. Additionally, the boundary conditions in which the heart functions, which determine the interactions between these components were defined as: a) wall properties such as tissue composition/elasticity, fibre structure and global geometry, and b) interaction between the heart and peripheral circulation, mostly described as (pressure & volume) loading conditions.

Furthermore, Doppler echocardiography data were analyzed in a study addressing flow remodelling as a consequence of cellular and force remodelling in ischaemically remodelled hearts. A dedicated automated quantification of the CW outflow Doppler traces was used to define specific trace parameters indicative of myocardial dysfunction. It was shown that decreased overall contractility results in a more symmetrical outflow velocity profile, which would suggest that the global development of contractile force has been remodelled to cope with the decreased output resulting from decreased contractility.

Similar automatic quantification of the aortic instantaneous peak velocities was further employed in patients with hypertrophic remodelling due to aortic stenosis. This study has shown that the values of trace asymmetry before surgery are predictive of the change in EF

pre- and postoperatively: all of the patients with markedly symmetric preoperative instantaneous peak velocities showed stagnation or deterioration of EF postoperatively. Furthermore, the study has proven that the symmetry of the shape of the instantaneous peak velocities is a more reliable predictor of functional improvement after the valve replacement procedure as compared to mean aortic gradient and aortic valve area which are widely used in preoperative assessment of patients with aortic stenosis.

An intraoperative Doppler myocardial imaging study was performed along with standard echocardiography in an analysis of electrical remodelling in patients with LBBB during the CRT implantation procedure. In addition to confirming the septal flash as a mechanical consequence of the underlying electrical problem and a valid marker of intraventricular dyssynchrony, an acute contractility recruitment, resolution of the septal flash as well as reverse remodelling immediately following CRT device activation was shown in these patients.

As opposed to remodelling induced by changes in loading conditions, evidence of hypertrophy and hypercontractility without an additional change in afterload resulting in increased cardiac output and inducing additional signs of vascular remodelling was demonstrated in patients with early stage acromegaly.

Finally, a comprehensive view on the changing role of echocardiography in the diagnosis of hypertrophic myopathies is presented. Previous knowledge as well as regional deformation data (including deformation pattern analysis) are combined to provide an indicator toward the disease underlying hypertrophic ventricular remodelling: in hypertensive heart disease LVH is predominantly localized in the basal septal region showing reduced systolic strain values with post-systolic shortening; systemic diseases such as Fabry's disease often affect a specific region - the basal (infero)lateral segment in which post-systolic deformation is often present. Hypertrophic cardiomyopathy is associated with regions of local fibre disarray, in which no myocardial deformation is present at all, while in the surrounding segments (often showing similar thickness) deformation is reduced, but almost normal as compared to undiseased hearts. The absence of deformation is mostly associated with the thickest segments. Amyloidosis seems to provide an exception in which the impairment of systolic function affects the myocardium globally – it is presented with global LVH and diffuse, severe reduction of longitudinal strain, while the radial strain is still preserved, but of low values.

Ispitivanje regionalne i globalne morfologije te funkcije miokarda u različitim oblicima srčanog remodeliranja

Sažetak

U suvremenoj kardiologiji ehokardiografija ima vodeću ulogu u dijagnostici i odabiru postupaka u raznim oblicima remodeliranja miokarda. Nadalje, to je najčešće primjenjivana metoda u rasvjetljavanju temeljnih supstrata i patofizioloških mehanizama zatajenja srca kao posljedice remodeliranja klijetki. Zahvaljujući širokoj dostupnosti, neinvazivnosti, lakoći primjene i relativno malenoj cijeni, ehokardiografija je i dalje nezamjenjiva u odnosu na druge metode oslikavanja u kardiologiji, koje bi valjalo prihvatiti kao komplementarne dijagnostičke metode.

Cilj je ove disertacije istražiti nekoliko oblika remodeliranja klijetki i njihovih posljedica na regionalnu i globalnu funkciju miokarda, primjenom različitih ehokardiografskih metoda i specifičnih algoritama analize signala i slike u otkrivanju disfunkcije srca.

Novije ehokardiografske tehnike temeljene na oslikavanju miokardnih brzina gibanja (*Myocardial Velocity Imaging*) omogućuju podrobniji i integrirani pogled u (dis)funkciju srca. Na temelju novijih spoznaja, na početku disertacije prikazan je originalni, integrirani pregled „srčane funkcije“, razlikujući intrinzičnu funkciju miocita (obično nazivanu kontraktilitetom) i crpnu funkciju klijetki, kao i glavne sastojnice srčane funkcije, to jest razvoj sile i deformaciju., Uvjeti u kojima srce radi, koji određuju odnos između navedenih sastavnica, definirani su kao: a) svojstva stijenke poput građe/elastičnosti tkiva, strukture vlakna i globalne geometrije, te b) interakcija srca i periferne cirkulacije koja se većinom opisuje kao stanje punjenja (tlačno i volumno opterećenje).

U ispitivanju remodeliranja protoka kao posljedici staničnog remodeliranja i remodeliranja sile u ishemijski remodeliranom srcu, obrađivali smo podatke Dopplerske ehokardiografije. Posebna automatska kvantifikacija Dopplerskih zapisa istiska lijeve klijetke primijenjena je u definiranju specifičnih svojstava krivulje, koja ukazuju na disfunkciju miokarda. Dokazali smo da smanjenje ukupne kontraktilnosti uzrokuje simetričniji oblik krivulje istiska lijeve klijetke, što sugerira remodeliranje globalne kontraktilne sile, kako bi se prilagodila smanjenju istiska zbog smanjene kontraktilnosti.

Slična automatska kvantifikacija trenutnih vršnih brzina protoka kroz aortni zalistak primijenjena je i u bolesnika s hipertrofijskim remodeliranjem klijetki u aortnoj stenozi. Ovo istraživanje pokazalo je da predoperativne vrijednosti asimetrije Dopplerskog zapisa predskazuju poslijeoperacijsku promjenu ejekcijske frakcije: u svih bolesnika sa značajno simetričnim predoperativnim vršnim brzinama kroz aortni zalistak dokazali smo pogoršanje ili

istovjetnu ejekcijsku frakciju nakon operacije. Nadalje, ovo je istraživanje dokazalo da je simetričnost vršnih brzina pouzdaniji predskazatelj funkcijskog oporavka nakon zamjene aortnog zalistka, u usporedbi sa srednjim transaortnim gradijentom i površinom aortnog ušća koji se često koriste u predoperativnoj evaluaciji bolesnika s aortnom stenozom.

U analizi električnog remodeliranja u bolesnika s blokom lijeve grane, provedeno je, uz standardnu ehokardiografiju, intraoperacijsko ispitivanje miokardnog Dopplera tijekom postupka ugradnje resinkronizacijskog elektrostimulatora. Uz potvrdu *flash* - septuma kao mehaničke posljedice temeljnog električnog problema te valjanog pokazatelja intraventrikulske disinkronije, u ovoj skupini bolesnika dokazano je i akutno poboljšanje kontraktilnosti, nestanak *flash* - septuma kao i povratno remodeliranje lijeve klijetke neposredno nakon uključivanja resinkronizacijskog elektrostimulatora.

Za razliku od remodeliranja uzrokovanog promjenom uvjeta punjenja, u skupini bolesnika s akromegalijom dokazali smo hipertrofiju i hiperkontraktilnost lijeve klijetke uz posljedično povećanje minutnog volumena srca te razvoj znakova vaskularnog remodeliranja, bez dodatnih promjena u tlačnom opterećenju srca.

Disertacija završava širim prikazom izmijenjene uloge ehokardiografije u dijagnozi hipertrofijskih bolesti miokarda. Prethodna saznanja kao i podatci o regionalnoj deformaciji (uključujući analizu uzoraka deformacije) povezani su u svrhu prepoznavanja bolesti koja je u podlozi hipertrofijskom remodeliranju klijetki: u hipertenzivnoj bolesti srca hipertrofija je većinom lokalizirana u bazalnom interventrikulskom septumu uz smanjenje vrijednosti sistoličkog *strain-a* te nastanak post-sistoličkog izduljenja. Sistemske bolesti poput Fabryjeve bolesti često zahvaćaju određenu regiju srca – bazalni (infero)lateralni segment u kojem je često prisutno post-sistoličko zadebljanje. Hipertrofijska kardiomiopatija je povezana s ograničenim područjima poremećene arhitekture srčanih vlakana, u kojima je deformacija u potpunosti odsutna, dok je u okolnim segmentima (često slične debljine stijenke) deformacija smanjena, no gotovo normalna. Odsutnost deformacije obično je povezana s najzadebljanijim segmentima. Čini se da amiloidoza predstavlja iznimku u kojoj smanjenje sistoličke funkcije globalno zahvaća miokard - nalazi se globalna hipertrofija lijeve klijetke te difuzno, teško oštećenje logitudinalnog *straina* dok je radijalni *strain* još očuvan, ali malenih vrijednosti.

References

1. Sutherland GR, Hatle L, Claus P, D'hooge J, Bijnens BH. Doppler Myocardial Imaging- A Textbook. Hasselt - Belgium: BSWK, 2006.
2. Perk G, Tunick PA, Kronzon I. Non-Doppler two-dimensional strain imaging by echocardiography--from technical considerations to clinical applications. J Am Soc Echocardiogr 2007;20:234-43
3. Jamal F, Strotmann J, Weidemann F, Kukulski T, D'hooge J, Bijnens B et al. Noninvasive quantification of the contractile reserve of stunned myocardium by ultrasonic strain rate and strain. Circulation 2001;104:1059-65.
4. Weidemann F, Jamal F, Sutherland GR, Claus P, Kowalski M, Hatle L et al. Myocardial function defined by strain rate and strain during alterations in inotropic states and heart rate. Am J Physiol Heart Circ Physiol 2002;283:H792-9.
5. Thibault H, Derumeaux G. Assessment of myocardial ischemia and viability using tissue Doppler and deformation imaging: the lessons from the experimental studies. Arch Cardiovasc Dis 2008;101:61-8.
6. Voigt JU, Nixdorff U, Bogdan R, Exner B, Schmiedehausen K, Platsch G et al. Comparison of deformation imaging and velocity imaging for detecting regional inducible ischaemia during dobutamine stress echocardiography. Eur Heart J 2004;25:1517-25.
7. Marciniak A, Claus P, Sutherland GR, Marciniak M, Karu T, Baltabaeva A et al. Changes in systolic left ventricular function in isolated mitral regurgitation. A strain rate imaging study. Eur Heart J 2007;28:2627-36.
8. Marciniak A, Sutherland GR, Marciniak M, Claus P, Bijnens B, Jahangiri M. Myocardial deformation abnormalities in patients with aortic regurgitation: a strain rate imaging study. Eur J Echocardiogr 2008 Jun 25. [Epub ahead of print]
9. Baltabaeva A, Marciniak M, Bijnens B, Moggridge J, He FJ, Antonios TF et al. Regional left ventricular deformation and geometry analysis provides insights in myocardial remodelling in mild to moderate hypertension. Eur J Echocardiogr 2008;9:501-8.
10. Vinereanu D, Florescu N, Sculthorpe N, Tweddel AC, Stephens MR, Fraser AG. Differentiation between pathologic and physiologic left ventricular hypertrophy by tissue Doppler assessment of long-axis function in patients with hypertrophic cardiomyopathy or systemic hypertension and in athletes. Am J Cardiol 2001;88:53-8.
11. Kato TS, Noda A, Izawa H, Yamada A, Obata K, Nagata K et al. Discrimination of nonobstructive hypertrophic cardiomyopathy from hypertensive left ventricular hypertrophy on the basis of strain rate imaging by tissue Doppler ultrasonography. Circulation 2004;110:3808-14.

12. Breithardt OA, Stellbrink C, Herbots L, Claus P, Sinha AM, Bijnens B et al. Cardiac resynchronization therapy can reverse abnormal myocardial strain distribution in patients with heart failure and left bundle branch block. J Am Coll Cardiol 2003;42:486-94.
13. Bellavia D, Pellikka PA, Abraham TP, Al-Zahrani GB, Dispenzieri A, Oh JK et al. Evidence of impaired left ventricular systolic function by Doppler myocardial imaging in patients with systemic amyloidosis and no evidence of cardiac involvement by standard two-dimensional and Doppler echocardiography. Am J Cardiol 2008;101:1039-45.
14. Eroglu E, D'hooge J, Sutherland GR, Marciniak A, Thijs D, Droogne W et al. Quantitative dobutamine stress echocardiography for the early detection of cardiac allograft vasculopathy in heart transplant recipients. Heart 2008;94(2):e3.
15. Weidemann F, Breunig F, Beer M, Sandstede J, Störk S, Voelker W et al. The variation of morphological and functional cardiac manifestation in Fabry disease: potential implications for the time course of the disease. Eur Heart J 2005;26:1221-7.
16. Mertens L, Ganame J, Claus P, Goemans N, Thijs D, Eyskens B et al. Early Regional Myocardial Dysfunction in Young Patients With Duchenne Muscular Dystrophy. J Am Soc Echocardiogr 2008 Apr 10. [Epub ahead of print]
17. Bijnens B, Claus P, Weidemann F, Strotmann J, Sutherland GR. Investigating cardiac function using motion and deformation analysis in the setting of coronary artery disease. Circulation 2007;116:2453-64.
18. Lang RM, Bierig M, Devereux RB, Flachskampf FA, Foster E, Pellikka PA et al; American Society of Echocardiography's Nomenclature and Standards Committee; Task Force on Chamber Quantification; American College of Cardiology Echocardiography Committee; American Heart Association; European Association of Echocardiography, European Society of Cardiology. Recommendations for chamber quantification. Eur J Echocardiogr 2006;7:79-108.
19. Aurigemma GP, Silver KH, Priest MA, Gaasch WH. Geometric changes allow normal ejection fraction despite depressed myocardial shortening in hypertensive left ventricular hypertrophy. J Am Coll Cardiol 1995;26:195-202.
20. Claus P, Weidemann F, Dommke C, Bito V, Heinzel FR, D'hooge J et al. Mechanisms of postsystolic thickening in ischemic myocardium: mathematical modelling and comparison with experimental ischemic substrates. Ultrasound Med Biol 2007;33:1963-70.
21. Weidemann F, Dommke C, Bijnens B, Claus P, D'hooge J, Mertens P et al. Defining the transmurality of a chronic myocardial infarction by ultrasonic strain rate imaging. The implications for identifying intramural viability - an experimental study. Circulation 2003;107:883–888.

22. Kowalski M, Herbots L, Weidemann F, Breithardt O, Strotmann J, Davidavicius G et al. One-dimensional ultrasonic strain and strain rate imaging: a new approach to the quantitation of regional myocardial function in patients with aortic stenosis. Ultrasound Med Biol 2003;29:1085–92.
23. Modesto KM, Cauduro S, Dispenzieri A, Khandheria B, Belohlavek M, Lysyansky P et al. Two-dimensional acoustic pattern derived strain parameters closely correlate with one-dimensional tissue Doppler derived strain measurements. Eur J Echocardiogr 2006;7: 315-321.
24. Sengupta PP, Krishnamoorthy VK, Korinek J, Narula J, Vannan MA, Lester SJ et al. Left ventricular form and function revisited: applied translational science to cardiovascular ultrasound imaging. J Am Soc Echocardiogr 2007;20:539-51.
25. Dokos S, Smaill BH, Young AA, LeGrice IJ. Shear properties of passive ventricular myocardium. Am J Physiol Heart Circ Physiol 2002;283:H2650-9.
26. Garot J, Pascal O, Diebold B, Derumeaux G, Gerber BL, Dubois-Rande JL et al. Alterations in systolic left ventricular twist after acute myocardial infarction. Am J Physiol Heart Circ Physiol 2002;281:H357–62.
27. Langeland S, Wouters PF, Claus P, Leather HA, Bijnens B, Sutherland GR et al. Experimental assessment of a new research tool for the estimation of two-dimensional myocardial strain. Ultrasound Med Biol 2006;32:1509-13.
28. Korinek J, Wang J, Sengupta PP, Miyazaki C, Kjaergaard J, McMahon E et al. Two-dimensional strain--a Doppler-independent ultrasound method for quantitation of regional deformation: validation in vitro and in vivo. J Am Soc Echocardiogr 2005;18:1247-53.
29. Helle-Valle T, Crosby J, Edvardsen T, Lyseggen E, Amundsen BH, Smith HJ et al. New noninvasive method for assessment of left ventricular rotation: speckle tracking echocardiography. Circulation 2005;112:3149-56.
30. Ng AC, Tran da T, Newman M, Allman C, Vidaic J, Kadappu KK et al. Comparison of myocardial tissue velocities measured by two-dimensional speckle tracking and tissue Doppler imaging. Am J Cardiol 2008;102:784-9.
31. Chan J, Hanekom L, Wong C, Leano R, Cho GY, Marwick TH. Differentiation of subendocardial and transmural infarction using two-dimensional strain rate imaging to assess short-axis and long-axis myocardial function. J Am Coll Cardiol 2006;48:2026-33.
32. Guccione JM, Le Prell GS, de Tombe PP, Hunter WC. Measurements of active myocardial tension under a wide range of physiological loading conditions. J Biomech 1997;30:189–92.
33. Grossman W, Jones D, McLaurin LP. Wall stress and patterns of hypertrophy in the human left ventricle. J Clin Invest 1975;56:56-64.

34. Guccione JM, Waldman LK, McCulloch AD. Mechanics of active contraction in cardiac muscle: Part II--Cylindrical models of the systolic left ventricle. J Biomech Eng 1993;115:82-90.
35. Edvardsen T, Aakhus S, Endresen K, Bjomerheim R, Smiseth O, Ihlen H. Acute regional myocardial ischaemia identified by 2-dimensional multiregion tissue Doppler imaging technique. J Am Soc of Echocardiogr 2000;13:986–94.
36. Derumeaux G, Ovize M, Loufoua J, Andre-Fouet X, Minaire Y, Cribier A et al. Doppler tissue imaging quantitates regional wall motion during myocardial ischaemia and reperfusion. Circulation 1998;97:1970–7.
37. Kukulski T, Jamal F, D'hooge J, Bijnens B, De Scheerder I, Sutherland GR. Acute changes in systolic and diastolic events during clinical coronary angioplasty: A comparison of regional velocity, strain rate and strain measurement. J Am Soc of Echocardiogr 2002;15:1–12.
38. Bragadeesh T, Jayaweera AR, Pascotto M, Micari A, Le DE, Kramer CM et al. Post-ischaemic myocardial dysfunction (stunning) results from myofibrillar oedema. Heart 2008;94:166-71.
39. Turschner O, D'hooge J, Dommke C, Claus P, Verbeken E, De Scheerder I et al. The sequential changes in myocardial thickness and thickening which occur during acute transmural infarction, infarct reperfusion and the resultant expression of reperfusion injury. Eur Heart J 2004;25:794-803.
40. Merli E, Sutherland GR, Bijnens B, Fischer A, Chaparro M, Karu T et al. Usefulness of changes in left ventricular wall thickness to predict full or partial pressure reperfusion in ST-elevation acute myocardial infarction. Am J Cardiol 2008;102:249-56.
41. Hawkins NM, Petrie MC, MacDonald MR, Hogg KJ, McMurray JJ. Selecting patients for cardiac resynchronization therapy: electrical or mechanical dyssynchrony? Eur Heart J 2006;27:1270–81.
42. Hayes D, Wang P, Sackner-Bernstein J, Asirvatham S. Resynchronization and Defibrillation for Heart Failure: A Practical Approach. Oxford, UK: Futura (Blackwell), 2004.
43. Marciniak M, Bijnens B, Baltabaeva A, Marciniak A, Parsai C, Claus P et al. Interventricular interaction as a possible mechanism for the presence of a biphasic systolic velocity profile in normal left ventricular free walls. Heart 2008;94:1058-64.
44. Chung ES, Leon AR, Tavazzi L, Sun JP, Nihoyannopoulos P, Merlino J et al. Results of the Predictors of Response to CRT (PROSPECT) trial. Circulation 2008;117:2608-16.
45. Nagueh SF, Middleton KJ, Kopelen HA, Zoghbi WA, Quiñones MA. Doppler tissue imaging: a noninvasive technique for evaluation of left ventricular relaxation and estimation of filling pressures. J Am Coll Cardiol 1997;30:1527-33.

46. Ommen SR, Nishimura RA, Appleton CP, Miller FA, Oh JK, Redfield MM et al. Clinical utility of Doppler echocardiography and tissue Doppler imaging in the estimation of left ventricular filling pressures: A comparative simultaneous Doppler-catheterization study. Circulation 2000;102:1788-94.
47. D'Souza KA, Mooney DJ, Russell AE, MacIsaac AI, Aylward PE, Prior DL. Abnormal septal motion affects early diastolic velocities at the septal and lateral mitral annulus, and impacts on estimation of the pulmonary capillary wedge pressure. J Am Soc Echocardiogr 2005;18:445-53.
48. Bruch C, Stypmann J, Gradaus R, Breithardt G, Wichter T. Usefulness of tissue Doppler imaging for estimation of filling pressures in patients with primary or secondary pure mitral regurgitation. Am J Cardiol 2004;93:324-8.
49. Bito V, Heinzel FR, Weidemann F, Dommke C, van der Velden J, Verbeken E et al. Cellular mechanisms of contractile dysfunction in hibernating myocardium. Circ Res 2004;94:794-801.
50. Bushberg J.T., Seibert J.A., Leidholdt E.M. jr, Boon J.M. The Essential Physics of Medical Imaging. 2nd Edition Philadelphia, 2002.
51. Hatle, L. Angelsen, B. Doppler ultrasound in cardiology – Physical principles and clinical applications. 2nd ed. Philadelphia: Lea & Febiger;1982.
52. Cikes M, Kalinic H, Baltabaeva A, Loncaric S, Parsai C, Milicic D et al. The shape of the aortic outflow velocity profile revisited. Is there a relation between its asymmetry and ventricular function in coronary artery disease? Eur J Echocardiogr. 2009; Jun 16. [Epub ahead of print] doi: 10.1093/ejechocard/jep088
53. Colocousis JS, Huntsman LL, Curreri PW. Estimation of stroke volume changes by ultrasonic Doppler. Circulation 1977;56;914-7.
54. Huntsman LL, Stewart DK, Barnes SR, Franklin SB, Colocousis JS, Hessel EA. Noninvasive Doppler determination of cardiac output in man. Clinical validation. Circulation 1983;67:593-602.
55. Ihlen H, Amlie JP, Dale J, Forfang K, Nitter-Hauge S, Otterstad JE et al. Determination of cardiac output by Doppler echocardiography. Br Heart J 1984;51:54-60.
56. Bennett ED, Barclay SA, Davis AL, Mannering D, Mehta N. Ascending aortic blood velocity and acceleration using Doppler ultrasound in the assessment of left ventricular function. Cardiovasc Res 1984;18:632-8.
57. Pearlman AS. Evaluation of ventricular function using Doppler echocardiography. Am J Cardiol 1982;49:1324-30.
58. Appelton CP, Hatle LK, Popp RL. Relation of transmitral flow velocity patterns to left ventricular diastolic function: new insights from a combined Doppler and hemodynamic study. J Am Coll Cardiol 1988;12:426-40.

59. Hatle L, Angelsen BA, Tromsdal A. Non-invasive assessment of aortic stenosis by Doppler ultrasound. Br Heart J 1980;43:284-92.
60. Hatle L, Brubakk A, Tromsdal A, Angelsen B. Non-invasive assessment of pressure drop in mitral stenosis by Doppler ultrasound. Br Heart J 1978;40:131-40.
61. Noble MIM, Trenchard D, Guz A. Left ventricular ejection in conscious dogs: measurement and significance of the maximum acceleration of blood flow from the left ventricle. Circ Res 1966;19:139-47.
62. Sabbah HN, Khaja F, Brymer JF, McFarland TM, Albert DE, Snyder JE et al. Noninvasive evaluation of left ventricular performance based on peak aortic blood acceleration measured with a continuous-wave Doppler velocity meter. Circulation 1986;74:323-9.
63. Murgo JP, Alter BR, Dorethy JF, Altobelli SA, McGranahan GM Jr. Dynamics of left ventricular ejection in obstructive and nonobstructive hypertrophic cardiomyopathy. J Clin Invest 1980;66:1369-82.
64. Schluter M, Langenstein BA, Hanrath P, Kremer P, Bleifeld W. Assessment of transesophageal pulsed Doppler echocardiography in the detection of mitral regurgitation. Circulation 1982;66:784-9.
65. Buchtal A, Hanson GC, Peisach AR. Transcutaneous aortovelography. Potentially useful technique in management of critically ill patients. Br Heart J 1976;38:451-6.
66. Schiller NB, Shah PM, Crawford M, DeMaria A, Devereux R, Feigenbaum H et al. Recommendations for quantitation of the left ventricle by two-dimensional echocardiography. American Society of Echocardiography Committee on Standards, Subcommittee on Quantitation of Two-Dimensional Echocardiograms. J Am Soc Echocardiogr 1989;2:358-67.
67. Devereux RB, Alonso DR, Lutas EM, Gottlieb GJ, Campo E, Sachs I et al. Echocardiographic assessment of left ventricular hypertrophy: comparison to necropsy findings. Am J Cardiol 1986;57:450-8.
68. Ganau A, Devereux RB, Roman R, de Simone G, Pickering TG, Saba PS et al. Patterns of left ventricular hypertrophy and geometric remodeling in essential hypertension. J Am Coll Cardiol 1992;19:1550-8.
69. Kalinic H, Loncaric S, Cikes M, Baltabaeva A, Parsai C, Separovic J et al. Analysis of Doppler Ultrasound Outflow Profiles for the Detection of changes in Cardiac Function. In: International Symposium on Image and Signal Processing and Analysis (ISPA), 2007, 326-31.
70. Pellikka PA, Oh JK, Bailey KR, Nichols BA, Monahan KH, Tajik AJ. Dynamic intraventricular obstruction during dobutamine stress echocardiography. A new observation. Circulation 1992;86:1429-32.

71. Bijnens B, Claus P, Parsai C, Cikes M, Loncaric S, Anderson L et al. An integrated framework for the assessment of cardiac function – Description and illustrated applications. In: International Symposium on Image and Signal Processing and Analysis (ISPA), 2007, 332-7.
72. Penny DJ, Mynard JP, Smolich JJ. Aortic wave intensity analysis of ventricular-vascular interaction during incremental dobutamine infusion in adult sheep. Am J Physiol Heart Circ Physiol 2008;294:H481-9.
73. Duncan AM, O'Sullivan CA, Gibson DG, Henein MY. Electromechanical interrelations during dobutamine stress in normal subjects and patients with coronary artery disease: comparison of changes in activation and inotropic state. Heart 2001;85:411-6.
74. Bito V, van der Velden J, Claus P, Dommke C, Van Lommel A, Mortelmans L et al. Reduced force generating capacity in myocytes from chronically ischemic, hibernating myocardium. Circ Res 2007;100:229-37.
75. Henein MY, Gibson DG. Long axis function in disease. Heart 1999; 81:229-31.
76. O'Sullivan CA, Henein MY, Sutton R, Coats AJ, Sutton GC, Gibson DG. Abnormal ventricular activation and repolarisation during dobutamine stress echocardiography in coronary artery disease. Heart. 1998;79:468-73.
77. Henein MY, O'Sullivan C, Davies SW, Sigwart U, Gibson DG. Effects of acute coronary occlusion and previous ischaemic injury on left ventricular wall motion in humans. Heart 1997;77:338-45.
78. Sasson Z, Yock PG, Hatle LK, Alderman EL, Popp RL. Doppler echocardiographic determination of the pressure gradient in hypertrophic cardiomyopathy. J Am Coll Cardiol 1988;11:752-6.
79. Panza JA, Petrone RK, Fananapazir L, Maron BJ. Utility of continuous wave Doppler echocardiography in the noninvasive assessment of left ventricular outflow tract pressure gradient in patients with hypertrophic cardiomyopathy. J Am Coll Cardiol 1992;19:91-9.
80. Henein MY, O'Sullivan C, Sutton GC, Gibson DG, Coats AJ. Stress-induced left ventricular outflow tract obstruction: a potential cause of dyspnea in the elderly. J Am Coll Cardiol 1997;30:1301-7.
81. Luria D, Klutstein MW, Rosenmann D, Shaheen J, Sergey S, Tzivoni D. Prevalence and significance of left ventricular outflow gradient during dobutamine echocardiography. Eur Heart J 1999;20:386-92.
82. Merli E, Sutcliffe S, Gori M, Sutherland GG. Tako-Tsubo cardiomyopathy: new insights into the possible underlying pathophysiology. Eur J Echocardiogr 2006;7:53-61.
83. Dal-Bianco JP, Khandheria BK, Mookadam F, Gentile F, Sengupta PP. Management of asymptomatic severe aortic stenosis. J Am Coll Cardiol 2008;52:1279-1292.

84. Hachicha Z, Dumesnil JG, Bogaty P, Pibarot P. Paradoxical low-flow, low-gradient severe aortic stenosis despite preserved ejection fraction is associated with higher afterload and reduced survival. Circulation 2007;115:2856-2864.
85. Wranne B, Baumgartner H, Flachskampf F, Kasenkam M, Pinto F. Stenotic lesions. Heart 1996;75:36-42.
86. Claus P, Weidemann F, Decramer I, Mc Laughlin M, Rademakers FE, Mertens L, Strotmann J, Bijnens B. Increased and prolonged active myocardial stress as compensation in aortic stenosis. Eur J Echocardiogr 2005;6:S75. Abstract.
87. Singer M, Allen MJ, Webb AR, Bennett ED. Effects of alterations in left ventricular filling, contractility, and systemic vascular resistance on the ascending aortic blood velocity waveform of normal subjects. Crit Care Med 1991;19:1138-1145.
88. Vahanian A, Baumgartner H, Bax J, Butchart E, Dion R, Filippatos G, Flachskampf F, Hall R, Iung B, Kasprzak J, Nataf P, Tornos P, Torracca L, Wenink A; Task Force on the Management of Valvular Hearth Disease of the European Society of Cardiology; ESC Committee for Practice Guidelines. Guidelines on the management of valvular heart disease: The Task Force on the Management of Valvular Heart Disease of the European Society of Cardiology. Eur Heart J 2007;28:230-268.
89. Skjaerpe T, Hegrenaes L, Hatle L. Noninvasive estimation of valve area in patients with aortic stenosis by Doppler ultrasound and two-dimensional echocardiography. Circulation 1985;72:810-818.
90. Zoghbi WA, Farmer KL, Soto JG, Nelson JG, Quinones MA. Accurate noninvasive quantification of stenotic aortic valve area by Doppler echocardiography. Circulation 1986;73:452-459.
91. Weissler AM, Harris WS, Schoenfeld CD. Systolic time intervals in heart failure in man. Circulation 1968:37;149-159.
92. Voelker W, Reul H, Nienhaus G, Stelzer T, Schmitz B, Steegers A, Karsch KR. Comparison of valvular resistance, stroke work loss, and Gorlin valve area for quantification of aortic stenosis. An in vitro study in a pulsatile aortic flow model. Circulation 1995;91:1196-1204.
93. Bermejo J, Antoranz JC, Burwash IG, Alvarez JL, Moreno M, García-Fernández MA, Otto CM. In-vivo analysis of the instantaneous transvalvular pressure difference-flow relationship in aortic valve stenosis: implications of unsteady fluid-dynamics for the clinical assessment of disease severity. J Heart Valve Dis 2002;11:557-566.
94. Otto CM. Aortic stenosis: echocardiographic evaluation of disease severity, disease progression, and the role of echocardiography in clinical decision making. In: Otto CM, ed. The Practice of Clinical Echocardiography. Philadelphia, PA:W.B. Saunders Company; 1997. p. 405-432.

95. Rosenhek R, Klaar U, Schemper M, Scholten C, Heger M, Gabriel H, Binder T, Maurer G, Baumgartner H. Mild and moderate aortic stenosis. Natural history and risk stratification by echocardiography. Eur Heart J 2004;25:199-205.
96. Bonner AJ, Sacks HN, Tavel ME. Assessing the Severity of Aortic Stenosis by Phonocardiography and External Carotid Pulse Recordings. Circulation 1973;48:247-252.
97. Beauchesne LM, de Kemp R, Chan KL, Burwash IG. Temporal Variations in Effective Orifice Area During Ejection in Patients with Valvular Aortic Stenosis. J Am Soc Echocardiogr 2003;16:958-964.
98. Agatston AS, Chengot M, Rao A, Hildner F, Samet P. Doppler Diagnosis of Valvular Aortic Stenosis in Patients Over 60 Years of Age. Am J Cardiol 1985;56:106-109.
99. Hein S, Arnon E, Kostin S, Schonburg M, Elsasser A, Polyakova V, Bauer EP, Klovekorn WP, Schaper J. Progression from compensated hypertrophy to failure in the pressure-overloaded human heart: structural deterioration and compensatory mechanisms. Circulation 2003;107:984-991.
100. Bauer F, Eltchaninoff H, Tron C, Lesault P, Agatiello C, Nercolini D, Derumeaux G, Cribier A. Aortic Stenosis After Percutaneous Heart Valve Implantation in Patients With Symptomatic Acute Improvement in Global and Regional Left Ventricular Systolic Function. Circulation 2004;110:1473-1476.
101. Iwahashi N, Nakatani S, Kanzaki H, Hasegawa T, Abe H, Kitakaze M. Acute improvement in myocardial function assessed by myocardial strain and strain rate after aortic valve replacement for aortic stenosis. J Am Soc Echocardiogr 2006;19:1238-1244.
102. Bermejo J, Antoranz JC, Garcia-Fernandez MA, Moreno MM, Delcan JL. Flow dynamics of stenotic aortic valves assessed by signal processing of Doppler spectrograms. Am J Cardiol 2000;85:611-617.
103. Derumeaux G, Mulder P, Richard V, Chagraoui A, Nafeh C, Bauer F, Henry JP,Thuillez C. Tissue Doppler imaging differentiates physiological from pathological pressure-overload left ventricular hypertrophy in rats. Circulation 2002;105:1602-1608.
104. Shim Y, Hampton TG, Straley CA, Harrison JK, Spero LA, Bashore TM, Pasipoularides AD. Ejection Load Changes in Aortic Stenosis. Observations Made after Balloon Aortic Valvuloplasty. Circ Res 1992;71:1174-1184.
105. Strotmann JM, Lengenfelder B, Blondelot J, Voelker W, Herrmann S, Ertl G, Weidemann F. Functional differences of left ventricular hypertrophy induced by either arterial hypertension or aortic valve stenosis. Am J Cardiol 2008;101:1493-1497.
106. Cleland JGF, Daubert J-C, Erdmann E, et al for the Cardiac Resynchronization-Heart Failure (CARE-HF) Study Investigators. The effect of cardiac resynchronization on morbidity and mortality in heart failure. N Engl J Med 2005;352:1539-1549.

107. Chung N, Nishimura RA, Holmes DR Jr, Tajik AJ. Measurement of left ventricular dp/dt by simultaneous Doppler echocardiography and cardiac catheterization. J Am Soc Echocardiogr 199;25:147-52.
108. Parsai C, Bijnens B, Sutherland GR, Baltabaeva A, Claus P, Marciniak M et al. Toward understanding response to cardiac resynchronization therapy: left ventricular dyssynchrony is only one of multiple mechanisms. Eur Heart J 2009;30:940-9.
109. Parsai C, Baltabaeva A, Anderson L, Chaparro M, Bijnens B, Sutherland GR. Low-dose dobutamine stress echo to quantify the degree of remodelling after cardiac resynchronization therapy. Eur Heart J 2009;30:950-8.
110. Hunt SA, Abraham WT, Chin MH et al; American College of Cardiology; American Heart Association Task Force on Practice Guidelines; American College of Chest Physicians; International Society for Heart and Lung Transplantation; Heart Rhythm Society. ACC/AHA 2005 Guideline update for the diagnosis and management of chronic heart failure in the adult: a report of the American College of Cardiology/American Heart Association Task Force on Practice Guidelines (Writing Committee to Update the 2001 Guidelines for the Evaluation and Management of Heart Failure): developed in collaboration with the American College of Chest Physicians and the International Society for Heart and Lung Transplantation: endorsed by the Heart Rhythm Society. Circulation 2005;112:e154-235.
111. Bargiggia GS, Bertucci C, Recusani F Bargiggia GS, Bertucci C, Recusani F et al. A new method for estimating left ventricular dP/dt by continuous wave Doppler echocardiography: Validation studies at cardiac catheterization. Circulation 1989;80:1287-92.
112. Weidemann F, Kowalski M, D'hooge J, Bijnens B, Sutherland GR. Doppler myocardial imaging. A new tool to assess regional inhomogeneity in cardiac function. Basic Res Cardiol 2001;96:595-605.
113. Yu CM, Bleeker GB, Fung JW, Schalij MJ, Zhang Q, van der Wall EE et al. Left ventricular reverse remodeling but not clinical improvement predicts long-term survival after cardiac resynchronization therapy. Circulation 2005;112:1580-6.
114. Sutton MS, Keane MG. Reverse remodelling in heart failure with cardiac resynchronisation therapy. Heart 2007;93:167-71.
115. Linde C, Leclercq C, Rex S, Garrigue S, Lavergne T, Cazeau S, McKenna W et al. Long-term benefits of biventricular pacing in congestive heart failure: results from the MUltisite STimulation in cardiomyopathy (MUSTIC) study. J Am Coll Cardiol 2002;40:111-8.

116. Molhoek SG, Bax JJ, van Erven L, Bootsma M, Boersma E, Steendijk P et al. Comparison of benefits from cardiac resynchronization therapy in patients with ischemic cardiomyopathy versus idiopathic dilated cardiomyopathy. Am J Cardiol 2004;93:860-3.
117. Yu CM, Chau E, Sanderson JE, Fan K, Tang MO, Fung WH et al. Tissue Doppler echocardiographic evidence of reverse remodeling and improved synchronicity by simultaneously delaying regional contraction after biventricular pacing therapy in heart failure. Circulation 2002;105:438-45.
118. Abraham WT, Leon AR, Young JB. Benefits of cardiac resynchronization therapy sustained for 18 months: results from the MIRACLE program. Circulation 2003;108:IV-629.
119. Ghio S, Freemantle N, Scelsi L, Serio A, Magrini G, Pasotti M et al. Long-term left ventricular reverse remodelling with cardiac resynchronization therapy: results from the CARE-HF trial. Eur J Heart Fail 2009;11:480-8.
120. Melmed S. Acromegaly. N Engl J Med. 1990;322:966-77.
121. Delafontaine P. Insulin-like growth factor I and its binding proteins in the cardiovascular system. Cardiovasc Res. 1995;30:825-34.
122. Ito H, Hiroe M, Hirata Y, Tsujino M, Adachi S, Shichiri M et al. Insulin-like growth factor-I induces hypertrophy with enhanced expression of muscle specific genes in cultured rat cardiomyocytes. Circulation. 1993;87:1715-21.
123. Chen DB, Wang L, Wang PH. Insulin-like growth factor I retards apoptotic signaling induced by ethanol in cardiomyocytes. Life Sci. 2000;67:1683-93.
124. Morvan D, Komajda M, Grimaldi A, Turpin G, Grosgogeat Y. Cardiac hypertrophy and function in asymptomatic acromegaly. Eur Heart J. 1991;12:666-72.
125. López-Velasco R, Escobar-Morreale HF, Vega B, Villa E, Sancho JM, Moya-Mur JL et al. Cardiac involvement in acromegaly: specific myocardiopathy or consequence of systemic hypertension? J Clin Endocrinol Metab. 1997;82:1047-53.
126. Colao A, Cuocolo A, Marzullo P, Nicolai E, Ferone D, Della Morte AM et al. Impact of patient's age and disease duration on cardiac performance in acromegaly: a radionuclide angiography study. J Clin Endocrinol Metab. 1999;84:1518-23.
127. Colao A, Vitale G, Pivonello R, Ciccarelli A, Di Somma C, Lombardi G. The heart: an end-organ of GH action. Eur J Endocrinol. 2004;151 Suppl 1:S93- 101.
128. Saccà L, Cittadini A, Fazio S. Growth hormone and the heart. Endocr Rev. 1994;15:555-73.
129. Colao A, Ferone D, Marzullo P, Lombardi G. Systemic complications of acromegaly: epidemiology, pathogenesis, and management. Endocr Rev. 2004;25:102-52.
130. Colao A, Marzullo P, Di Somma C, Lombardi G. Growth hormone and the heart. Clin Endocrinol (Oxf). 2001;54:137-54.

131. Lie JT. Pathology of the heart in acromegaly: anatomic findings in 27 autopsied patients. Am Heart J. 1980;100:41-52.
132. Oscarsson J, Wiklund O, Jakobsson KE, Petruson B, Bengtsson BA. Serum lipoproteins in acromegaly before and 6-15 months after transsphenoidal adenomectomy. Clin Endocrinol (Oxf). 1994;41:603-8.
133. Møller N, Jørgensen JO, Abildgård N, Orskov L, Schmitz O, Christiansen JS. Effects of growth hormone on glucose metabolism. Horm Res. 1991;36 Suppl 1:32-5.
134. Nabarro JD. Acromegaly. Clin Endocrinol (Oxf). 1987;26:481-512.
135. Bengtsson BA, Edén S, Ernest I, Odén A, Sjögren B. Epidemiology and long-term survival in acromegaly. A study of 166 cases diagnosed between 1955 and 1984. Acta Med Scand. 1988;223:327-35.
136. Fazio S, Cittadini A, Sabatini D, Merola B, Colao A, Biondi B et al. Growth hormone and heart performance. A novel mechanism of cardiac wall stress regulation in humans. Eur Heart J. 1997;18:340-7.
137. Mercuro G, Zoncu S, Colonna P, Cherchi P, Mariotti S, Pigliaru F et al. Cardiac dysfunction in acromegaly: evidence by pulsed wave tissue Doppler imaging. Eur J Endocrinol. 2000;143:363-9.
138. van der Klaauw AA, Bax JJ, Smit JW, Holman ER, Delgado V, Bleeker GB et al. Increased aortic root diameters in patients with acromegaly. Eur J Endocrinol. 2008;159:97-103.
139. Mancia G, De Backer G, Dominiczak A, Cifkova R, Fagard R, Germano G et al, The task force for the management of arterial hypertension of the European Society of Hypertension, The task force for the management of arterial hypertension of the European Society of Cardiology. 2007 Guidelines for the management of arterial hypertension: The Task Force for the Management of Arterial Hypertension of the European Society of Hypertension (ESH) and of the European Society of Cardiology (ESC). Eur Heart J. 2007;28:1462-536.
140. Thuesen L, Christiansen JS, Sørensen KE, Jørgensen JOL, Ørskov H, Henningsen P. Increased myocardial contractility following growth hormone administration in normal men. Dan Med Bull. 1988;35:193–6.
141. Freestone NS, Ribaric S, Mason WT. The effect of insulin-like growth factor-1 on adult rat cardiac contractility. Mol Cell Biochem. 1996;163:223–9.
142. Stroemer H, Cittadini A, Douglas PS, Morgan JP. Exogenously administered growth hormone and insulin-like growth factor-1 alter intracellular Ca2 handling and enhance cardiac performance. In vitro evaluation in the isolated isovolumic buffer-perfused rat heart. Circ Res. 1996;79:227–35.

143. Herrmann BL, Bruch C, Saller B, Bartel T, Ferdin S, Erbel R et al. Acromegaly: evidence for a direct relation between disease activity and cardiac dysfunction in patients without ventricular hypertrophy. Clin Endocrinol (Oxf). 2002;56:595-602.
144. Colao A, Cuocolo A, Marzullo P, Nicolai E, Ferone D, Della Morte AM et al. Impact of patient's age and disease duration on cardiac performance in acromegaly: a radionuclide angiography study. J Clin Endocrinol Metab. 1999;84:1518–23.
145. Bijnens BH, Cikes M, Claus P, Sutherland GR. Velocity and deformation imaging for the assessment of myocardial dysfunction. Eur J Echocardiogr 2009;10:216-26.
146. Fazio S, Cittadini A, Biondi B, Palmieri EA, Riccio G, Bonè F et al. Cardiovascular effects of short-term growth hormone hypersecretion. J Clin Endocrinol Metab. 2000;85:179-82.
147. Ikkos D, Luft R, Siogren B. Water and sodium in patients with acromegaly. J Clin Invest. 1954;33:989 –94.
148. Ludens JH, Back RR, Williamson HE. Characteristics of the antinatriuretic action of growth hormone. Proc Soc Exp Biol Med. 1969;130:1156 –8.
149. Møller J, Joergensen JOL, Moeller N, Hansen KW, Pedersen EB, Christiansen JS. Expansion of extracellular volume and suppression of atrial natriuretic peptide after growth hormone administration in normal man. J Clin Endocrinol Metab. 1991;72:768 – 72.
150. Davies PF. Hemodynamic shear stress and the endothelium in cardiovascular pathophysiology. Nat Clin Pract Cardiovasc Med. 2009;6:16-26.
151. Bogazzi F, Lombardi M, Strata E, Aquaro G, Di Bello V, Cosci C et al. High prevalence of cardiac hypertophy without detectable signs of fibrosis in patients with untreated active acromegaly: an in vivo study using magnetic resonance imaging. Clin Endocrinol (Oxf). 2008;68:361-8.
152. Opie L.H., Commerford P.J., Gersh B.J, Pfeffer M.A. Controversies in ventricular remodelling. Lancet. 2006;367,356-67.
153. Maron BJ. Structural features of the athlete heart as defined by echocardiography. J Am Coll Cardiol. 1986;7:190-203.
154. Perseghin G, De Cobelli F, Esposito A, Lattuada G, Terruzzi I, La Torre A et al. Effect of the sporting discipline on the right and left ventricular morphology and function of elite male track runners: a magnetic resonance imaging and phosphorus 31 spectroscopy study. Am Heart J. 2007;154:937-42.
155. Pluim BM, Lamb HJ, Kayser HW, Leujes F, Beyerbacht HP, Zwinderman AH et al. Functional and metabolic evaluation of the athlete's heart by magnetic resonance imaging and dobutamine stress magnetic resonance spectroscopy. Circulation. 1998;97:666-72.

156. Abergel E, Chatellier G, Hagege AA, Oblak A, Linhart A, Ducardonnet A et al. Serial left ventricular adaptations in world-class professional cyclists: implications for disease screening and follow-up. J Am Coll Cardiol. 2004;44:144-9.
157. Morganroth J, Maron BJ, Henry WL, Epstein SE. Comparative left ventriculardimensions in trained athletes. Ann Intern Med. 1975;82:521-4.
158. D'Andrea A, Limongelli G, Caso P, Sarubbi B, Della Pietra A, Brancaccio P et al. Association between left ventricular structure and cardiac performance during effort in two morphological forms of athlete's heart. Int J Cardiol. 2002;86:177-84.
159. Blomqvist CG, Saltin B. Cardiovascular adaptations to physical training. Annu Rev Physiol. 1983;45:169-89.
160. Medugorac I. Myocardial collagen in different forms of heart hypertrophy in the rat. Res Exp Med. 1980;177:201–11.
161. Moore RL, Korzick DH. Cellular adaptations of the myocardium to chronic exercise. Prog Cardiovasc Dis. 1995;37:371-96.
162. Caso P, D'Andrea A, Galderisi M, Liccardo B, Severino S, De Simone L et al. Pulsed Doppler tissue imaging in endurance athletes: relation between left ventricular preload and myocardial regional diastolic function. Am J Cardiol. 2000;85:1131-6.
163. Herbots L. Assessment of Contractile Function in Endurance Trained Athletes using Strain Rate and Strain. PhD Thesis, University Hospital Gasthuisberg, Leuven, Belgium, 2006.
164. Teske AJ, Prakken NH, De Boeck BW, Velthuis BK, Doevendans PA, Cramer MJ. Echocardiographic deformation imaging reveals preserved regional systolic function in endurance athletes with left ventricular hypertrophy. Br J Sports Med. 2009 Jan 9. [Epub ahead of print].
165. Palka P, Lange A, Nihoyannopoulos P. The effect of long-term training on age-related left ventricular changes by Doppler myocardial velocity gradient. Am J Cardiol 1999;84:1061–7.
166. D'Andrea A, D'Andrea L, Caso P, Scherillo M, Zeppilli P, Calabrò R. The usefulness of Doppler myocardial imaging in the study of the athlete's heart and in the differential diagnosis between physiological and pathological ventricular hypertrophy. Echocardiography. 2006;23:149-57.
167. Poulsen SH, Hjortshøj S, Korup E, Poenitz V, Espersen G, Søgaard P et al. Strain rate and tissue tracking imaging in quantitation of left ventricular systolic function in endurance and strength athletes. Scand J Med Sci Sports. 2007;17:148-55.
168. Richand V, Lafitte S, Reant P, Serri K, Lafitte M, Brette S et al. An ultrasound speckle tracking (two-dimensional strain) analysis of myocardial deformation in professional

soccer players compared with healthy subjects and hypertrophic cardiomyopathy. Am J Cardiol. 2007;100:128-32.

169. Frohlich ED, Apstein C, Chobanian AV, Devereux RB, Dustan HP, Dzau V et al. The heart in hypertension. N Engl J Med 1992;327:998-1008.

170. Hatford M, Wikstrand JCM, Wallentin I, Ljungman SMJ. Left ventricular wall stress and systolic function in untreated primary hypertension. Hypertension 1985;7:97-104.

171. Przewlocka-Kosmala M, Kosmala W, Mazurek W. Left ventricular circumferential function in patients with essential hypertension. J Hum Hypertens. 2006;20:666-71.

172. Park SJ, Miyazaki C, Bruce CJ, Ommen S, Miller FA, Oh JK. Left ventricular torsion by two-dimensional speckle tracking echocardiography in patients with diastolic dysfunction and normal ejection fraction. J Am Soc Echocardiogr. 2008;21:1129-37.

173. Kosmala W, Plaksej R, Strotmann JM, Weigel C, Herrmann S, Niemann M et al. Progression of left ventricular functional abnormalities in hypertensive patients with heart failure: an ultrasonic two-dimensional speckle tracking study. J Am Soc Echocardiogr. 2008;21:1309-17.

174. Palmon LC, Reichek N, Yeon SB, Clark NR, Brownson D, Hoffman E, et al. Intramural myocardial shortening in hypertensive left ventricular hypertrophy with normal pump function. Circulation. 1994;89:122-31.

175. Heng MK, Janz RF, Jobin J. Estimation of regional stress in the left ventricular septum and free wall: an echocardiographic study suggesting a mechanism for asymmetric septal hypertrophy. Am Heart J. 1985;110:84-90.

176. Orlando S et al. Hypertrophic cardiomyopathy can be effectively discriminated from others forms by the presence of localised non-deforming segments - a deformation imaging study. Eur Heart J. 2007;Suppl 28(1):370.

177. Schwartzkopff B, Frenzel H, Dieckerhoff J, Betz P, Flasshove M, Schulte HD, et al. Morphometric investigation of human myocardium in arterial hypertension and valvular aortic stenosis. Eur Heart J 1992;13(suppl):17–23.

178. Weidemann F, Herrmann S, Störk S, Niemann M, Frantz S, Lange V et al. Impact of Myocardial Fibrosis in Patients with Symptomatic Severe Aortic Stenosis. Circulation. 2009;120:577-84.

179. Kato TS, Noda A, Izawa H, Yamada A, Obata K, Nagata K et al. Discrimination of nonobstructive hypertrophic cardiomyopathy from hypertensive left ventricular hypertrophy on the basis of strain rate imaging by tissue doppler ultrasonography. Circulation. 2004;110:3808–14.

180. Elliott P, Andersson B, Arbustini E, Bilinska Z, Cecchi F, Charron P et al. Classification of the cardiomyopathies: a position statement from the European Society Of Cardiology Working Group on Myocardial and Pericardial Diseases. Eur Heart J. 2008;29:270-6.

181. Maron BJ, McKenna WJ, Danielson GK, Kappenberger LJ, Kuhn HJ, Seidman CE et al; American College of Cardiology Foundation Task Force on Clinical Expert Consensus Documents; European Society of Cardiology Committee for Practice Guidelines. American College of Cardiology/European Society of Cardiology Clinical Expert Consensus Document on Hypertrophic Cardiomyopathy. A report of the American College of Cardiology Foundation Task Force on Clinical Expert Consensus Documents and the European Society of Cardiology Committee for Practice Guidelines. Eur Heart J. 2003;24:1965–91.
182. Elliott P, McKenna WJ. Hypertrophic cardiomyopathy. Lancet. 2004;363:1881–91.
183. Niimura H, Bachinski LL, Sangwatanaroj S, Watkins H, Chudley AE, McKenna W et al. Mutations in the gene for cardiac myosin-binding protein C and late-onset familial hypertrophic cardiomyopathy. N Engl J Med. 1998;338:1248-57.
184. Maron BJ, Niimura H, Casey SA, Soper MK, Wright GB, Seidman JG et al. Development of left ventricular hypertrophy in adults in hypertrophic cardiomyopathy caused by cardiac myosin-binding protein C gene mutations. J Am Coll Cardiol. 2001;38:315-21.
185. Charron P, Dubourg O, Desnos M, Isnard R, Hagege A, Millaire A et al. Diagnostic value of electrocardiography and echocardiography for familial hypertrophic cardiomyopathy in a genotyped adult population. Circulation. 1997;96:214-9.
186. Charron P, Dubourg O, Desnos M, Bouhour JB, Isnard R, Hagege A et al. Diagnostic value of electrocardiography and echocardiography for familial hypertrophic cardiomyopathy in genotyped children. Eur Heart J. 1998;19:1377-82.
187. Panza JA, Maron BJ. Relation of electrocardiographic abnormalities to evolving left ventricular hypertrophy in hypertrophic cardiomyopathy during childhood. Am J Cardiol. 1989;63:1258-65.
188. Maron BJ, Spirito P, Wesley Y, Arce J. Development and progression of left ventricular hypertrophy in children with hypertrophic cardiomyopathy. N Engl J Med. 1986;315:610-4.
189. Erdmann J, Raible J, Maki-Abadi J, Hummel M, Hammann J, Wollnik B et al. Spectrum of clinical phenotypes and gene variants in cardiac myosin-binding protein C mutation carriers with hypertrophic cardiomyopathy. J Am Coll Cardiol. 2001;38:322-30.
190. Maron BJ, Gardin JM, Flack JM, Gidding SS, Kurosaki TT, Bild DE. Prevalence of hypertrophic cardiomyopathy in a general population of young adults. Echocardiographic analysis of 4111 subjects in the CARDIA Study. Coronary Artery Risk Development in (Young) Adults. Circulation. 1995;92:785-9.
191. Klues HG, Schiffers A, Maron BJ. Phenotypic spectrum and patterns of left ventricular hypertrophy in hypertrophic cardiomyopathy: morphologic observations and significance

as assessed by two-dimensional echocardiography in 600 patients. J Am Coll Cardiol. 1995;26:1699-708.

192. Richardson P, McKenna W, Bristow M, Maisch B, Mautner B, O'Connell J et al. Report of the 1995 World Health Organization/International Society and Federation of Cardiology Task Force on the definition and classification of cardiomyopathies. Circulation. 1996;93:841–2.
193. Goodwin JF. The frontiers of cardiomyopathy. Br Heart J. 1982;48:1–18.
194. Abelmann WH. Classification and natural history of primary myocardial disease. Prog Cardiovasc Dis. 1984;27:73–94.
195. Report of the WHO/ISFC Task Force on the definition and classification of cardiomyopathies. Br Heart J. 1980;44:672–3.
196. Shapiro LM, McKenna WJ. Distribution of left ventricular hypertrophy in hypertrophic cardiomyopathy: a two-dimensional echocardiographic study. J Am Coll Cardiol. 1983;2:437– 44.
197. Charron P, Forissier JF, Amara ME, Isnard R, Hagege A, Bénaïche A et al. Accuracy of European diagnostic criteria for familial hypertrophic cardiomyopathy in a genotyped population. Int J Cardiol 2003, 90:33–8.
198. Verdecchia P, Porcellati C, Zampi I, Schillaci G, Gatteschi C, Battistelli M et al. Asymmetric left ventricular remodeling due to isolated septal thickening in patients with systemic hypertension and normal left ventricular masses. Am J Cardiol 1994;73:247-52.
199. Conrady AO, Rudomanov OG, Zaharov DV, Krutikov AN, Vahrameeva NV, Yakovleva OI et al. Prevalence and determinants of left ventricular hypertrophy and remodelling patterns in hypertensive patients: the St. Petersburg study. Blood Press. 2004:13:101-9.
200. Wachtell K, Bella JN, Liebson PR, Gerdts E, Dahlöf B, Aalto T et al. Impact of different partition values on prevalences of left ventricular hypertrophy and concentric geometry in a large hypertensive population: the LIFE study. Hypertension 2000; 35(1 Pt 1):6-12.
201. Nagueh SF, Lakkis NM, Middleton KJ, Spencer WH III, Zoghbi WA, Quinones MA. Doppler estimation of left ventricular filling pressures in patients with hypertrophic cardiomyopathy. Circulation. 1999;99:254–61.
202. McMahon CJ, Nagueh SF, Pignatelli RH, Denfield SW, Dreyer WJ, Price JF et al. Characterization of left ventricular diastolic function by tissue Doppler imaging and clinical status in children with hypertrophic cardiomyopathy. Circulation. 2004;109:1756–62.
203. Severino S, Caso P, Galderisi M, De Simone L, Petrocelli A, de Divitiis O et al. Use of pulsed Doppler tissue imaging to assess regional left ventricular diastolic dysfunction in hypertrophic cardiomyopathy. Am J Cardiol. 1998;82:1394–8.

204. Maron BJ, Spirito P, Green KJ, Wesley YE, Bonow RO, Arce J. Noninvasive assessment of left ventricular diastolic function by pulsed Doppler echocardiography in patients with hypertrophic cardiomyopathy. J Am Coll Cardiol. 1987;10:733–42.
205. Kato T, Noda A, Izawa H, Nishizawa T, Somura F, Yamada A et al. Myocardial velocity gradient as a noninvasively determined index of left ventricular diastolic dysfunction in patients with hypertrophic cardiomyopathy. J Am Coll Cardiol. 2003;42:278–85.
206. Connelly KA, Prior DL, Kelly DJ, Feneley MP, Krum H, Gilbert RE. Load sensitive measures may overestimate global systolic function in the presence of left ventricular hypertrophy: a comparison with load-insensitive measures. Am J Physiol Heart Circ Physiol. 2006;290:H1699–H1705.
207. Hirota Y, Furubayashi K, Kaku K, Shimizu G, Kino M, Kawamura K et al. Hypertrophic nonobstructive cardiomyopathy: a precise assessment of hemodynamic characteristics and clinical implications. Am J Cardiol. 1982;50:990–7.
208. Shimizu G, Hirota Y, Kita Y, Keishero K, Saito T, Gaasch WH. Left ventricular midwall mechanics in systemic arterial hypertension: myocardial function is depressed in pressure-overload hypertrophy. Circulation. 1991;83:1676–84.
209. Geisterfer-Lowrance AA, Christe M, Conner DA, Ingwall JS, Schoen FJ, Seidman CE et al. A mouse model of familial hypertrophic cardiomyopathy. Science. 1996;272:731-4.
210. Karlon WJ, McCulloch AD, Covell JW, Hunter JJ, Omens JH. Regional dysfunction correlates with myofiber disarray in transgenic mice with ventricular expression of ras. Am J Physiol Heart Circ Physiol. 2000;278:H898–H906.
211. Rajiv C, Vinereanu D, Fraser AG. Tissue Doppler imaging for the evaluation of patients with hypertrophic cardiomyopathy. Curr Opin Cardiol. 2004;19:430-6.
212. Serri K, Reant P, Lafitte M, Berhouet M, Le Bouffos V, Roudaut R et al. Global and regional myocardial function quantification by two-dimensional strain: application in hypertrophic cardiomyopathy. J Am Coll Cardiol. 2006;47:1175-81.
213. Ito T, Suwa M, Tonari S, Okuda N, Kitaura Y. Regional postsystolic shortening in patients with hypertrophic cardiomyopathy: its incidence and characteristics assessed by strain imaging. I Am Soc Echocardiogr 2006;19:987-93.
214. Yang H, Sun JP, Lever HM, Popovic ZB, Drinko JK, Greenberg NL et al. Use of strain imaging in detecting segmental dysfunction in patients with hypertrophic cardiomyopathy. J Am Soc Echocardiogr. 2003;16:233–9.
215. Sengupta PP, Mehta V, Arora R, Mohan JC, Khandheria BK. Quantification of Regional Nonuniformity and Paradoxical Intramural Mechanics in Hypertrophic Cardiomyopathy by High Frame Rate Ultrasound Myocardial Strain Mapping. J Am Soc Echocardiogr. 2005;18:737-42.

216. Maron BJ, Anan TJ, Roberts WC. Quantitative analysis of the distribution of cardiac muscle cell disorganization in the left ventricular wall of patients with hypertrophic cardiomyopathy. Circulation. 1981;63:882-94.
217. Ganame J, Mertens L, Eidem BW, Claus P, D'hooge J, Havemann LM et al. Regional myocardial deformation in children with hypertrophic cardiomyopathy: morphological and clinical correlations. Eur Heart J. 2007;28:2886-94.
218. Weidemann F, Niemann M, Herrmann S, Kung M, Störk S, Waller C et al. A new echocardiographic approach for the detection of non-ischaemic fibrosis in hypertrophic myocardium. Eur Heart J. 2007;28:3020-6.
219. Sun JP, Stewart WJ, Yang XS, Donnell RO, Leon AR, Felner JM et al. Differentiation of hypertrophic cardiomyopathy and cardiac amyloidosis from other causes of ventricular wall thickening by two-dimensional strain imaging echocardiography. Am J Cardiol. 2009;103:411-5.
220. Kato TS, Izawa H, Komamura K, Noda A, Asano H, Nagata K et al. Heterogeneity of regional systolic function detected by tissue Doppler imaging is linked to impaired global left ventricular relaxation in hypertrophic cardiomyopathy. Heart. 2008;94:1302-6.
221. Dong SJ, MacGregor JH, Crawley AP, McVeigh E, Belenkie I, Smith ER et al. Left ventricular wall thickness and regional systolic function in patients with hypertrophic cardiomyopathy. A three-dimensional tagged magnetic resonance imaging study. Circulation. 1994;90:1200–9.
222. Kim YI, Choi BW, Hur J, Lee HJ, Seo JS, Kim TH et al. Delayed enhancement in hypertrophic cardiomyopathy: Comparison with myocardial tagging MRI. Journal of Magn Reson Imaging. 2008;27:1054-60.
223. Piella G, De Craene M, Oubel E, Larrabide I, Bijnens B, Frangi A. Myocardial deformation from tagged MRI in hypertrophic cardiomyopathy using an efficient registration strategy. In Proceedings of SPIE. 2009;7262.
224. Moon JC, Mogensen J, Elliott PM, Smith GC, Elkington AG, Prasad SK et al. Myocardial late gadolinium enhancement cardiovascular magnetic resonance in hypertrophic cardiomyopathy caused by mutations in troponin I. Heart. 2005;9:1036-40.
225. Falk RH. Diagnosis and management of the cardiac amyloidoses. Circulation. 2005;112:2047-60.
226. Merlini G, Bellotti V. Molecular mechanisms of amyloidosis. N Engl J Med. 2003;349:583–96.
227. Dubrey SW, Cha K, Anderson J, Chamarthi B, Reisinger J, Skinner M et al. The clinical features of immunoglobulin light-chain (AL) amyloidosis with heart involvement. QJM. 1998;91:141–57.

228. Kyle RA, Gertz MA. Primary systemic amyloidosis: clinical and laboratory features in 474 cases. Semin Hematol. 1995;32:45–59.
229. Dubrey SW, Cha K, Simms RW, Skinner M, Falk RH. Electrocardiography and Doppler echocardiography in secondary (AA) amyloidosis. Am J Cardiol. 1996;77:313-5.
230. Gertz MA, Kyle RA. Secondary systemic amyloidosis: response and survival in 64 patients. Medicine (Baltimore). 1991;70:246-56.
231. Robbins MA, Pizzarello RA, Stechel RP, Chiaramida SA, Gulotta SJ. Resting and exercise hemodynamics in constrictive pericarditis and a case of cardiac amyloidosis mimicking constriction. Cathet Cardiovasc Diagn. 1983;9:463– 71.
232. Westermark P, Sletten K, Johansson B, Cornwell GG. Fibril in senile systemic amyloidosis is derived from normal transthyretin. Proc Natl Acad Sci U S A. 1990;87:2843–5.
233. Ng B, Connors LH, Davidoff R, Skinner M, Falk RH. Senile systemic amyloidosis presenting with heart failure: a comparison with light chain– associated (AL) amyloidosis. Arch Intern Med. 2005;165:1425–9.
234. Cornwell GG, Murdoch WL, Kyle RA, Westermark P, Pitkanen P. Frequency and distribution of senile cardiovascular amyloid: a clinicopathologic correlation. Am J Med. 1983;75:618–23.
235. Wright JR, Calkins E. Amyloid in the aged heart: frequency and clinical significance. J Am Geriatr Socy. 1975;23:97–103.
236. Ardehali H, Qasim A, Cappola T, Howard D, Hruban R, Hare JM et al. Endomyocardial biopsy plays a role in diagnosing patients with unexplained cardiomyopathy. Am Heart J.2004;147:919 –23.
237. Gertz MA, Grogan M, Kyle RA, Tajik AJ. Endomyocardial biopsy proven light chain amyloidosis (AL) without echocardiographic features of infiltrative cardiomyopathy. Am J Cardiol. 1997;80:93–5.
238. Klein AL, Hatle LK, Taliercio CP, Taylor CL, Kyle RA, Bailey KR et al. Serial Doppler echocardiographic follow-up of left ventricular diastolic function in cardiac amyloidosis. J Am Coll Cardiol. 1990;16:1135–41.
239. Shah KB, Inoue Y, Mehra MR. Amyloidosis and the heart: a comprehensive review. Arch Intern Med. 2006;166:1805-13.
240. Brenner DA, Jain M, Pimentel DR, Wang B, Connors LH, Skinner M et al. Human amyloidogenic light chains directly impair cardiomyocyte function through an increase in cellular oxidant stress. Circ Res. 2004;94:1008-10.
241. Koyama J, Ray-Sequin PA, Davidoff R, Falk RH. Usefulness of pulsed tissue Doppler imaging for evaluating systolic and diastolic left ventricular function in patients with AL (primary) amyloidosis. Am J Cardiol. 2002;89:1067–71.

242. Koyama J, Davidoff R, Falk RH. Longitudinal myocardial velocity gradient derived from pulsed Doppler tissue imaging in AL amyloidosis: a sensitive indicator of systolic and diastolic dysfunction. J Am Soc Echocardiogr. 2004;17:36–44.
243. Bellavia D, Pellikka PA, Abraham TP, Al-Zahrani GB, Dispenzieri A, Oh JK et al. Evidence of impaired left ventricular systolic function by Doppler myocardial imaging in patients with systemic amyloidosis and no evidence of cardiac involvement by standard two-dimensional and Doppler echocardiography. Am J Cardiol. 2008;101:1039-45.
244. Maceira AM, Joshi J, Prasad SK, Moon JC, Perugini E, Harding I et al. Cardiovascular magnetic resonance in cardiac amyloidosis. Circulation. 2005;111:186–93.
245. Weidemann F, Niemann M, Breunig F, Herrmann S, Beer M, Störk S et al. Long-term effects of enzyme replacement therapy on fabry cardiomyopathy: evidence for a better outcome with early treatment. Circulation. 2009;119:524-9.
246. Buyse G, Mertens L, Di Salvo G, Matthijs I, Weidemann F, Eyskens B et al. Idebenone treatment in Friedreich's ataxia: neurological, cardiac, and biochemical monitoring. Neurology. 2003;60:1679–81.
247. Weidemann F, Breunig F, Beer M, Sandstede J, Turschner O, Voelker W et al. Improvement of cardiac function during enzyme replacement therapy in patients with Fabry disease: a prospective strain rate imaging study. Circulation. 2003;108:1299–1301.
248. Dutka DP, Donnelly JE, Palka P, Lange A, Nunez DJ, Nihoyannopoulos P. Echocardiographic characterization of cardiomyopathy in Friedreich's ataxia with tissue Doppler echocardiographically derived myocardial velocity gradients. Circulation 2000;102:1276–82.
249. Pieroni M, Chimenti C, Ricci R, Sale P, Russo MA, Frustaci A. Early detection of Fabry cardiomyopathy by tissue Doppler imaging. Circulation. 2003;107:1978–84.
250. Weidemann F, Breunig F, Beer M, Sandstede J, Stork S, Voelker W et al. The variation of morphological and functional cardiac manifestation in Fabry disease: potential implications for the time course of the disease. Eur Heart J. 2005;26:1221-7.
251. Desnick RJ, Ioannou YA, Eng CM. α -Galactosidase A deficiency: Fabry disease. In: Scriver CR, Beaudet AL, Sly WS, Valle D, editors. The Metabolic and Molecular Bases of Inherited Disease, 8th edn. New York: McGraw-Hill;2001,3733–74.
252. Desnick, Meikle PJ, Hopwood JJ, Clague AE, Carey WF. Prevalence of lysosomal storage disorders. JAMA. 1999;281:249-54.
253. Mehta A, Ricci R, Widmer U, Dehout F, Garcia de Lorenzo A, Kampmann C et al. Fabry disease defined: baseline clinical manifestations of 366 patients in the Fabry Outcome Survey. Eur J Clin Invest. 2004;34:236–42.

254. Linhart A, Palecek T, Bultas J, Ferguson JJ, Hrudova J, Karetova D et al. New insights in cardiac structural changes in patients with Fabry's disease. Am Heart J. 2000;139:1101-12.
255. Weidemann F, Strotmann JM. Use of tissue Doppler imaging to identify and manage systemic diseases. Clin Res Cardiol. 2008;97:65-73.
256. Bogaert J, Rademakers FE. Regional nonuniformity of normal adult human left ventricle. Am J Physiol Heart Circ Physiol. 2001;280:H610–20.
257. Moon JC, Sachdev B, Elkington AG, McKenna WJ, Mehta A, Pennell DJ et al. Gadolinium enhanced cardiovascular magnetic resonance in Anderson-Fabry disease. Evidence for a disease specific abnormality of the myocardial interstitium. Eur Heart J. 2003;24:2151-5.
258. Eng CM, Guffon N, Wilcox WR, Germain DP, Lee P, Waldek S et al. Safety and efficacy of recombinant human alpha-galactosidase A – replacement therapy in Fabry's disease. N Engl J Med. 2001;345:9–16.
259. Beer M, Weidemann F, Breunig F, Knoll A, Koeppe S, Machann W et al. Impact of enzyme replacement therapy on cardiac morphology and function and late enhancement in Fabry's cardiomyopathy. Am J Cardiol. 2006;97:1515–8.
260. Bradley JL, Blake JC, Chamberlain S, Thomas PK, Cooper JM, Schapira AH. Clinical, biochemical and molecular genetic correlations in Friedreich's ataxia. Hum Mol Genet. 2000;9:275–82.
261. Hewer R. The heart in Friedreich's ataxia. Br Heart J. 1969;31:5–14.
262. Child JS, Perloff JK, Bach PM, Wolfe AD, Perlman S, Kark RA. Cardiac involvement in Friedreich's ataxia: a clinical study of 75 patients. J Am Coll Cardiol 1986;7:1370–8.
263. Weidemann F, Eyskens B, Mertens L, Di Salvo G, Strotmann J, Buyse G et al. Quantification of regional right and left ventricular function by ultrasonic strain rate and strain indexes in Friedreich's ataxia. Am J Cardiol. 2003;91:622–6.
264. Rustin P, von Kleist-Retzow JC, Chantrel-Groussard K, Sidi D, Munnich A, Rotig A. Effect of idebenone on cardiomyopathy in Friedreich's ataxia: a preliminary study. Lancet. 999;354:477–9.
265. Biggar WD. Duchenne muscular dystrophy. Pediatr Rev 2006;27,83-8.
266. Hoffman EP, Brown RH Jr, Kunkel LM. Dystrophin: the protein product of the Duchenne muscular dystrophy locus. Cell 1987;51,919-28.
267. Mertens L, Ganame J, Claus P, Goemans N, Thijs D, Eyskens B et al. Early regional myocardial dysfunction in young patients with Duchenne muscular dystrophy. J Am Soc Echocardiogr. 2008,21,1049-54.

Curriculum vitae

Maja Čikeš was born in Zagreb, 1980. where she has graduated from the Classical Gymnasium in 1998 and the School of Medicine, University of Zagreb in 2004. During the medical studies, she has taken part in student clerkship programmes in Nottingham, United Kingdom as well as at the Department for Cardiovascular Diseases, Mayo Clinic, Rochester, Minnesota, USA where she has been introduced to clinical research, resulting in her first publications. Upon returning to Zagreb, Maja Čikeš has continued with scientific work at the Department of Cardiovascular Diseases, University Hospital Centre Zagreb, for which she was awarded the Rector's award in 2004. Following her graduation, she has been appointed as Research fellow – assistant at the Chair of Internal medicine and has enrolled to the PhD study "Biomedicine and Health Sciences", both at the School of Medicine, Zagreb. During the same year, doctor Čikeš has started the Internal medicine – cardiology residency programme. As a research fellow, she has been collaborating on the Brain – Gain "Senior" Programme of the National Foundation for Science, Higher Education and Technological Development of the Republic of Croatia (mentored by Professor B. Bijnens). Currently, she is a collaborator on a research project by the Ministry of Science, Education and Sport of the Republic of Croatia (mentored by Professor J. Separović Hanževački). As an assistant, Dr. Čikeš is involved in medical teaching of undergraduate and postgraduate students. In 2008 she has spent 6 months as a research fellow at the Echocardiography laboratory, St. George's Hospital, St George's University, London, United Kingdom.

So far Dr. Čikeš has actively taken part in 23 international meetings with 41 abstracts and 4 scientific papers in meeting proceedings. She has published 9 articles, 8 of which in the Current Contents database, while further 3 are currently under review in acclaimed international cardiology journals. For her scientific work, she was awarded the L'Oreal-UNESCO Scholarship for Women in Science in 2008.

Bibliography

Articles Published in Journals:

1. Mookadam F, Cikes M. Images in clinical medicine. Cullen's and Turner's signs. N Engl J Med. 2005;353(13):1386.
2. Separovic-Hanzevacki J, Cikes M, Lovric-Bencic M, Sonicki Z, Cekovic S, Ernst A, Drinkovic N, Cikes I. Early detection of left ventricular diastolic dysfunction in hypertensive heart disease by color Doppler myocardial imaging. Croat Med J. 2005;46(6):913-21.
3. Mookadam F, Cikes M, Baddour LM, Tleyjeh IM, Mookadam M. Corynebacterium jeikeium endocarditis: a systematic overview spanning four decades. Eur J Clin Microbiol Infect Dis. 2006;25(6):349-53.
4. Mookadam F, Haley JH, Olson LJ, Cikes M, Mookadam M. Dynamic left ventricular outflow tract obstruction in senile cardiac amyloidosis. Eur J Echocardiogr. 2006;7:465-8.
5. Cikes M, Mookadam M, Asirvatham SJ, Mookadam F. Pseudomonas infection of implantable cardioverter-defibrillator generator and leads as a complication of gastrostomy. Int J Infect Dis. 2007;11(3):281-2.
6. Bijnens BH, Cikes M, Claus P, Sutherland GR. Velocity and deformation imaging for the assessment of myocardial dysfunction. Eur J Echocardiogr. 2009;10(2):216-26
7. Cikes M, Kalinic H, Baltabaeva A, Loncaric S, Parsai C, Milicic D, Cikes I, Sutherland G, Bijnens B. The shape of the aortic outflow velocity profile revisited: is there a relation between its asymmetry and ventricular function in coronary artery disease? Eur J Echocardiogr. 2009;10(7):847-57
8. Čikeš M, Bijnens B, Đurić Ž, Lovrić Benčić M, Gošev I, Velagić V, Gašparović H, Miličić D, Biočina B. Detecting Volume Responders prior to Implantation of a Cardiac Resynchronization Therapy Device via Minithoracotomy: The Septal Flash as a Predictor of Immediate Left Ventricular Reverse Remodeling. Heart Surg Forum. 2009;12(6):in press
9. Jelaković B, Kuzmanić D, Milicić D, Reiner Z, Aganović I, Basić-Jukić N, Bozikov J, Cikes M, Dika Z, Delmis J, Galesić K, Hrabak-Zerjavić V, Ivanusa M, Juresa V, Katić M, Kern J, Kes P, Laganović M, Pavlović D, Pećin I, Pocanić D, Racki S, Sabljar-Matovinović M, Sonicki Z, Vrcić-Keglević M, Vuletić S, Zaputović L; Croatian Working Group for Hypertension. [Guidelines for diagnostics and treatment of arterial hypertension. Practical recommendations of the Croatian Working Group for Hypertension. Consideration on the ESH-ESC 2007 guidelines]. Lijec Vjesn. 2008;130(5-6):115-32.

Articles under Review:

1. M. Cikes, H Kalinic, S Hermann, S. Loncaric, D. Milicic, M. Beer, L Hatle, I Cikes, G Sutherland, F. Weidemann, B. Bijnens. The Symmetry of the Aortic Outflow Velocity Profile in Aortic Stenosis: Does it Predict Functional Recovery After Aortic Valve Replacement?
2. Cikes M, Bijnens B, Anderson L, Sutherland G. The New Role of Echocardiography in the Diagnosis and Assessment of Hypertrophic Myopathies.
3. Cikes M, Separovic Hanzevacki J, Kastelan D, Dusek T, Lovric Bencic M, Ernst A, Korsic M, Bijnens B. Early Stage Acromegalic Cardiomyopathy: Evidence of Left Ventricular Hypertrophy without Increased Afterload and Increased Contractility Associated with Increased Cardiac Output.

Meeting Abstracts Published in Journals:

1. Čikeš M, Miličić D, Strozzi M, Separović-Hanževački J, Čikeš I, Štern-Padovan R, Karadža J, Seiwewrth S. Retrokardijalni paragangliom koji oponaša tumor lijeve pretkijetke. Liječ vjesn 2004;126(supl.1):43
2. Šeparović-Hanževački J, Lovrić-Benčić M, Putarek K, Čikeš M, Biškup I, Bobić L, Ernst A. Do late diastolic parameters change in mild hypertensive heart disease? Liječ vjesn 2004; 126(supl.1):46
3. Šeparović-Hanževački J, Lovrić-Benčić M, Putarek K, Čikeš M, Biškup I, Bobić L, Ernst A. Regional diastolic dysfunction as early manifestation of hypertensive heart disease. Liječ vjesn 2004; 126(supl.1):47
4. Separovic-Hanzevacki J, Lovric-Bencic M, Putarek K, Ernst A, Cikes M. Do late diastolic parameters change in mild hypertensive heart disease? Eur J Echocardiogr 2004;5(suppl 1):162
5. Separovic-Hanzevacki J, Lovric-Bencic M, Putarek K, Ernst A, Cikes M. Regional diastolic dysfunction as early manifestation of hypertensive heart disease. Eur J Echocardiogr 2004;5(suppl 1):162
6. Separovic Hanzevacki J, Cikes M, Lovric Bencic M, Jelakovic B, Biskup I, Bobic L. Early detection of hypertensive heart disease by measuring regional myocardial diastolic dysfunction. Journal of Hypertension 2005;23(suppl 2):162
7. Separovic Hanzevacki J, Cikes M, Lovric Bencic M, Jelakovic B, Biskup I, Bobic L. Deterioration of left ventricular compliance in mild hypertensive heart disease assessed by color Doppler myocardial imaging. Journal of Hypertension 2005;23(suppl 2):290
8. Separovic Hanzevacki J, Cikes M, Lovric Bencic M, Cekovic S, Biskup I, Bobic L, Ernst A. Is There Decreased Left Ventricular Diastolic Distensibility in Mild Hypertensive Heart

Disease? - a Color Doppler Myocardial Imaging Study. Eur J Echocardiogr 2005;6(suppl.1):179
9. Cikes M, Separovic Hanzevacki J, Lovric Bencic M, Ernst A, Sonicki Z, Bijnens B. Is it possible to measure interventricular mechanical delay from a single heart cycle? – Colour Doppler myocardial imaging study. Liječ Vjesn 2006;128(Suppl 2):115
10. Cikes M, Separovic Hanzevacki J, Lovric Bencic M, Ernst A, Sonicki Z. Assessment of regional vs. global diastolic function in early detection of myocardial involvement in acromegaly - Colour Doppler myocardial imaging study. Liječ Vjesn 2006;128(Suppl 2):122
11. Cikes M, Separovic Hanzevacki J, Lovric Bencic M, Sonicki Z, Ernst A. Early detection of hypertensive heart disease by measuring regional myocardial diastolic dysfunction assessed by color Doppler myocardial imaging. Eur Heart J 2006;27(Suppl 1):115
12. Separovic Hanzevacki J, Cikes M, Lovric Bencic M, Ernst A, Sonicki Z, Bijnens B. Measurement of interventricular delay by color Doppler myocardial imaging from a single heart cycle. Eur Heart J 2006;27(Suppl 1):816
13. Separovic Hanzevacki J, Cikes M, Lovric Bencic M, Ernst A, Cikes I. Single heart cycle measurement of interventricular delay by color Doppler myocardial imaging in right ventricular paced patients. Eur J Echocardiogr 2006; 7(suppl.1):152
14. Separovic Hanzevacki J, Cikes M, Lovric Bencic M, Ernst A. Is color Doppler myocardial imaging superior to conventional echocardiography in early detection of myocardial dysfunction in acromegaly? Eur J Echocardiogr 2006; 7(suppl.1):164
15. Čikeš M, Šeparović Hanževački J, Kaštelan D, Dušek T, Ernst A, Koršić M, Bijnens B. Does pituitary adenoma size influence left ventricular hypertrophy in acromegaly? Liječ Vjesn 2007;129(Suppl 1):42
16. Šeparović Hanževački J, Čikeš M, Kaštelan D, Dušek T, Lovrić Benčić M, Ernst A, Koršić M, Bijnens B. Early acromegalic cardiomyopathy – a model for left ventricular hypertrophy and hypercontractility. Liječ Vjesn 2007;129(Suppl 1):43
17. Čikeš M, Kalinić H, Baltabaeva A, Loncarić S, Parsai C, Šeparović Hanževački J, Čikeš I, Sutherland GR, Bijnens B. Is there a relation between the shape of the aortic outflow velocity profile and contractile function in coronary artery disease? A dobutamine stress echo study. Liječ Vjesn 2007;129(Suppl 2):65
18. Šeparović Hanževački J, Čikeš M, Lovrić Benčić M, Sonicki Z, Ernst A, Bijnens B. Early detection of hypertensive heart disease by measuring regional myocardial diastolic dysfunction assessed by color Doppler myocardial imaging. Liječ Vjesn 2007;129(Suppl 2):58
19. Čikeš M, Kalinić H, Baltabaeva A, Lončarić S, Parsai C, Šeparović Hanževački J, Čikeš I, Sutherland G.R, Bijnens B. The Shape of the Aortic Outflow Velocity Profile in Coronary

Artery Disease. Might it be Related to Contractile Function? An Automated Analysis Using Mathematical Modelling. Liječ Vjesn 2007;129(Suppl 4):67

20. Keller N, Čikeš M, Pezo Nikolić B, Buljević B, Puljević D, Tomašić D, Šeparović Hanževački J, Miličić D, Bijnens B. The Acute Impact of Cardiac Resynchronization Therapy on Left Ventricular Function - The Role of Intraoperative Echocardiography. Liječ Vjesn 2007;129(Suppl 4):150

21. Cikes M, Keller N, Kalinic H, Loncaric S, Separovic Hanzevacki J, Cikes I, Bijnens B. Aortic Outflow Doppler Trace – The Relation Between Left Ventricular Function, Increased Afterload and Trace Symmetry. Liječ Vjesn 2007;129(Suppl 4):163

22. Cikes M, Kalinic H, Baltabaeva A, Loncaric S, Parsai C, Separovic J, Cikes I, Sutherland GR and Bijnens B. The shape of the aortic outflow velocity profile in coronary artery disease. Might it be related to contractile function ? An automated analysis using mathematical modeling. Eur J Echocardiogr 2007;(Suppl 1):645

23. Cikes M, Separovic J, Kastelan D, Dusek T, Ernst A, Korsic M, Bijnens B. Left ventricular hypertrophy in acromegalic heart disease: is there an impact of pituitary adenoma size? Eur J Echocardiogr 2007; (Suppl 1):859

24. Separovic J, Cikes M, Kastelan D, Dusek T, Lovric M, Ernst A, Korsic M, Bijnens B. Early stage acromegalic cardiomyopathy: a model for LV hypertrophy and increased contractility without an increase in loading. Eur J Echocardiogr 2007; (Suppl 1):834

25. Baltabaeva AT, Parsai C, Bijnens B, Cikes M, Nistor M, Sutherland GR. The prevalence and clinical significance of the development of a left ventricular cavity/outflow pressure gradient during dobutamine stress echocardiography. Eur J Echocardiogr 2007;(Suppl 1):637

26. Cikes M, Kalinic H, Baltabaeva A, Loncaric S, Parsai C, Separovic Hanzevacki J, Cikes I, Sutherland G, Bijnens B. Does symmetry of the aortic outflow velocity profile reflect contractile function in coronary artery disease? An automated analysis using mathematical modeling. Circulation 2008;117(19):196

27. Cikes M, Kalinic H, Baltabaeva A, Loncaric S, Parsai C, Milicic D, Cikes I, Sutherland GR, Bijnens B. The shape of the aortic outflow velocity profile revisited. Is there a relation to contractile function in coronary artery disease? An automated analysis using mathematical modeling. Liječ Vjesn 2008;130(Suppl 3):60

28. Cikes M, Kalinic H, Herrmann S, Loncaric S, Milicic D, Cikes I, Sutherland GR, Weidemann F, Bijnens B. The symmetry of the aortic outflow velocity profile in aortic stenosis: a novel predictor of functional improvement after aortic valve replacement? Liječ Vjesn 2008;130(Suppl 3):61

29. Ivanac I, Milicic D, Lovric D, Reskovic V, Cikes M, Hrabak M, Stern – Padovan R. Implementation of contrast-enhanced cardiac magnetic resonance in diagnosis of myocarditis. Liječ Vjesn 2008;130(Suppl 3):62

30. Bulum J, Cikes M, Separovic Hanzevacki J, Lovric Bencic M, Ernst A, Ivanac I, Strozzi M, Milicic D. Myocardial bridging and apical ballooning syndrome in the patient presented with pulmonary edema. Liječ Vjesn 2008;130(Suppl 3):86

31. Lovric D, Skoric B, Cikes M, Reskovic V, Baricevic Z, Velagic V, Brida M, Smalcelj A, Milicic D. Fibrinolytic therapy for artificial mechanical valve thrombosis – a series report and single center experience. Liječ Vjesn 2008;130(Suppl 3):87

32. Cikes M, Kalinic H, Hermann S, Loncaric S, Milicic D, Sutherland GR, Weidemann F, Bijnens B. Symmetry of the aortic outflow velocity profile in aortic stenosis: does it predict functional changes before and after aortic valve replacement? Eur J Echocardiogr 2008;(Suppl 1):136

33. Čikeš M, Kalinić H, Hermann S, Lange V, Lončarić S, Miličić D, Beer M, Čikeš I, Weidemann F, Bijnens B. Odražava li oblik spektra aortnog protoka u stenozi aortnog zalistka više od težine stenoze? Utjecaj miokardne fibroze na simetriju spektra aortnog protoka. Liječ Vjesn 2009;131(Suppl 2):89

34. Baričević Ž, Velagić V, Čikeš M, Skorić B, Samardžić J, Miličić D. Fondaparinux u liječenju heparinom inducirane trombocitopenije. Liječ Vjesn 2009;131(Suppl 2):100

35. Cikes M, Kalinic H, Hermann S, Lange V, Loncaric S, Milicic D, Beer M, Cikes I, Weidemann F, Bijnens B. Does the aortic velocity profile in aortic stenosis patients reflect more than stenosis severity? The impact of myocardial fibrosis on aortic flow symmetry. Eur Heart J 2009;30(Suppl 1):605

36. Cikes M, Kalinic H, Hermann S, Lange V, Loncaric S, Milicic D, Beer M, Cikes I, Weidemann F, Bijnens B. The symmetry of the shape of the instantaneous peak velocities in aortic stenosis: does it predict functional recovery after aortic valve replacement? Liječ Vjesn 2009;131(Suppl 5):21

37. Cikes M, Separovic Hanzevacki J, Kastelan D, Dusek T, Lovric Bencic M, Ernst A, Milicic D, Bijnens B. Non pressure overload LV hypertrophy in acromegaly leads to increased contractility and cardiac output whereas hypertensive hypertrophy does not. Hineka 2009;24:39

Scientific Papers Published in Meeting Proceedings:

1. Bijnens B, Claus P, Parsai C, Cikes M, Loncaric S, Anderson L and Sutherland GR. An integrated framework for the assessment of cardiac function – Description and illustrated applications. In *International Symposium on Image and Signal Processing and Analysis (ISPA)*, 2007, 332-337.

2. Kalinic H, Loncaric S, Cikes M, Baltabaeva A, Parsai C, Separovic J, Cikes I, Sutherland GR and Bijnens B. Analysis of Doppler Ultrasound Outflow Profiles for the Detection of

changes in Cardiac Function. In *International Symposium on Image and Signal Processing and Analysis (ISPA)*, 2007, 326-331.

3. Kalinić H, Lončarić S, Čikeš M, Miličić D, Čikeš I, Sutherland G, Bijnens B. A method for registration and model-based segmentation of Doppler ultrasound images. In *Proceedings of SPIE Medical Imaging.* 2009;7259:72590S-72590S-8. doi: 10.1117/12.811331

4. Kalinic H, Loncaric S, Cikes M, Milicic D and Bijnens B. Comparison of different methods for atlas construction In: *17th European Signal Processing Conference (EUSIPCO 2009),* Glasgow 2009, 1319-1323

Abstracts Published in Meeting Proceedings:

1. Čikeš M. Diastolic dysfunction of the left ventricle and recent evaluation methods. 1st International Croatian Student Summit for Biomedical Students and Young Scientists Abstract Book; 2005, p. 57

2. Cikes M, Separovic Hanzevacki J, Kastelan D, Cekovic S, Dusek T, Korsic M. Early detection of heart affection in acromegaly assesed by color Doppler myocardial imaging. European Congress of Endocrinology Abstract Book, 2005, p.141

3. Čikeš M, Bijnens B, Gjurić Ž, Saade K, Gošev I, Matasić R, Velagić V, Lovrić Benčič M, Puljević D, Hrabak M, Ferek-Petrić B, Gašparović H, Miličić D, Biočina B. Detecting volume responders prior to CRT device implantation via mini-thoracotomy. The septal flash as a predictor of immediate LV reverse remodeling detectable by intraoperative echocardiography. 6th Annual Meeting of the Euro-Asian Bridge Book of abstracts; 2009, p30.

4. Gošev I, Gašparović H, Burcar I, Đurić Ž, Čikeš M, Petričević M, Biočina B. Aortic score – quantification of atherosclerosis altered ascending aorta by epiaortic ultrasound. 6th Annual Meeting of the Euro-Asian Bridge Book of abstracts; 2009, p56.